INVESTIGATION OF TEMPERATURE EFFECTS FOR MODELIZATION AND SIMULATION OF THE TREAT FACILITY

A Thesis

by

LOGAN MICHAEL SCOTT

Submitted to the Office of Graduate and Professional Studies of
Texas A&M University
in partial fulfillment of the requirements for the degree of

MASTER OF SCIENCE

Chair of Committee,	Jean Ragusa
Committee Members,	Lin Shao
	Amine Benzerga
Head of Department,	Yassin Hassan

August 2017

Major Subject: Nuclear Engineering

ABSTRACT

From the initiation of operations in 1959, the Transient Reactor Test (TREAT) facility at Idaho National Laboratories possessed the potential to serve as the foremost transient testing site in the world. From 1959 to 1994, thousands of tests were conducted to investigate fission heating of test fuel, non-destructive test data through fuel radiography, and test fuels under severe criticality conditions. However, experiments have not been conducted since 1994. A resurging interest in fuel-motion testing has ignited new interest in the facility. Even after nearly 20 years, the return to operable conditions and resumption of testing at TREAT is believed to be feasible by the Department of Energy (DOE). As the facility prepares to resume testing, systematic and safety checks ensure the optimization of the facility. In preparation of testing resumption, models have been constructed to investigate the effects of temperature change in the experimental fuels on neutron flux observed in the hodoscope fuel-mass surveillance. Because of a wide range of expected fuel samples, it was necessary to determine the effects of temperature changes in the experimental test vehicle, if any, on neutron behavior at the center of the reactor system. Using Monte Carlo simulations, this study demonstrates that the temperature changes in the experimental test vehicle have no effect neutron flux response from the fuel samples tested within TREAT.

DEDICATION

For Kenzie's patience,

For my family's guidance,

And for a dog's love.

ACKNOWLEDGEMENTS

I would like to thank my committee chair, Dr. Jean Ragusa, for his unwavering patience and insight. I would also like to thank my committee members, Dr. Lin Shao, and Dr. Amine Benzerga, for their guidance and support throughout the course of this research.

Special thanks is due to Dr. Samuel Bays for his continued mentorship and expertise in research and in life through this process.

Thanks also go to my friends and colleagues and the department faculty and staff for making my time at Texas A&M University a great experience.

Finally, thanks to my mother and father for their encouragement and to my wife for her patience and love.

CONTRIBUTORS AND FUNDING SOURCES

This work was supervised by a dissertation committee consisting of Jean Ragusa, advisor, and Lin Shao of the Department of Nuclear Engineering, and Amine Benzerga of the Department of Aerospace Engineering.

Financial and laboratory support was provided by Samuel Bayes of Idaho National Laboratory.

NOMENCLATURE

TREAT	Transient Reactor Test Facility
INL	Idaho National Laboratory
ATF	Accident-Tolerant Fuels
MCNP	Monte Carlo N-Particle Code
HEU	High Enriched Uranium
Al-2	Aluminum-II Alloy
SERTTA	Static Environment Rodlet Transient Test Apparatus
mSERTTA	Multi Static Environment Rodlet Transient Test Apparatus
ENDF	Evaluated Nuclear Data Files
ACE	A Compact ENDF
OTFDB	On-The-Fly Doppler Broadening
PWR	Pressurized Water Reactor
UOx	Uranium Oxide Fuel
SSW	Surface Source Write
SSR	Surface Source Read
LEU	Light Enriched Uranium
HPC	High-Performance Computing Center

TABLE OF CONTENTS

Page

LIST OF FIGURES

Page

LIST OF TABLES

Page

1. INTRODUCTION

The Transient Reactor Test (TREAT) facility is an air cooled, graphite moderated thermal reactor located at Idaho National Laboratories (INL) that specialized in transient testing of nuclear fuels. Transient tests use high levels of neutron flux to expose experimental test fuels to extreme conditions. The intent is to observe how various types of nuclear fuels perform under severe conditions.

Transient tests at the TREAT facility rely on the fast neutrons born from fission events inside the experimental vehicle during testing. These fast neutrons are then collimated in the hodoscope system and detected behind the hodoscope using neutron detectors ("Hornyak buttons"). However, fast neutron can slow-down, or thermalize, in the material surrounding the fuel, such as water or reactor graphite. Since thermal neutrons move at speeds comparable to the thermal vibration motion of nuclei, it is possible that temperature changes in the experimental capsule affect the rate of detection of neutrons behind the detector.

As TREAT prepares to resume testing, notably to test novel, accident-tolerant nuclear fuels (ATF), systematic optimization and safety checks are being preformed and enhanced to ensure the optimal use of the facility. The response of materials during transient conditions may cause discrepancies in the experimental and simulated results if temperature effects be deemed important and yet unaccounted for in the modeling and simulation.

This work focuses on the construction of a model that accurately simulates the temperature effects on neutron flux observed at the front of the hodoscope. Geometric models of the reactor were constructed using Monte Carlo N-Particle (MCNP) code. Then, multiple programs were used to develop neutron cross-section value at various temperatures to most accurately characterize the neutronic behavior within the TREAT core. Finally, simulations provided insight to the effect of observed neutron flux in the performance monitoring instrumentation because of changes in experimental fuel temperature.

2. TREAT BACKGROUND AND THEORY

2.1 History of TREAT

From the initiation of operations in 1959, the TREAT facility at INL possessed the potential to serve as the foremost transient testing site in the world. From 1959 to 1994, thousands of tests were conducted to investigate fission heating of test fuel, non-destructive test data through fuel radiography, and test fuels under severe criticality conditions. During this timeframe, TREAT generated over 720 MWh of energy over 6604 reactor startups while irradiating over 2884 tests. However, experiments have not been conducted since 1994 [1]. A resurging interest in fuel-performance testing has ignited new interest in the facility. After 20 years of interruption, the Department of Energy (DOE) has scheduled a return to operable conditions and resumption of testing at TREAT by year 2018. This current work is carried out to support this larger goal.

2.2 Facility Overview of TREAT

TREAT was originally designed as a multi-faceted system to simulate accident conditions and measure the damage to fuel experiments. This air-cooled, graphite-moderated reactor uses a core configuration of HEU-graphite matrix fuel rods and control rods to shape energy pulses towards the center of the reactor, where the experimental fuel tests are placed. Figure 1 shows the three-dimensional rendering of the reactor, labeled with key components [3].

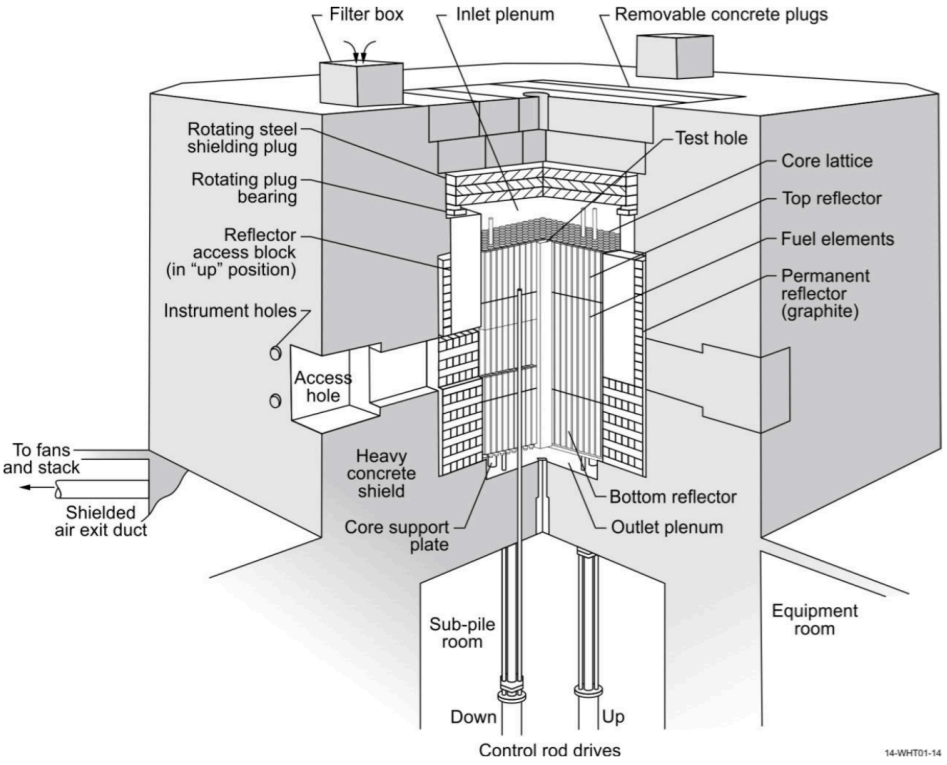

Figure 1. Three-dimensional rendering of TREAT showing the internal components of the system.

To produce a transient pulse, the reactor is initiated in a sub-critical state. By changing the height of the control rods within the reactor core, the reactor is gradually brought closer and closer to critical. Once the reactor system is primed, the transient rods are ejected, inserting a large amount of positive reactivity into the system. This produces more neutrons through fission that streams directly to the experimental test slot. The experimental fuel becomes super-critical instantaneously, allowing observable phenomena by the supporting instrumentation systems.

One of these systems is the hodoscope. This system monitors the deformation of experimental fuel as it melts by recording the time and spatial resolution fast neutrons emitted by the experimental fuel samples under transient conditions. To show the degree of fracture, fast-aperture cameras are position to gather images throughout the testing process. The cross-section planar view of TREAT is show in Figure 2. In Fig. 2, the hodoscope is placed in the cardinal-north oriented viewing slot. The other directionally oriented slots allow for the implementation both optical and gamma camera systems for the experimental testing procedures.

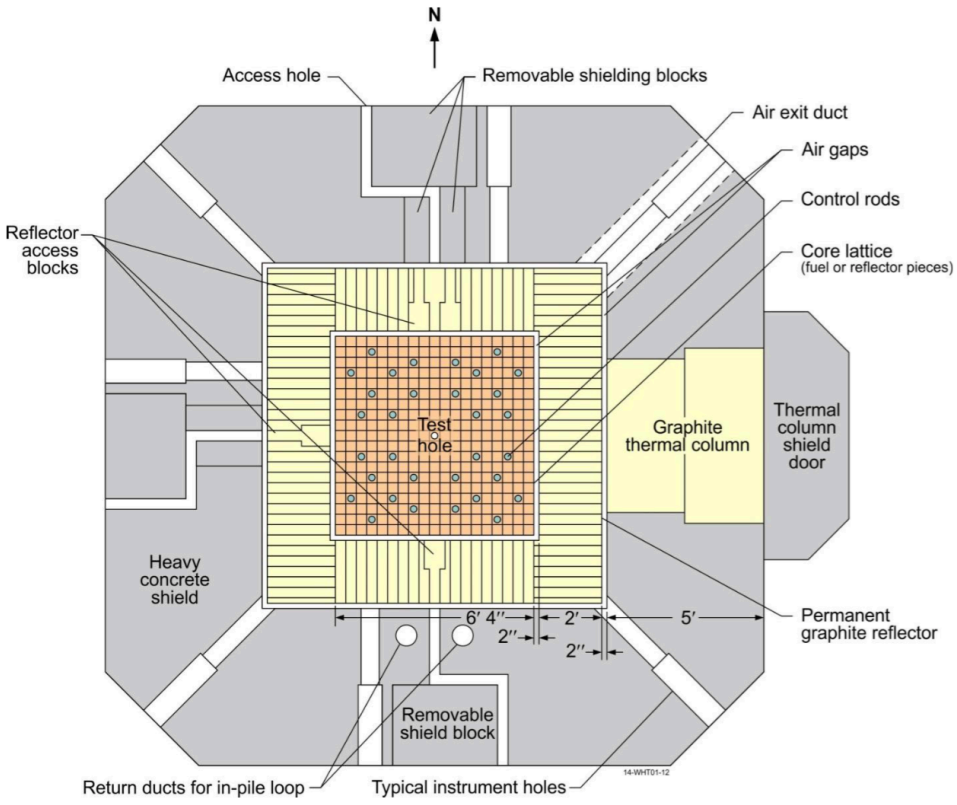

Figure 2. Planar cross-section of the TREAT core, graphite reflector, and biological shielding concrete.

TREAT is designed with passive safety features. The driving fuel in the core is comprised of a HEU-graphite matrix at a ratio of $1{:}1x10^4$. This causes the thermal range of the neutron of the overall cross section to shift drastically from in an increased neutron leakage, resulting in a large negative temperature feedback coefficient. The graphite also works to absorb most of the primary thermal spikes. For the delayed head from secondary fission, the air surrounding reactor core acts to remove the remaining heat from transient during experimentation.

2.3 Reactor Specifics

The TREAT core is a 19x19 slotted assembly matrix of 10.16 cm slotted lattices. The lattice container is a 193.04 cm by 193.03 cm matrix grid that stands 244.00 cm in height. An example core configuration is shown in Figure 3. The large unit in the center is the test vehicle. The assemblies extending up from the test vehicle are the half-slotted assemblies leading to the hodoscope. All of the assemblies with protruding wires are thermocouples [4].

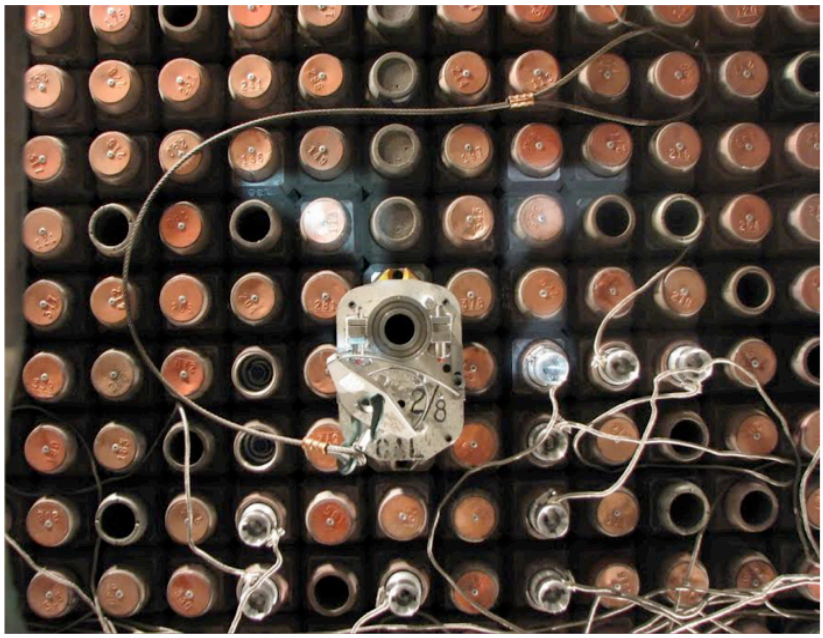

Figure 3. Photograph showing the TREAT core assembly.

A typical fuel rod assembly is shown in Figure 4. Most importantly, the fuel region shown is 122.24 cm in height and surrounded by graphite on the top and bottom. All the control rods have the same assembly as the fuel rod with a hole bored through the center to allow for insertion and withdrawal. The slotted assembly is missing the either fuel portion to allow neutrons to stream towards the north-viewing slot. For reference, all the engineering renderings from 1960 are given in inches [5].

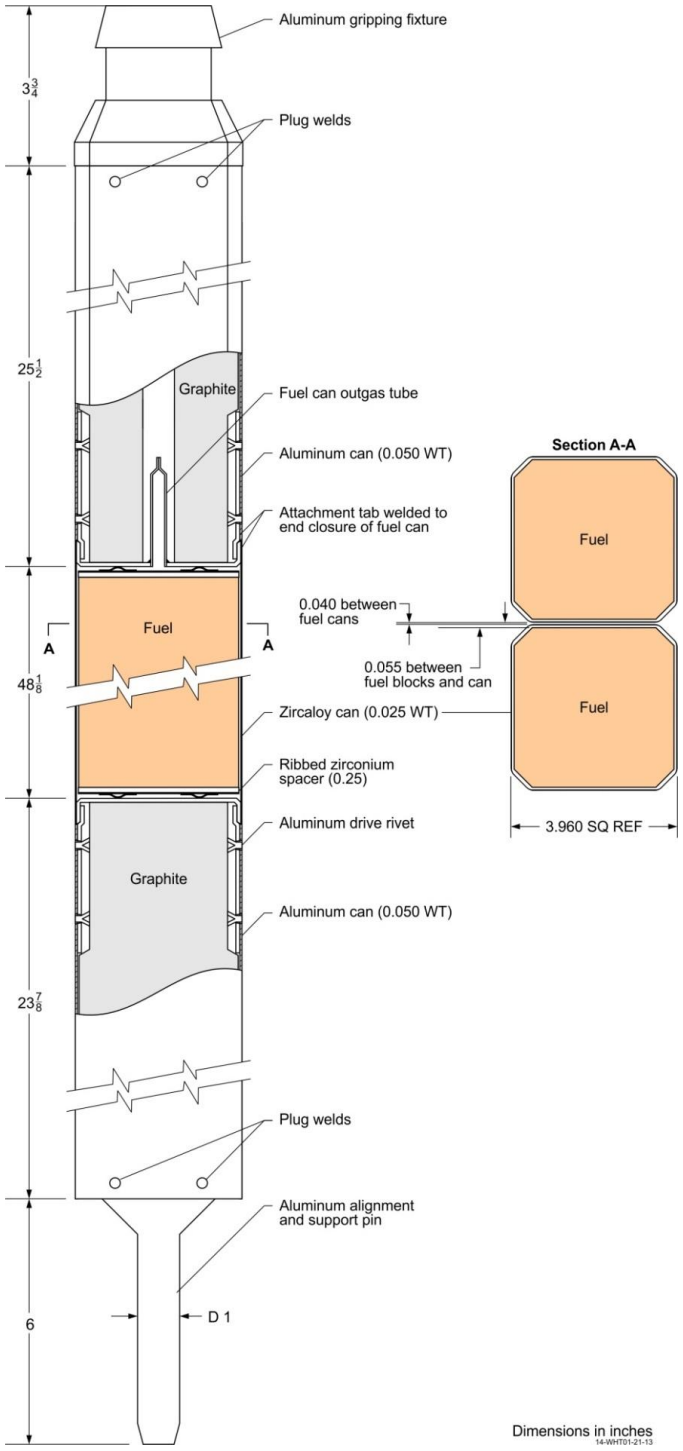

Figure 4. Standard fuel rod assembly inside the TREAT core. All dimensions are in inches.

The slotted assembly in the core leads to hodoscope slot, which is oriented cardinal north from the experimental test section. The TREAT reactor shielding, the transient gap between the reactor core, and the lead collimator are shown from the plan and elevation view in Figure 5 and Figure 6, respectively [6]. Additionally, to 0.635 cm aluminum-2 alloy (Al-2) plates are positioned immediately adjacent to the front collimator opening and the graphite reflector. They are depicted with the bold line on Fig. 6. For reference, the origin of these plots is located in the center of the experimental test slot in the center of the reactor core.

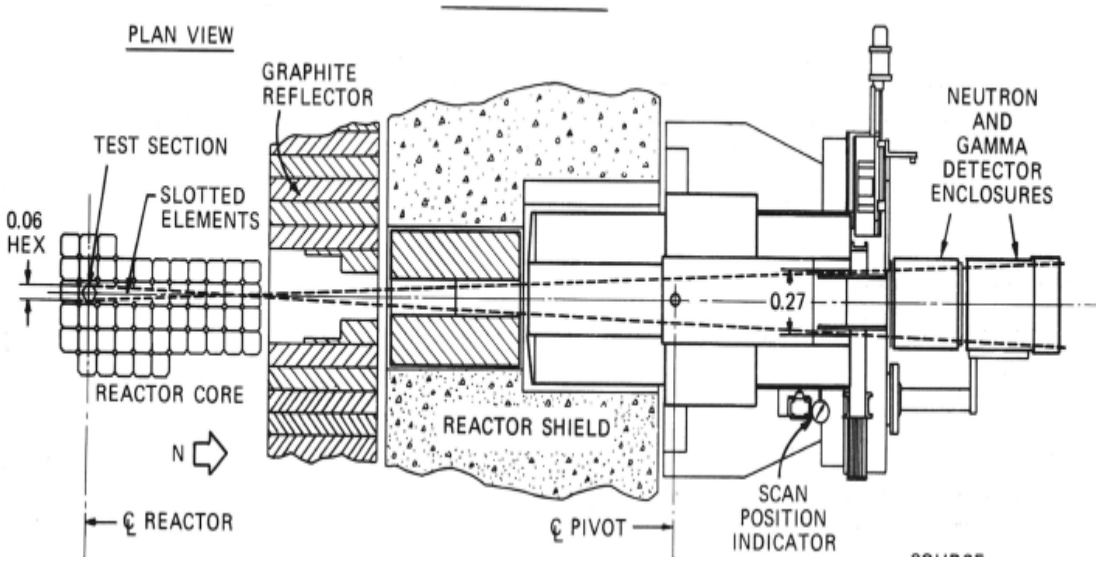

Figure 5. TREAT reactor shown from the plan view (X-Y Plane).

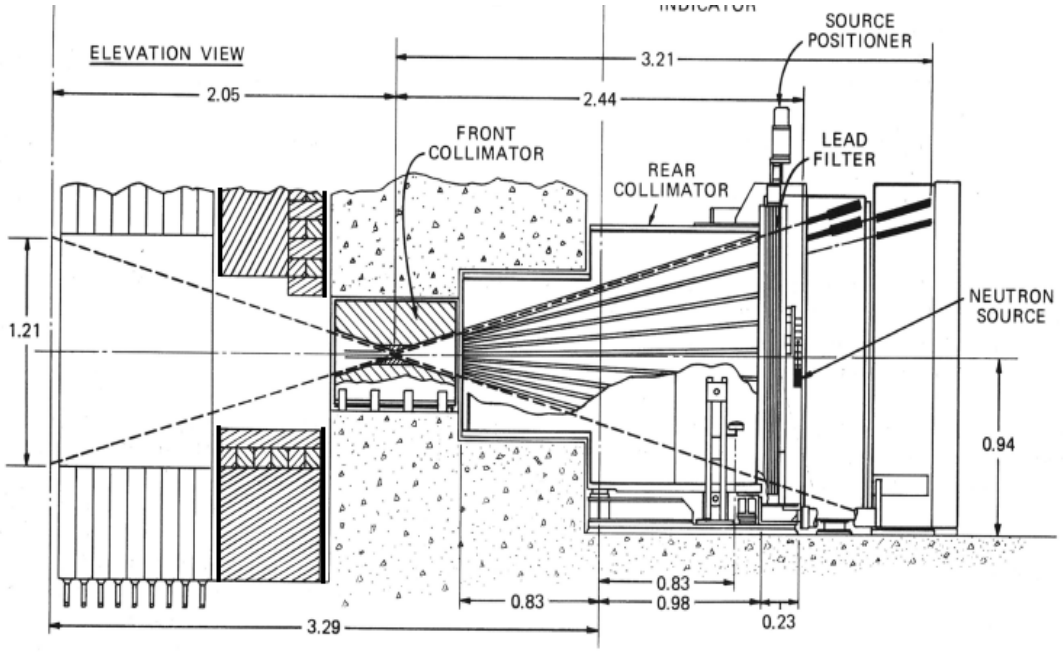

Figure 6. TREAT reactor shown from the elevation view (Y-Z Plane).

A summary of model dimensions is displayed in Table 1. These dimensions were obtained from parts lists and other engineering renderings of both TREAT and the hodoscope slot. In some instances, measurements were converted from U.S. customary to metric units. All elements are described in the Y-Axis, unless stated otherwise [6].

Table 1. TREAT reactor-hodoscope interface dimensions.

Interface Element	Length (cm)	Distance from Origin (cm)
Reactor Core	95.0	95.0
Air Gap	5.08	100.1
Al-2 Alloy Plate	0.64	100.7
Graphite Reflector/Transient Air Gap	60.9	161.0
Air Gap	5.08	166.1
Al-2 Alloy Plate	0.64	166.7
Front Collimator Interface to Focus	38.2	205.0
Reactor Height (Z-Axis)	244.0	-
Assembly Gap Height (Z-Axis)	244.0	-
Assembly Gap Width (X-Axis)	7.62	-

2.4 mSERTTA Test Apparatus

The Static Environment Rodlet Transient Test Apparatus (SERTTA) is a new vehicle for test samples was designed with the re-initiation of TREAT. The device includes multiple capsule-type irradiation containers with a static water coolant. It is designed with the intent of containing multiple types of accident tolerant fuels currently scheduled for when TREAT resumes operations; however, it is easily adaptable for other fuel types [7].

The mSERTTA vehicle consists of four individual and separate containers assembled vertically. Each individual apparatus is contained within a 10.13 cm by 20.29 cm by 34.94 cm unit and able to accommodate test fuels up to 12 cm in length [8]. With the goal of pushing the irradiating the fuels to failure under extreme conditions, primary containment instrumentation includes a crucible for heat resistance, a small bowl to catch any melted fuels, and expansion tank for any fission gases produced during testing. A 47.63 cm tall graphite block underneath the four SERTTA units acts a neutron, and a

15.24 cm lead brick acts as a gamma shield on top of the four SERTTA units. All four apparatuses are then set into the secondary containment. This 244 cm tall sheet metal test vehicle easily be inserted into its appropriate slot at the center of the TREAT core. A computer rendering of mSERTTA is shown in Figure 7. Moving left to right, the images show each subsequent layer with key design features.

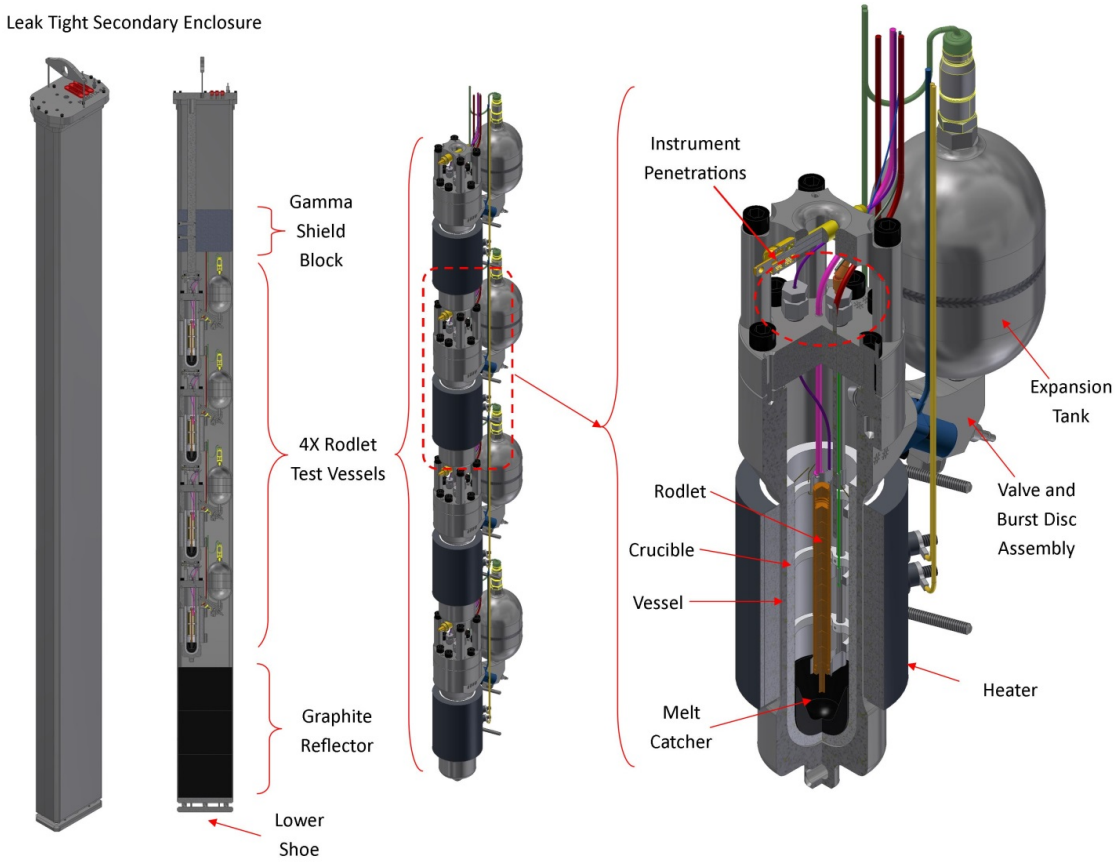

Figure 7. mSERTTA experimental test vehicle.

3. OVERVIEW OF THERMAL NEUTRONS AND DOPPLER BROADENING

There are three broad regions neutrons based on the energy of the neutron: thermal, epithermal, and fast. Generally, the boundaries between thermal-epithermal neutrons and epithermal-fast neutrons lie at about $1x10^{-6}$ MeV and $1x10^{-1}$ MeV, respectively. Neutrons are more commonly born as fast neutrons through fission; however, as they interact, they scatter and slow to epithermal and thermal energies.

In reference to TREAT, all of the experiments are conducted under transient conditions. These neutrons flood the experiment with fast neutrons that stream towards the fuel motion modeling instrumentation. While the hodoscope only detects fast neutrons, temperature changes in the experimental fuels may affect the neutron flux spectra observed by the hodoscope. This work aims to describe and model these effects under transient conditions in TREAT.

3.1 Thermal Neutron Theory

At room temperature, thermal neutrons are moving at speeds comparable to the speed of the thermal motion of the ambient atoms with an average kinetic energy of only about 0.025 eV. In the overall spectrum of neutron energies, the energy distribution of thermal neutrons is approximated by a Maxwellian energy distribution. When thermal neutrons absorb or leak, the pure Maxwellian shifts and deforms as a function of neutron energy, as shown in Equation 1, where N_0 is the initial number of neutrons, E is the energy of the neutron, T is the ambient temperature, and k Boltzmann's constant.

Equation 1 can be used to characterize the average velocity of 2200 m/s and energy of 0.0253 eV for a general ambient temperature of 293 K [9].

$$N(E) = \frac{2\pi N_0}{(\pi kT)^{3/2}} \sqrt{E} e^{-\frac{E}{kT}} \quad (1)$$

3.2 Doppler Broadening Physics

Understanding the effects of Doppler broadening of cross sections is crucial in understanding the physics and operations of nuclear reactors. The relative motion between incident neutrons and target nuclei can cause changes in the resonance cross sections that have a significant effects on the neutronic behavior observed by the fuel-motion monitoring system. Using codes such as *MCNP* to investigate and quantify this phenomenon within the experimental test tray can provide insight for future operations while minimizing computational power and time associated with more traditional methods of cross-section generation.

As a neutron moves through a material, the relative center-of-mass energies between the incident neutron and the target nucleus causes effects on the incident neutron's capture probability. When the energy level of the resultant compound nucleus nears the capacity relative energy is combined with the neutron binding energy, the probability of capture spikes in a phenomenon known as neutron resonance absorption. This phenomenon is integral in explaining several forms of negative feedback within nuclear reactor systems modeled by this work [10].

The most effective means of demonstrating this phenomenon begins with the concept of resonance integrals. Resonance integrals allow the complex resonance structure of various isotopes to be broken down and simplified by calculating the individual effects contributed by each resonance. Through the superposition of the Breit-Wigner resonances using known parameters, known energy and temperature dependencies of each resonance can be combine to allowing the total resonance cross sections to dramatically simplified for energies between 1 eV and 100 keV [11].

The Breit-Wigner single-level resonance formula shows the neutron capture cross section averaged over the motion of the nucleus, demonstrated in Equation 2, where E is the neutron energy, T is the Maxwellian temperature, σ_γ is the neutron capture cross section, σ_0 is the maximum value of the total cross section, E_0 is the energy at which the resonance occurs, E_c is the relative energy between the nucleus and the neutron, Γ_γ is the radiative capture partial width, Γ is the resonance width, and ψ is the integral over the relative motion of the neutron and nucleus.

$$\sigma_\gamma(E,T) = \sigma_0 \frac{\Gamma_\gamma}{\Gamma} \left(\frac{E_0}{E_c}\right)^{1/2} \psi(\xi,\chi) \tag{2}$$

However, as a neutron moves through a material, its velocity relative to the target nucleus can change because of the relative thermal motion of the target nucleus. For Doppler broadening effect, a specific cross section must be used to accurately characterize the effect, shown in Equation 3, where σ_{eff} is the effective neutron cross-section, v is the incident neutron velocity, V is the target nucleus velocity, and P is the Maxwell-Boltzmann distribution [12].

$$\sigma_{eff}(v) = \int \frac{\left|\vec{v} - \vec{V}\right|}{v} \sigma\left(\left|\vec{v} - \vec{V}\right|\right) P\left(\vec{V}\right) d\vec{V} \tag{3}$$

As noted previously, a Maxwell-Boltzmann characterizes the velocity distribution for a target material, shown in Equation 4, where *v* is the velocity of the neutron.

$$P\left(\vec{V}\right) = (\alpha)^{\frac{3}{2}} e^{-(\frac{M}{2kT})V^2} \tag{4}$$

The coefficient α is the Maxwell-Boltzmann functional relationship, as shown in Equation 5, where *M* is the particle mass, *k* is the Boltzmann's constant, *T* is the thermal temperature of the material.

$$\alpha(T) = \frac{M}{2\pi kT} \tag{5}$$

As a result of the thermal motion of the nuclei, the incident neutron appears to have a continuous energy distribution relative to the target nucleus. The broadening of the cross-section distribution to nuclei at rest dictates neutron resonance integral of interaction compared. While the shape of the resonance integral changes with Doppler broadening, the total area remains constant. As resonances overlap during Doppler broadening, relative changes in resonance escape probability or thermal utilization can cause the system to experience either positive or negative feedback. All these changes can affect the observed changes in the experiments because *kT* aspect of Eq. 4 represents

energy on the scale of 0.2 eV, demonstrating that this will only have significant effects on neutrons in the thermal energy range. The temperature effects on thermal neutrons can lead to secondary fissions in the experimental test tray and must be captured by the fuel-motion monitoring system within TREAT.

4. NEUTRONIC MODELING WITH MCNP

MCNP is a general-purpose particle transport code used in nuclear modeling and design to solve the neutron transport equation. The program allows the user to construct geometric-shell models and fill them with specified materials. A set of physics packages allows the user to simulate various particle interactions within the constructed model. As the simulation progresses, the code tracks the history of interactions of the particle along the resultant particle's energy, direction, and position. Once the initial particle is absorbed into the medium of the model, the code records the entire particle history and initiates a new incident particle. This process repeats in a number of user-specified times to generate statistics and distributions useful to understanding the physics of the modeled system.

This versatile and simple tool was invaluable in simulating the response to temperature changes in the experimental test slot. Every model was constructed using MCNP; every simulation relied on the code packages to accurately describe the physics expected in the reactor. However, the results and models produced from the code are only acceptable within the accuracy of the various aspects of the program itself. This section will describe the stochastic nature of the program itself, as well as the comparative benefits of the files used to describe incident particle interactions within individual simulations.

4.1 Stochastic Error

MCNP uses a numerical technique centered upon the Monte Carlo method. This method produces a modeled solution of physical interactions based on multiple simulations of the model physics. Stochastic modeling relies on the random sampling of probability distributions. This provides the user with meaningful statistics to determine the precision of the simulation. For each tally, ten statistical checks are provided to ensure the overall precision of the simulation [13].

4.1.1 Ten Statistical Checks

MCNP provides ten statistical checks to the user for each model run that demonstrate components of the mathematical precision of the simulation from the point of view of statistic convergence. If any of the ten tests fails for a given simulation, the code prints a section to the output file that contains a plot of the probability distribution function for the given test, indicating the relative importance of the failed test.

The check tests are not absolute, and they require the judgment of the user. Some models may not be concerned with all of the ten tests due to the relative complexity of the model; however, they are have value in determining the overall merit of a specific model for a given exercise. The ten statistical checks are summarized below.

1. Tally Mean, $\bar{x}$: the mean must exhibit only random flux fluctuations as the number of particles increases.

2. Relative Error, *R*: the relative error must be less than 0.1 for area or volume detector tallies and less than 0.05 for point and ring detector tallies.
3. Relative Error, *R*: the relative error must decrease monotonically with the number of particles for the last half of the particle histories in a simulation.
4. Relative Error, *R*: the relative error must decrease proportionally with the square root of the number of particles for the last half of the particle histories in a simulation.
5. Variance of the Variance, *VOV*: the magnitude of the variance of the variance must be less than 0.1 for all types of tallies.
6. Variance of Variance, *VOV*: the variance of the variance must decrease monotonically for the last half of the particle histories in a simulation.
7. Variance of Variance, *VOV*: the variance of the variance must decrease proportionally with the number of particles for the last half of the particle histories in a simulation.
8. Figure of Merit, *FOM*: the figure of merit must remain statistically constant for the last half of the particle histories in a simulation.
9. Figure of Merit, *FOM*: the figure of merit must not exhibit any up or down monotonic trends in the last half of the particle histories in a simulation.
10. Tally Probability Distribution Function, *f(x)*: the slope from the 201 largest scoring events must be larger than three.

4.1.2 Tally Mean

The mean is just an average of the tally, signified by $\bar{x}$. All of the other statistical tests are based off this value. Because of the random seed number, each particle history should have some variance about the statistical mean. As more and more particles histories are added to the simulation tally, the distribution of the particle histories should for a standard Gaussian distribution. If it does not, the first of the ten statistical checks within *MCNP* is not valid, and the model precision is almost always very low.

4.1.3 Relative Error

The relative error, *R*, is the estimated uncertainty of the tally mean determined by the ratio of the standard deviation of the tally mean to the mean. Its value is determined by two separate quantities. For most of the simulations preformed in the evaluation of the TREAT model, an *R* value less than 0.1 is considered reliable for a given simulation [14]. Equation 6 shows the calculation of relative error as described within the statistical check tests.

$$R = \frac{\sigma_{\bar{x}}}{\bar{x}} \tag{6}$$

The scoring efficiency, *q*, is the fraction of particle histories for a given simulation that produce a value other than zero. If every particle is tallied in a given history, then *q* is perfect and represented by *q=1*; however, if the variance produced by the model is high, *q* will approach zero. Variance reduction techniques in models aim to maximize the value of *q* for the model as a whole.

In addition, MCNP divides R into two components. The first, R_{eff}, quantifies the distribution spread of R caused by q; the second, R_{int}, inherent randomness provided by the simulation based on the scoring efficiency [14]. The relationship between these two values is shown in Equation 7.

$$R^2 = R_{eff}^2 + R_{int}^2 \tag{7}$$

4.1.4 Figure of Merit

The figure of merit, *FOM*, is relates R to the simulation run time, τ, which varies machine to machine. For a single simulation, the *FOM* should remain relatively constant as the simulation reaches statistical convergence. In reference to variance techniques, a higher *FOM* is preferred. The relationship for *FOM* is shown in Equation 8.

$$FOM = \frac{1}{R^2 \tau} \tag{8}$$

4.1.5 Variance of the Variance

The variance of the variance, *VOV*, is the estimated relative variance of R as a function of the variance of R. The relationship is defined in Equation 9.

$$VOV = \frac{S^2(S_{\bar{x}}^2)}{S_{\bar{x}}^2} = \frac{\sum_{i=1}^{N}(x_i - \bar{x})^4}{\left[\sum_{i=1}^{N}(x_i - \bar{x})^2\right]^2} - \frac{1}{N} \tag{9}$$

VOV is more sensitive to large fluctuations than R because it of its relationship with the probability distribution function. The statistical test for *VOV* examine its behavior proportional to number of particles run in a given simulation. For every case,

the *VOV* should be less than 0.1.

4.1.6 Probability Distribution Function for the Tally

MCNP prints a probability distribution function to show the confidence intervals for a given tally. This shows the statistical trends sampled throughout all particle histories for a given simulation. The printed function shows the relationship between the tally's mean and *R* as it relates to the *FOM*. Doing this allows the user to decide whether or not the tally lies within meaningful confidence intervals.

As a statistical check, the largest tallies are scored to calculate the slope of the function's tail. For the tally to pass the check, the slope must be greater than or equal to three when fitted to a general Pareto function. Equation 10 and Equation 11 shows the relationship between the general Pareto function as a function of tally and the calculation of the statistical check, respectively. Slope values range between zero and ten.

$$f_P(x) = \frac{1}{a(1 + \frac{kx}{a})^{1 + (\frac{1}{k})}} \tag{10}$$

$$m(f_P) = 1 + \frac{1}{k} \tag{11}$$

4.2 Tally Mathematics

4.2.1 Surface Tallies (f2)

The *f2* tally measures the neutrons crossing over an averaged surface, A, with an angular distribution, θ. For a specific energy distribution, E, the sum of the contributions to the neuron behavior crossing a surface is show for the particle flux as a function of position. This relationship is shown in Equation 12, where r is a position of the tallied neutron, E is the energy of the tallied neutron, and Ω is the angle of the tallied neutron.

$$f_2\ tally = \frac{1}{A}\int_A dA \int_E dE \int_{4\pi} d\Omega\ \Phi(r, E, \Omega) \tag{12}$$

For man simple surfaces, MCNP calculates the area. For a given energy bins, the flux, shown as ϕ as a function of position, is calculated using Equation 13. These tallies will be output into a table within the MCNP output file with a relative error for each specified energy bin of group g.

$$\phi(E_{g+\frac{1}{2}}, r) = \frac{f_2\ tally}{\Delta E_{g+\frac{1}{2}}} \tag{13}$$

Then, to represent the flux as a function of lethargy, shown as u, the energy dependent flux was multiplied by the average energy of the bin to generate the lethargy dependent flux, as reflected in Equation 14.

$$\phi\left(u_{g+\frac{1}{2}}, r\right) = E_{g,avg}\phi(E_{g+\frac{1}{2}}) \tag{14}$$

4.2.2 Volume Tallies (f4)

For the *f4* tally, the MCNP tracks neutron path length as a function of radius for a given cell volume, *V*. The maximum path length is a function of the geometric dimensions. Equation 15 shows this relationship.

$$f_4\ tally = \frac{1}{V}\int_A dV \int_E dE \int_{4\pi} d\Omega\ \Phi(r, E, \Omega) \tag{15}$$

For the MCNP output, a similar method to the *f2* tallies was used to manipulate the data into energy dependent flux spectra. This relationship is shown in Equation 16.

$$\phi(E_{g+\frac{1}{2}}, r) = \frac{f_4 tally}{\Delta E_{g+\frac{1}{2}}} \tag{16}$$

4.2.3 Mesh Tallies (f-mesh)

For more complicated geometries, a mesh tally (*fmesh*) can be set to cover all surfaces within a given set of Cartesian boundaries. Mesh tallies are *f4* tally grids superimposed over a specified geometry. Unlike more traditional tallies in MCNP, the tally output is written to a separate file. This superposition allows for a spatially customizable tally superimposed onto complex geometries.

The user must specify the Cartesian bounds of the *fmesh* tally, as well as the number of intervals for the superimposed grid in for each Cartesian axis. These tallies are spatially dependent, as opposed to traditional tallies that are energy dependent. However, for a specific *fmesh* tally, several energy tally bins can be declared. This

allows for an easy comparison of the spatial flux profile compared at various energy intervals to show the energy dependent particle flux within a given spatial distribution.

4.3 Source Definitions and Biasing

MCNP allows users to specify the characteristics of the source for simulations. This includes things like the geometry of a source, ranging from a point source to a volumetric source. The initial energy of source particles can be described as monoenergetic or as characteristic distributions, such as the Watt fission spectrum. The user can specify the direction of source particles, as well as their angular distribution.

Several different source definitions were used in the simulation of models constructed in the course of this research. Each new model will describe the source used in a specific simulation in terms of geometry (point or volumetric), energy distribution, and directional bias with angular distribution. Along with temperature, these become the characteristic details from simulation to simulation.

5. TEMPERATURE-DEPENDENT CROSS SECTIONS

MCNP relies on specific cross-sections files to most accurately describe the physical interactions occurring in models. These cross-sections provide the probabilistic distributions of the neutron interaction with a target material in a given incident energy. The files are generated through three main pathways: ACE files included in the MCNP package; ACE file generation using NJOY modules; and, new physics sub-modules for On-the-Fly manipulation of stock ACE files.

The two-non included cross-section file generation methods were explored for the simulation of the experimental test vehicle to ensure the accuracy of the constructed models in the thermal energy range. The merits of each are described, as well as a simulated comparison using a simple pressurized water reactor (PWR) fuel rodlet.

5.1 NJOY Cross-Section Files

The nuclear data processing system, NJOY, is a code system designed to produces point-wise and multi-group nuclear cross section in the U.S. Evaluated Nuclear Data Files (ENDF) format. NJOY utilizes a set of modules to modify and produce neutron cross-section files. Each module, acting as its own computer program, is designed for a unique processing task, and they are linked together through input and output files called “tapes” using the NJOY code [15].

NJOY is usually initiated by generation a “point-ENDF” file that is used to produce a common energy grid for all the pertinent transformations by the individual modules. Produced using the RECONR module, the generated PENDF file can be designated with specific tolerances for the linear interpolation conducted by individual NJOY modules. Other modules then subsequently add or manipulate that PENDF file at the specification of the user. After all desired manipulations have been preformed on the PENDF file, the PENDF file is prepared for MCNP use in “A Compact ENDF” (ACE) format using the ACER module [16].

Within the scope of TREAT cross-section files, several modules were used to generation of cross-sectional files needed to model the mSERTTA experiment. Working as linked programs through the NJOY framework, these modules reconstruct resolved and unresolved, point-wise cross section resonance structures for specified material isotopes, treats the cross sections for Doppler broadening effects within the thermal energy range, and outputs the cross section files in ACE format for continuous energy MCNP codes. The theory and implementation of each module is described in following sections.

For this simulation, several modules were used to generate specific ACE files. The RECONR module reconstruct resonance cross sections using user specified reconstruction parameters from ENDF nonlinear interpolation schemes. The cross section is generated in a pointwise manner using different methods in different regions of incident neutron energies. RECONR uses linear-linear interpolation for all cross sections with respect to energy to allow for easy plotting and manipulation by other

modules. Because this format allow for the easy retrieval by the continuous-energy MCNP codes, all individual interaction cross sections are placed on the same unionized grid and summed to generate the total cross sections. This module must be initiated in any NJOY calculation.

Integral to the thermal treatment of the mSERTTA experiment, the BROADR module allows for Doppler-broadened cross sections in the PENDF format provided from either RECONR or a previous BROADR execution. This code uses the kernel broadening method to integrate the cross section over the relative velocity between the incident neutron and the target nucleus [16].

The effective cross section is derived similarly to the Doppler-broadened cross section, a piecewise linear function of energy to the accuracy defined by the user. Making use of reduction variables and a Taylor expansion, a polynomial recursion relation can directly generate the terms of the effective cross section to a desired number of significant figures. This recursive function will allow the module to keep accuracy to temperatures equivalent to 100 keV, as related by the Boltzmann's constant [16].

The THERMR module acts as a compliment to the BROADR module and generates pointwise neutron cross sections in the thermal energy range to provide interactions for both coherent and incoherent scattering. Monte Carlo modeling for neutrons in the thermal range are heavily dependent on the inelastic scattering interactions with free or bound atoms, typically referred to as the $S(\alpha, \beta)$ scattering functions [16].

The PURR module then produces probability tables to treat unresolved-resonance self-shielding interactions within MCNP, specifically for the radiative capture, fission, and total cross sections. ENDF files provide the mean values for the resonance spacing along with other statistical probability distributions for specific isotopic resonances. The PURR module uses these values to define a plausible set of cross sections correlated to the union grid from the RECONR module through the "narrow-resonance assumption". Because the energy loss from scattering is assumed large with respect the width, a random sample within the peak can reduce the truncation errors associated with the unresolved region. PURR can accumulate cross sections for one possible set of all cross sections for a defined, unresolved resonance, giving the module the ability to handle the temperature correlations within MCNP. As a particle goes through a system with various "tmp" declarations, the code will periodically check the total cross section and readjust for the next collisional interaction [16].

When all the modules have modified the ENDF file, the ACE module prepares libraries in the ACE format for the Los Alamos continuous-energy Monte Carlo code, MCNP. It output the cross section files in a format identical to the MCNP stock files, and it also outputs a file that can be incorporated into the working cross-sectional directory file, or "xsdir" file, that dictates the files selected during simulation runs.

5.2 On-the-Fly Cross-Section File Manipulation

The traditional ways of modeling thermal broadening effects on absorption cross sections involved generating broadened cross section using more traditional NJOY file

library generation however, these files can be large and require immense working memory and computational time. Beginning with a MCNP5 beta, an OTFDB physics card allowed for quick development of material cross sections at specific temperatures with functional expansions that represent the detailed energy and temperature dependence of the cross sections. This provides the capability to analyze coupled neutronic and thermal calculations without the need to generate cross-section libraries at all temperatures that are anticipated during the simulation [17].

To use this feature, a secondary utility code included with MCNP software must be executed for each isotope that will be treated with the OTFDB physics card. The code generates a secondary file including the unionized temperature and energy grids that must be included in the cross-section directory. Within the MCNP code, temperature declaration can occurs as the pairing of two steps. Because the cross-section files are temperature dependent, the appropriate ACE cross-section file must be declared in the material composition cards. Then, for the specific cells that are wished to treat with OTFBD, the temperature, signified with "tmp", must be declared in units of MeV. The OTFDB code reads this input and uses the unionized grid to interpolate the correct cross-section value for a given interaction.

As developed, the OTF Doppler processing within MCNP uses the thermal dependence of a particular cross-section as a functional expansion in temperature for each cross section type subject to Doppler effects [18]. The method uses unified temperature and energy grids to broaden the cross-sections of any specified nuclide within the model. The temperature grid is comprised of five temperatures in equal

intervals between the minimum and maximum for respective grids. This expansion fitting is shown in Equation 17, where σ_γ is the Doppler broadened cross section, $a_{g,i}$, $b_{g,i}$, and c_g are expansion coefficients, N is the expansion bound, and T is the examined temperature.

$$\sigma_\gamma(T, E_g) \cong \sum_{i=1}^{N} \frac{a_{g,i}}{T^{\frac{i}{2}}} + \sum_{i=1}^{N} b_{g,i} T^{\frac{i}{2}} + c_g \tag{17}$$

This method simplifies the steps needed to examine Doppler broadening effects on the vehicle test slot within TREAT over the operational temperature range. Since TREAT is air-cooled at room temperature, the lower limit of temperature range is set at 293 K. For the testable limits of the temperature grid, the safety and accident limit of TREAT at 873 K and 1093 K, respectively, must be included within the upper bounds of the set temperature grid [19].

5.3 Manipulating Temperature for Cross Sections within MCNP

MCNP allows users three ways to change the temperature of specific aspects of a given model. This occurs in a two-step process using either the NJOY cross-section generation method or the OTFDB utility within MCNP. Regardless of the chosen pathway, the user must preform some modifications to the underlying files used by MCNP code.

All cross-section files have a specified temperature in eV, differentiated by the ACE file designator suffix (ex: [ZAID].80c, where “80c” is the file designator suffix) within the material card definition. More common materials also include specific cross-

sections for thermal neutron scattering, called the $S(\alpha,\beta)$ data sets. These files correspond to the line within the cross-section directory (xsdir), that direct the MCNP code to the exact file within the working pathway of the machine. Declaring different cross-section designator suffixes for both the ACE and $S(\alpha,\beta)$ files can change the baseline temperature for a given cross-section in a single simulation.

For NJOY cross-section generation, additional ACE files with specific file subscripts must be added to the specified working pathway within MCNP, and the ACE file tape must be added to the xsdir file. To include these cross-section files in the MCNP model, the specified ACE file designator suffix must be used for the appropriate isotope within a material card. Then, if the user wants to modify the temperature of a cell that includes this material, a specific "tmp" must be specified on the specific cell card in eV. However, this only treats the free-gas temperature of the cross-section files.

Using the OTFDB feature, the On-the-Fly utility allows for an OTFDB cross-section file to be generated. This file takes five ACE files at different temperatures and develops the energy and temperature grid around these files. It outputs a specific file that must be in the same directory. This allows the user to declare the specific cross-section files that will be treated with the OTFDB feature. Then, to modify the temperature of the cross-section file using OTFDB, the user can change the temperature using the same "tmp" declaration on the specified cell cards. This gives the temperature that OTFDB uses to interpolate the cross-section values within the generated temperature grid for all interaction mechanics at the specified temperature designated.

5.4 Comparison Using a UOx Pin

Initial trials for the temperature dependence were tested on a single fuel pin, modeled with the fuel compositions within the mSERTTA experiment. The exercise aimed to demonstrate the effectiveness of OTF Doppler broadening within the uranium isotopics in the fuel sample, compared to NJOY and default MCNP cross-section libraries. The model is constructed as a simple PWR fuel pin using MCNP, provided by Dr. Jean Ragusa. The pin is a zirconium clad, 3% enriched uranium oxide (UOx) fuel moderated by borated water. An example of this pin is shown in Figure 8.

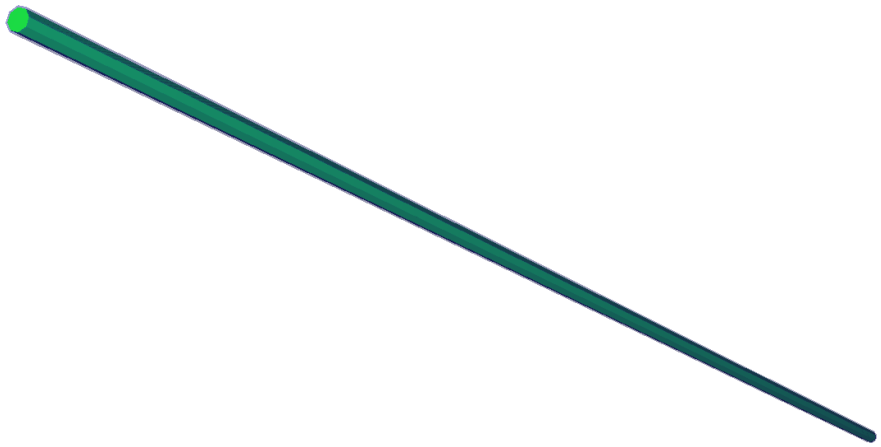

Figure 8. PWR fuel pin used to investigate OTFDB and NJOY utility.

This pin provides a simple way to examine the Doppler effects by altering the temperature of the cross-section files for uranium isotopics. Using this model allows for a quick comparison of neutronic behavior of the OTFDB physics cards prior to their application in the mSERTTA test vehicle. By using the cross-section libraries provided

within ENDF/B-VII.1 and generated using NJOY, a quick comparator can show the accuracy of the OTFDB as a means of demonstrating the thermal effects attributed to Doppler broadening.

While OTF methods can save computational time with equally accurate results, its implementation is not widely tested. The OTF executable code is initiated over a range of temperatures. It must only be run once for each material in the UOx fuel pin. The time for each code ranges, but the longest was around 45 minutes of computational time. Once the material OTF file is generated, only modification of corresponding of the TMP and OTFDB cards within MCNP is required.

Comparatively, NJOY methods were generated at each temperature for each of the three materials in the UOx fuel pin: uranium-235, uranium-238, and elemental oxygen. Each of these code executions takes around 5 minutes of computational time. Other measures must then transpire to place the newly generated cross-sectional files into the directories utilized by MCNP simulations. For each material, the NJOY module would take upwards of 15 to 20 minutes per isotope. While the computational time was comparable for a simple UOx fuel pin, a more complicated system would present accuracy versus time decision between using NJOY and OTFDB.

This is critical for efforts moving forward. The OTF method is crucial to develop a power-fitting factor for the TREAT. As an air-cooled reactor, TREAT has safety and accident temperatures of 973 K and 1093 K, respectively. These exercises were able to minimize error with the OTF method well below the stochastic uncertainty, where the k_{eff} derived in this range can be expected to be within +250 pcm to +50 pcm of NJOY

with a 95% confidence. The comparison of NJOY to OTFDB for each temperature between these limits is shown in Figure 9.

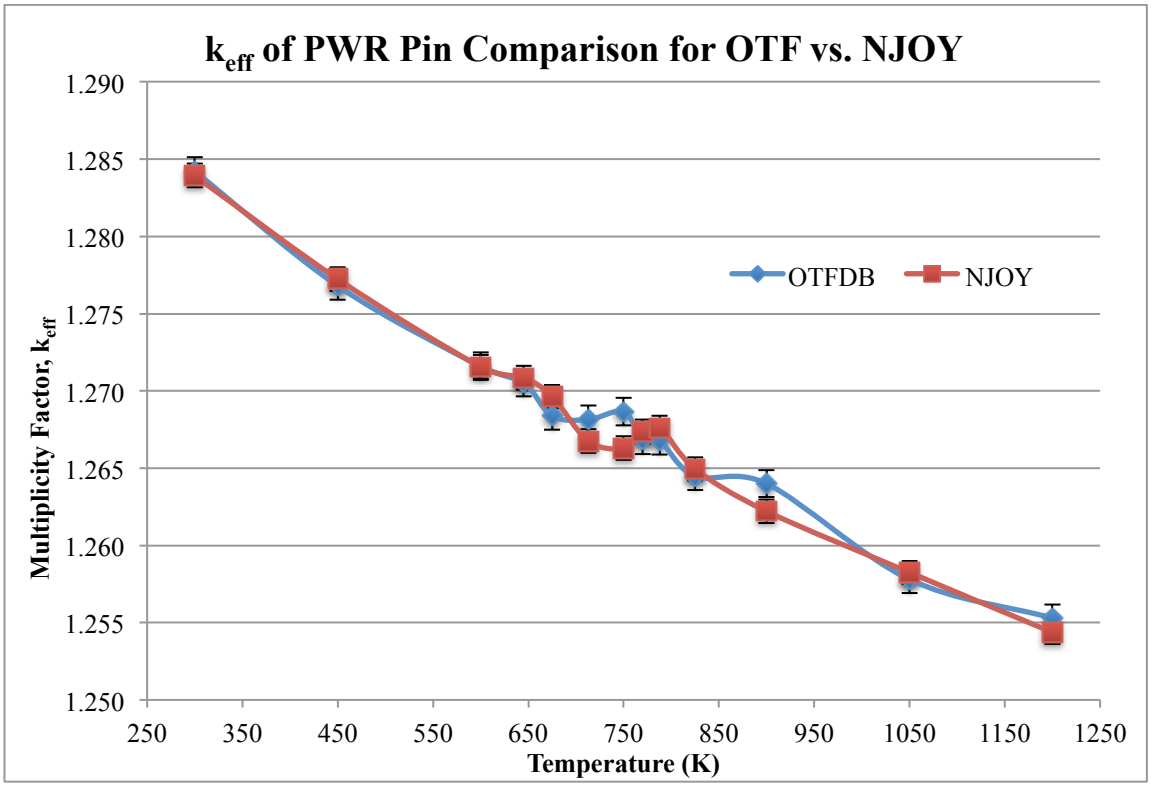

Figure 9. Changes in k_{eff} plotted as a function of temperature using the OTF temperature gridding within MCNP.

A great benefit of the OTFDB functionality is the flexibility for the temperature range. Also, generating NJOY cross sections for each temperature can prove tedious and time consuming when many temperature cross sections are needed for simulations. However, the single execution of the OTFDB file generation of temperature and energy grids allows which takes about seven computational minutes.

Table 2 through Table 5 show the comparison of models using OTF generated cross-section files with NJOY and ACE cross-section files for the specified temperatures. The propagated total error is also shown for a comparative benchmark.

Table 2. Comparison of k_{eff} for UOX Pin at 300 K using NJOY and OTF methods.

	300 K			
	k_{eff}	Error	Difference from NJOY	Total Error
OTF	1.28424	0.00059	---	---
NJOY	1.28394	0.00058	0.0003	0.000827345

Table 3. Comparison of k_{eff} from generated ACE file for UOX Pin at 600 K using NJOY and OTF methods.

	600 K				
	k_{eff}	Error	Difference from NJOY	Difference from ACE	Total Error
OTF	1.27159	0.00060	0.00003	0.00052	---
NJOY	1.27156	0.00061	---	0.00049	0.00086
ACE	1.27107	0.00060	0.00049	---	0.00085

Table 4. Comparison of k_{eff} from generated ACE file for UOX Pin at 900 K using NJOY and OTF methods.

	900 K				
	k_{eff}	Error	Difference from NJOY	Difference from ACE	Total Error
OTF	1.26400	0.00059	0.00179	0.00201	---
NJOY	1.26221	0.00057	---	0.00022	0.00082
ACE	1.26199	0.00059	0.00022	---	0.00083

Table 5. Comparison of k_{eff} from generated ACE file for UOX Pin at 1200 K using NJOY and OTF methods.

	1200 K				
	k_{eff}	Error	Difference from NJOY	Difference from ACE	Total Error
OTF	1.25530	0.00057	0.00093	0.00118	---
NJOY	1.25437	0.00058	---	0.00025	0.00081
ACE	1.25412	0.00061	0.00025	---	0.00083

For these simulations, only models at temperatures of 300 K and 600 K were accurate within the stochastic uncertainty. Simulations at 900 K were the least accurate with a difference of 1.8 pcm.

6. MODEL DEVELOPMENT AND METHODOLOGY

The Full-Core TREAT model was constructed in stages by multiple people and integrated into a single model during the summer of 2016 at the INL. For the purpose of this report, the three components shall be described as the following:

- Core Model (C. Hill and J. Bess),
- Transient-Gap Model (L. Scott), and
- Hodoscope Model (C. Townsend).

A 3D rendering of these models are shown in Figure 10, along with the boundaries of each respective model. The three colored boxes show the portions of TREAT included in each of the models [3].

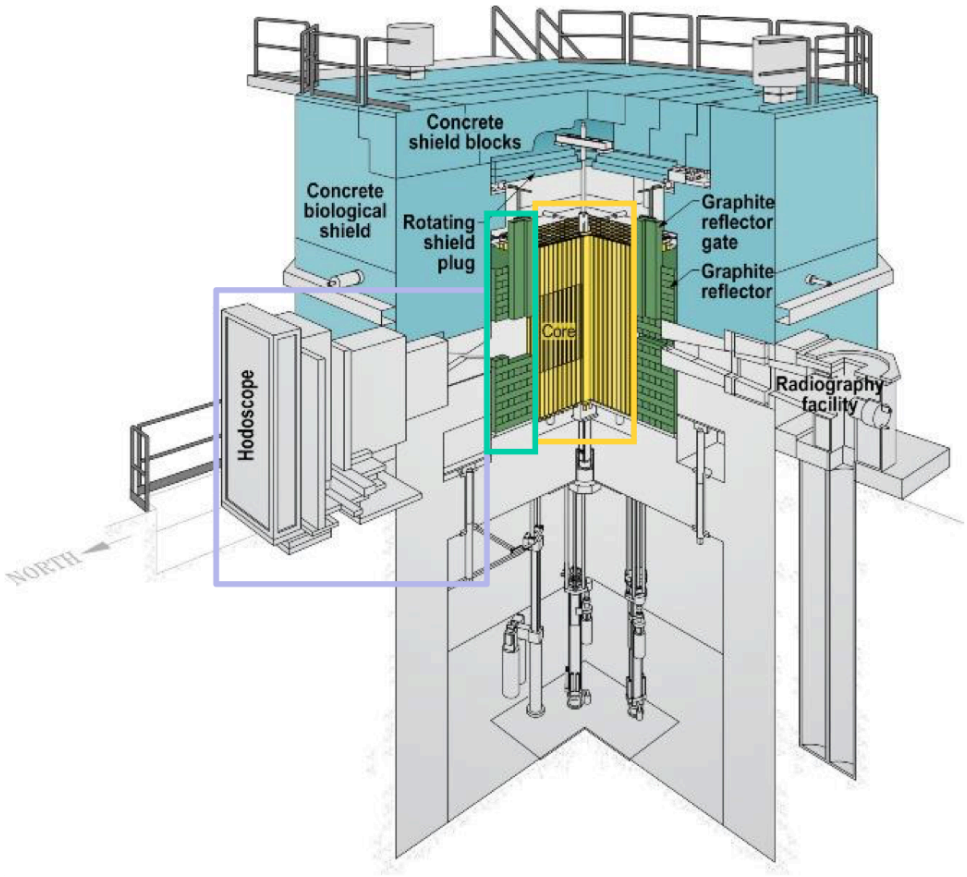

Figure 10. TREAT 3D rendering showing the tree component model boundaries where the Full-Core Model is in yellow, the Transient-Gap Model is in green, and the Hodoscope Model is in purple.

6.1 TREAT Core Model from M8CAL and ANCAL

Most of the preliminary models for TREAT reconstruct the reactor assemblies utilized in the M8CAL experiments from 1994 [1]. Figure 11 shows the experimental assembly for these experiments. For this assembly, *X* is the slotted assembly, *F* is the fuel cell, *Z* is the zirconium dummy cell. *S* is the zirconium clad source assembly, and *CC*, *CT*, and *CS* are control compensation, shutdown, and transient rods, respectively. The slotted assembly acts as the aperture for fast-neutrons from the test vehicle, *MK*, and

the half assemblies with zirconium cladding, *Z2*, and air streaming, *X2*. The center of the *MK* cell serves as the origin for this model, For the thermocouples, *T1* marks the 4-Fuel thermocouple assembly; *T2* represents the reflector-fuel gradient thermocouple assembly, *T3* represents the mid-fuel, reflector and skin thermocouple assembly; and *T4* represents the transient thermocouple assembly.

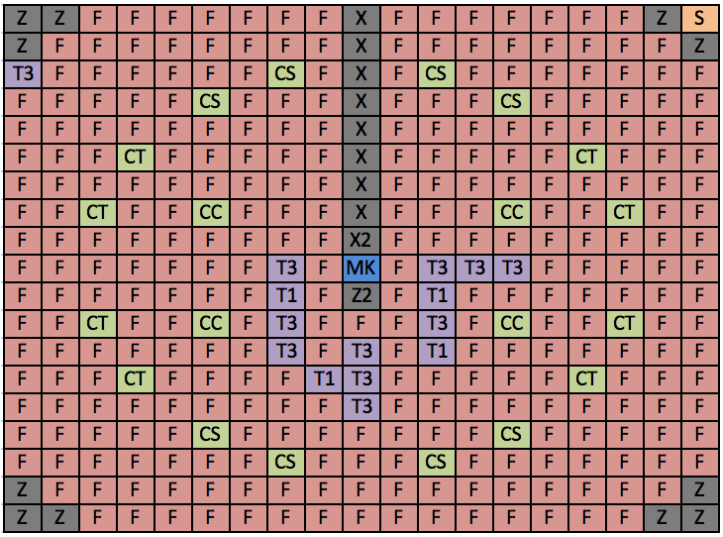

Figure 11. Core configuration lattice for TREAT.

The Core Model was previously constructed for multi-physics and coupled variable analysis. These models also serve as a result comparator for the k-eigenvalue solution of the interface model presented in this work. The reactor core configuration is shown in Figure 12. The model utilizes this simplified configuration when reconstructing its core lattice, where *X* is the slotted assembly, *F* is the fuel cell, *Z* is the zirconium dummy cell, and *CC*, *CT*, and *CS* are control compensation, shutdown, and transient rods, respectively. The slotted assembly acts as the aperture for fast-neutrons

from the test vehicle, *MK*, and the half assemblies with zirconium cladding, *Z2*, and air streaming, *X2*. The center of the *MK* cell serves as the origin for this model.

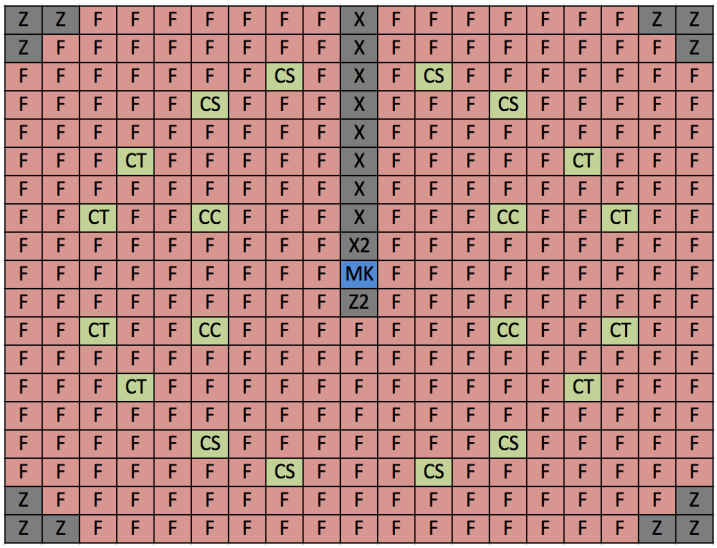

Figure 12. Core Model core assembly modeled with half-slotted assembly within TREAT.

The half-slotted assembly leads to north viewing slot on the positive Y-Axis from the origin towards the Hodoscope Model, as shown in Fig. 9. Surrounding the TREAT core are air gaps, aluminum plates, and the moderating graphite. The MCNP models in the plain and elevation view are shown in Figure 13 and Figure 14, respectively.

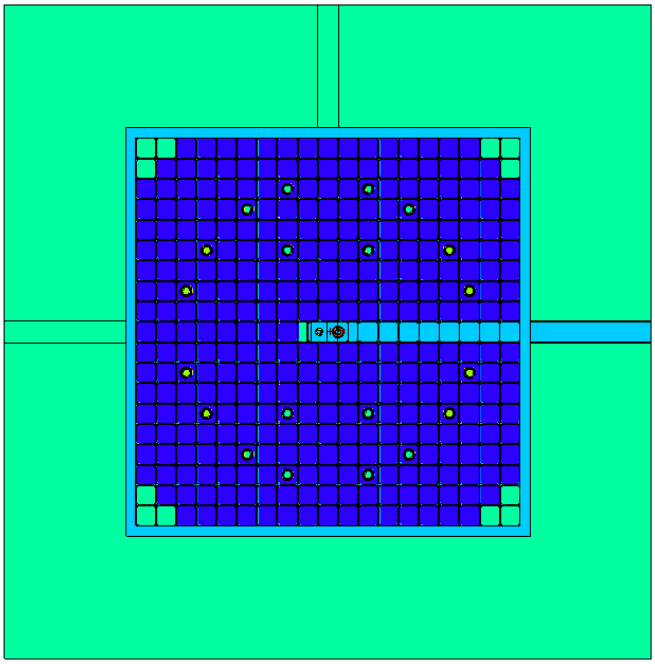

Figure 13. TREAT core model for *M8CAL* experiment in the X-Y Plane.

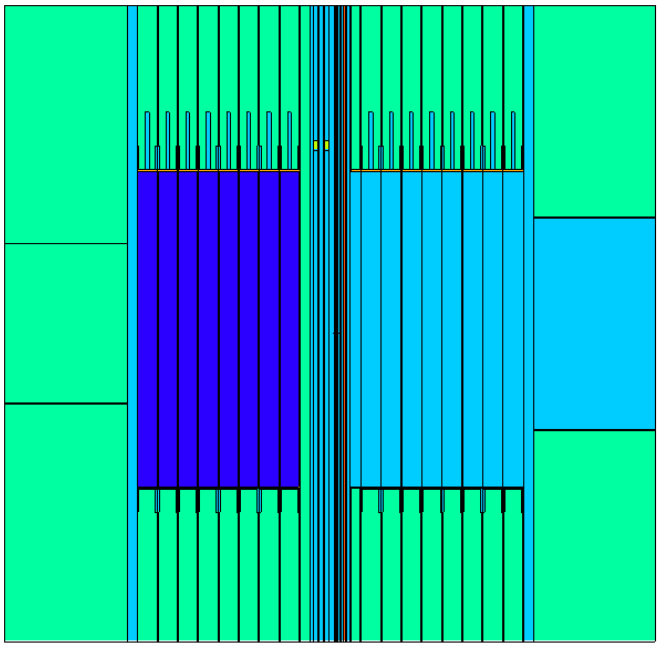

Figure 14. TREAT core model for the *M8CAL* experiment in the Y-Z Plane.

6.2 Transient Gap Model

The Transient-Gap Model was then combined with the Core Model to simulate the concentrated neutron signal leaving the TREAT core. This model was developed as a viable method to integrate models of the angular, spatial, and energy dependent fast-neutrons from the TREAT core with the two-dimensional models of fuel-motion hodographs. Neutron distribution paths from the core can be compiled into a planar source necessary to fit the two-dimensional dependence of the hodoscope models. Compiling the neutron histories at the interface planes will allow for collimated streaming through the initial and secondary collimators prior to incident flux tallies on the hodoscope model array. When compared to a similar geometric model utilizing surface source write (SSW) and read cards (SSR), this method can be used to verify both models.

The model draws all of the Core Model into a single universe to simplify any changes. Graphite was then distributed around the core and the transient gap consistent with all the dimensions from A. DeVolpi shown in Fig. 5 and Fig. 6. The MCNP models in the plain and elevation view are shown in Figure 15 and Figure 16, respectively.

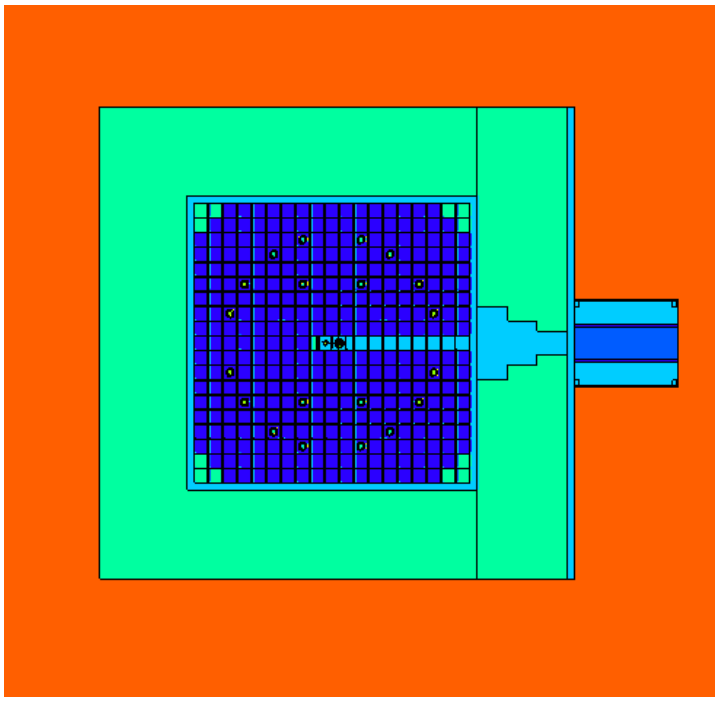

Figure 15. Transient-Gap Model shown from the plane view (X-Y Plane).

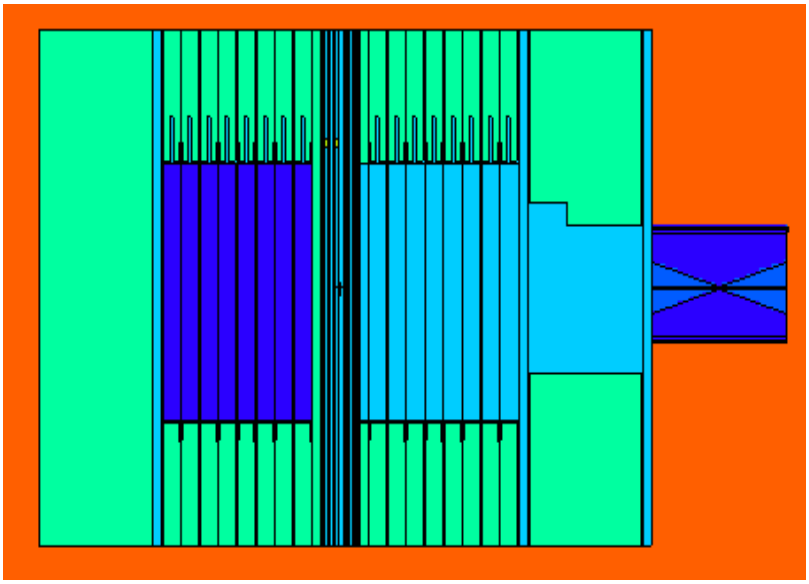

Figure 16. Transient-Gap Model shown from the elevation view (Y-Z Plane).

6.3 Full-Core Model with mSERTTA Integration

Finally, the Hodoscope Model was integrated with the Transient-Gap Model to make the Full-Core Model. This model can be broken down into five main sections: the TREAT core, the transient gap, the front collimator, the back collimator, and the hodoscope. Figure 17 and Figure 18 show the Full-Core Model in the plane and elevation view, respectively. Boundaries have been included around each of the five sections for clarity.

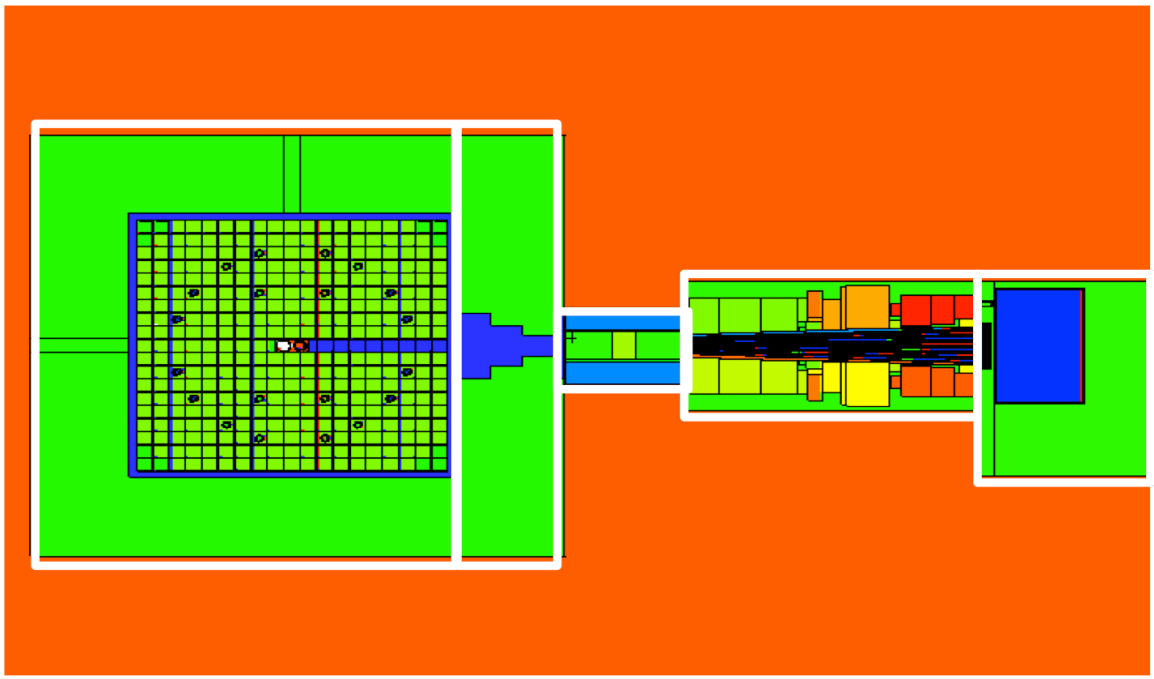

Figure 17. Full-Core Model shown from the plane view (X-Y Plane).

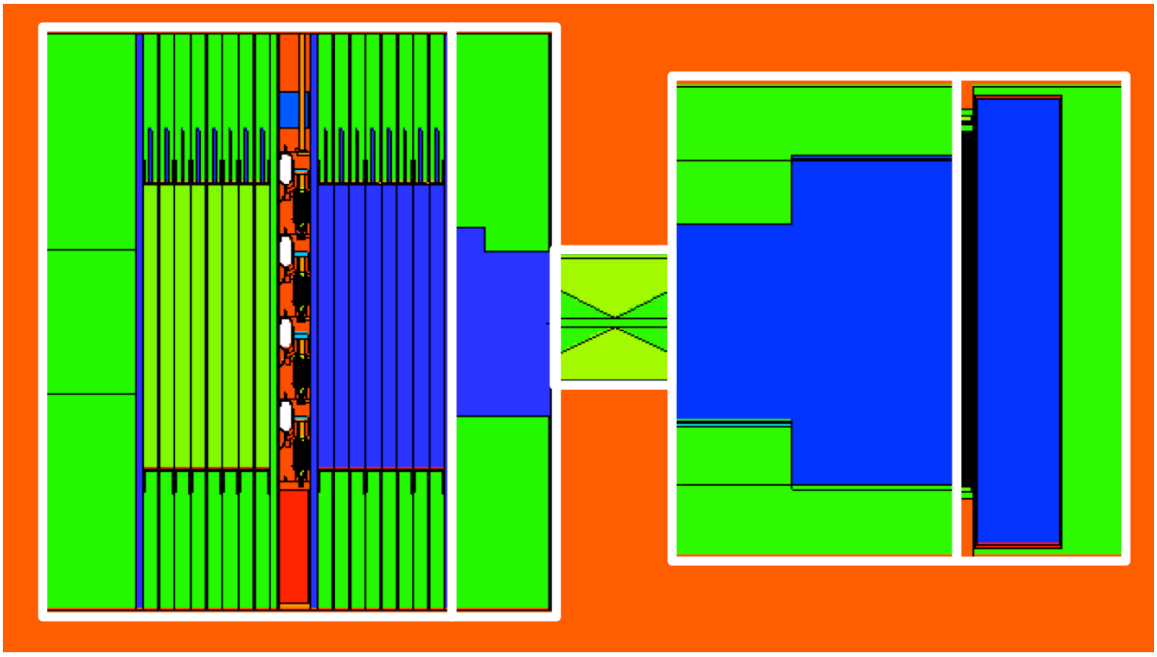

Figure 18. Full-Core Model shown from the elevation view (Y-Z Plane).

Various tally features are also included within the Full-Core Model. Mesh tallies are placed at the front of the front collimator, the back of the front collimator, and the back of the back collimator to track the progression of neutron collimation on the way to the hodoscope. Volumetric tallies are included around the fuel pellets within mSERTTA, in the transient gap, in the front collimator, and behind the back collimator to show the changing of the neutron flux shape at various points down the north-viewing slot.

7. RESULTS

With the completion of the Full-Core model, individual models were constructed with small modifications to demonstrate the change in neutron flux attributable to various factors. While this investigation aims to demonstrate how the neutron flux changes with respect to temperature changes, the amount of graphite in the TREAT core did not allow for an unbiased source characterization. Changes to the definition of source particles were necessary for the simulations to run to completion in a realistic time frame. Simple models were constructed to gain insight on the physics of the Full-Core model and to verify the observed results.

Overall, these investigations provided a check on the recorded neutron spectra provided in MCNP, insight into the use of source biasing to aid neutron streaming through the model, and verifications of the changes in neutron flux with changes in experimental fuel temperature. Initial simplified models demonstrated the accuracy of MCNP models compared to an analytical solution for neutron tallies. Then, simplified models of TREAT were constructed to demonstrate the ability to produce a characteristic spectrum for the full TREAT reactor core. These models yielded insight that was incorporated into Full-Core model simulations to isolate the change in neutron flux with temperature changes in the experimental fuel. Finally, simplified models of the mSERTTA vehicle aimed to verify the results in the Full-Core model.

7.1 Verification of MCNP Models with Analytical Solutions

At its most fundamental level, this research focuses on neutron interactions and streaming effects. Neutrons born in the TREAT core then escape the experimental instrumentation and stream towards the detection instrumentation in the north-viewing slot. While this work is focused at describing and identifying the phenomena occurring prior to escaping the TREAT core, the core physics governing the response at the front collimator interface can be simplified to neutrons streaming in space. This allows for the investigation of effects on neutron flux as a function of distance from the source. Understanding the underlying physics governing MCNP code is crucial in establishing the foundation for subsequent TREAT models.

7.1.1 Sphere in Void

A source of $1x10^{10}$ neutrons was placed inside a model consisting of concentric spheres to demonstrate the streaming and attenuation of particles in all directions. Included are both surface tallies (*f2*) and volume tallies (*f4*) for concentric spheres centered on the origin.

The *f2* tally measures the flux crossing over an averaged surface. Surface area is a function of only the distance between the source and the surface of question. In a void, the assumption that no scattering interactions occur in the void; thus, the neutrons counted at the surfaces of the concentric radii are relative to the averaged surface area at a given radius. This relationship is showed in Equation 18. The chi distribution of

neutrons for the source, demonstrated by a Watt fission spectrum, is described in Equation 19.

$$\phi(E, r_i) = \frac{\chi_{Watts}(E)}{4\pi(\, r_i^2)} \tag{18}$$

$$\chi_{Watts}(E, a, b) = \; e^{-E/a} \sinh\left(\sqrt{bE}\right) \tag{19}$$

Using this relationship, an analytical solution was determined to verify the MCNP output. The analytical solution and the output solution from MCNP are plotted for comparison. Representing these plots in for both energy and lethargy dependent flux helps validate the MCNP models. Figure 19 shows a geometric representation of this model. For comparison, each void shell has been filled with a separate color for comparison.

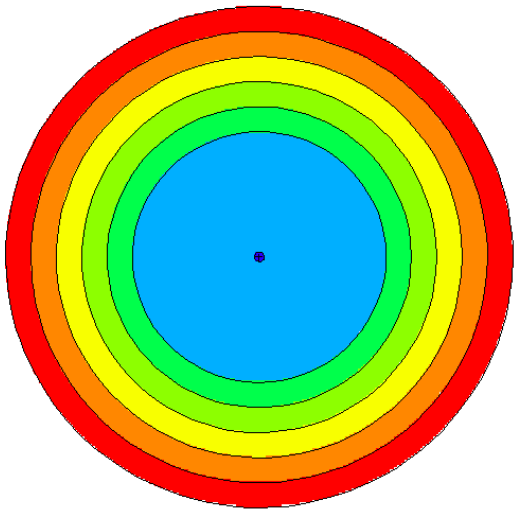

Figure 19. Cross-section representation of void spheres for *f2* tallies.

The analytical solution and the output solution from MCNP are plotted for comparison. Representing these plots in for both energy and lethargy dependent flux helps validate the MCNP models. These plots show the neutron flux for inner and outer radii in units of lethargy in Figure 20 and Figure 21, respectively. For the figures, the orange line represents the analytical solutions and the blue line represents the MCNP output. It should be noted that the incongruence at the spectrum peaks comes from energy binning.

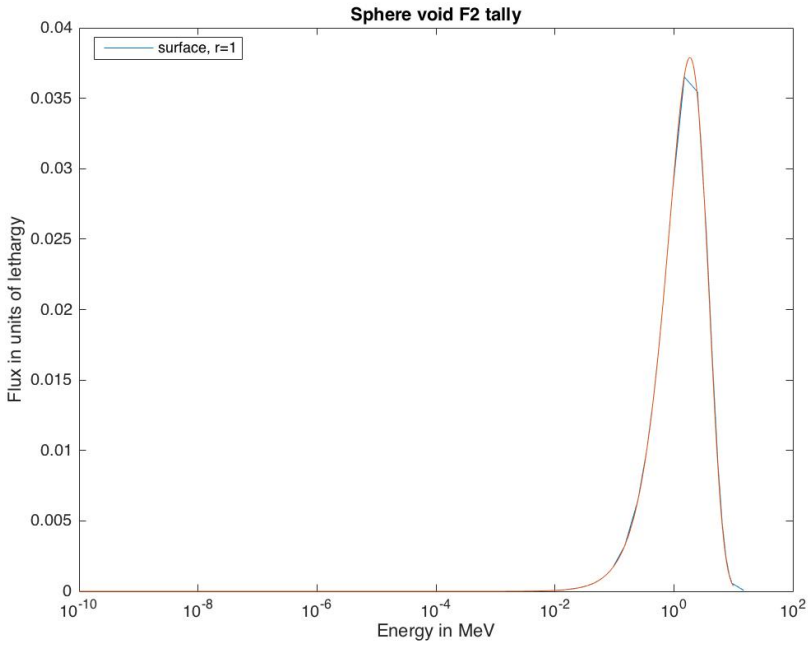

Figure 20. Neutron flux, in units of lethargy, tallied on a surface (*f2*) of a sphere with the radius of 1 cm.

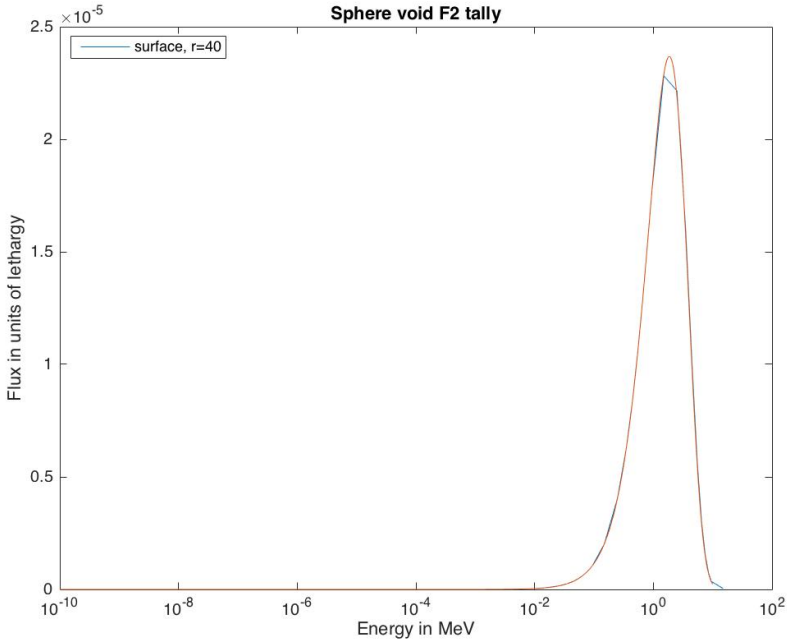

Figure 21. Neutron flux, in units of lethargy, tallied on a surface (*f2*) of a sphere with the radius of 40 cm.

For the *f4* tally, the MCNP tracks neutron path length as a function of radius for a given shell. The maximum path length is a difference in the shell's inner and outer radii (to show neutron path length through the shell). The analytical solution is derived by integrating the source term and point kernel for a point source within the volume of the sphere. This relationship is show in Equation 20.

$$< \phi(E) >_{Ci} = \frac{1}{V_{Ci}} \int_{r_i}^{r_{i+1}} \left(\frac{\chi_{Watts}(E)}{4\pi r^2}\right) dr^3 \tag{20}$$

For our shell tally volume, we assume that the volume of the shell can be derived as surface area as a function of the shell's radius multiplied by some distance, *dr*. In

doing so, the Green's theorem term and the surface area cancel out to yield the relationship shown in Equation 21.

$$< \phi(E) >_{Ci} = \frac{1}{V_{Ci}} \int_{r_i}^{r_{i+1}} \chi_{Watts}(E) dr = \frac{\chi_{Watts}(E)}{V_{Ci}} [r]_{r_i}^{r_{i+1}} \quad (21)$$

Figure 22 shows a geometric representation of this model. Again, for comparison, each void shell has been filled with a separate color for comparison.

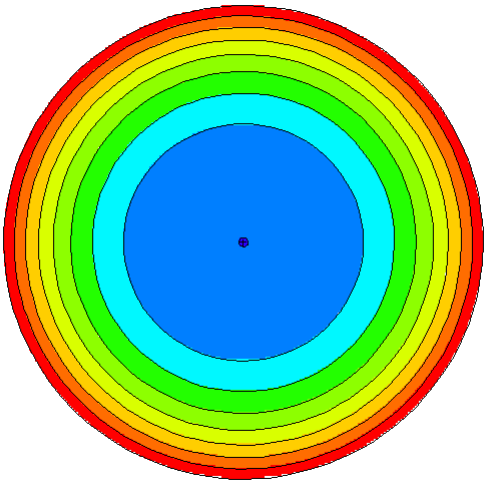

Figure 22. Cross-section representation of void spheres for *f4* tally.

For *f4* tallies, the analytical plots for energy and lethargy are shown comparatively in Figure 23 through Figure 25 with the plot from the MCNP data for outer radii of 1, 25, and 45.4 cm. This represents the flux for two different volumetric shells in the void, and it can be determined that the analytical solution matches the MCNP simulations for all radii. For these plots, the orange represents the MCNP output and the blue represents the analytical solution.

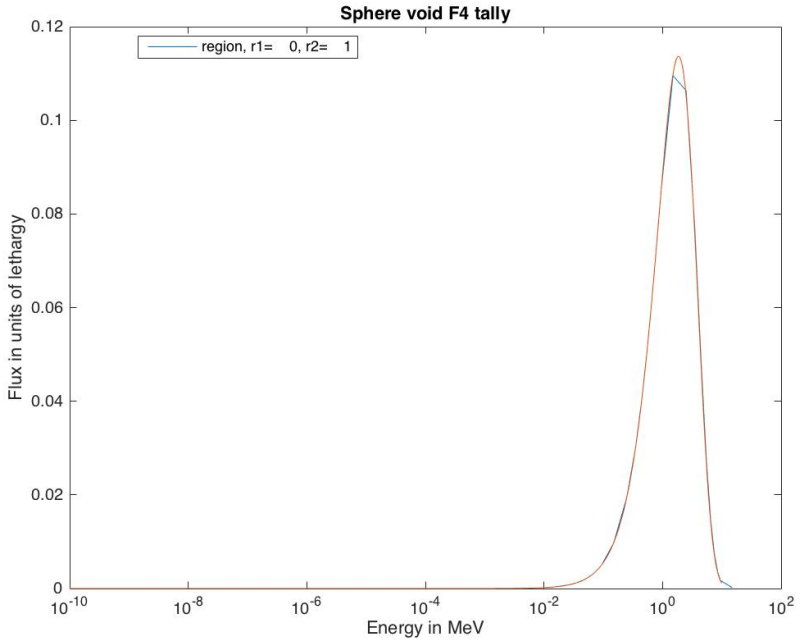

Figure 23. Neutron flux, in units of lethargy, tallied in a volume (*f4*) of a sphere with the radius of 1 cm.

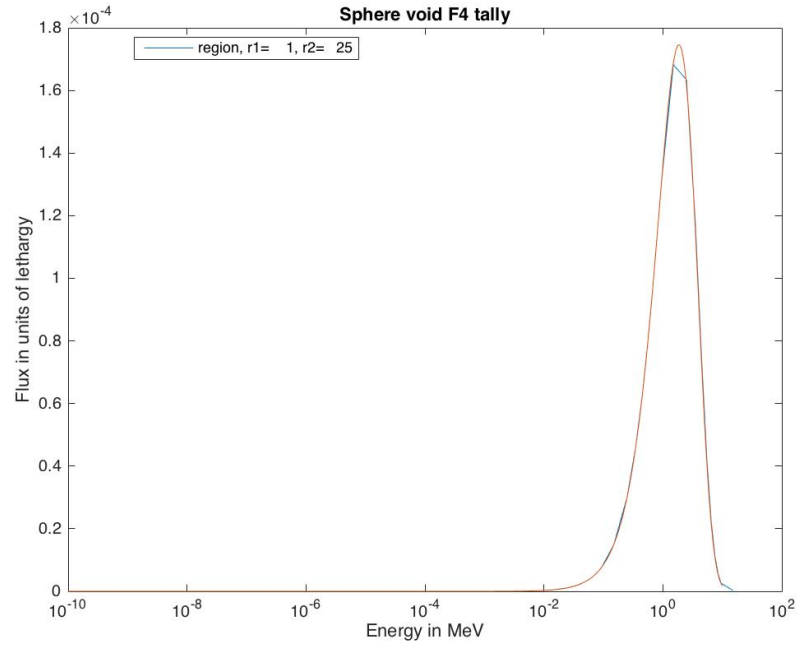

Figure 24. Neutron flux, in units of lethargy, tallied in a volume (*f4*) of a sphere shell with the radii of 1 cm and 25 cm.

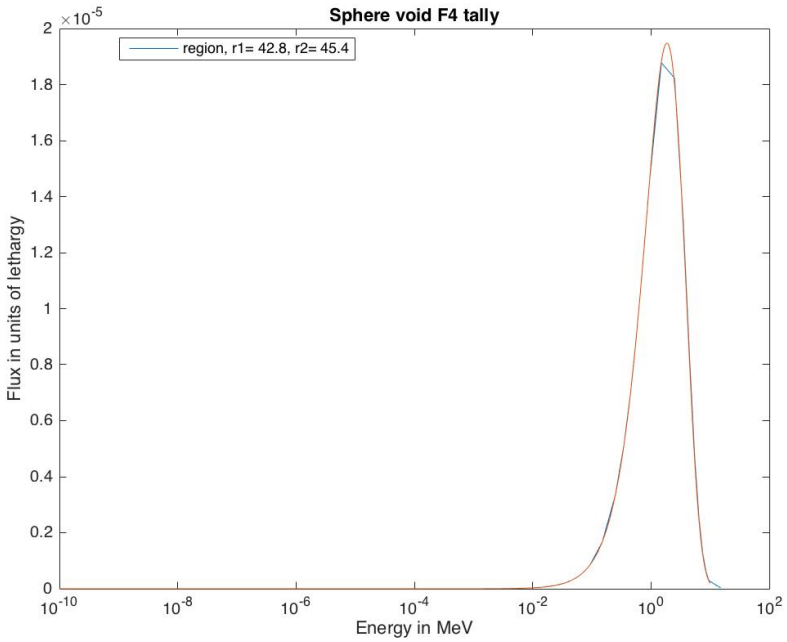

Figure 25. Neutron flux, in units of lethargy, tallied in a volume (*f4*) of a sphere shell with the radii of 42.8 cm and 45.4 cm.

7.2 Model Verification with Simple Models

After constructing the TREAT core model to include the transient gap, simple investigations looking at the deformation of the Watt fission spectrum at various points into the north viewing slot. Because the transient gap is air filled, we expect that the flux observed will degrade as the neutrons move down the north-viewing slot. However, upon gathering the initial run data, this was not observed. This resulted in a gradual deconstruction of the model to investigate the physical behavior on a smaller scale.

The first model investigated the streaming effects of neutrons to demonstrate an expected relationship between neutron tally and the distance from the source. The next model examined the effect of a graphite moderator on the neutron flux spectrum as a

function of energy. Next, the shape of the neturon flux was examined when neutron channeling was introduced using a small graphite collimation wrap. Finally, the TREAT Core and Transient Gap models were exercised to verify the same spectra characteristics as the simplified models.

All these models aimed to gradually add features to more accurately model the geometric construction of TREAT and to simulate a neutron flux spectra typical of a thermal reactor. All of these models included similar tally boxes showing the neutron flux spectra at various distances from the central fuel cell. However, as the neutrons leave the tallied area, they stream through void to the model boundary. Because the models aim to show the flux change as a function of a distance in a single direction, much like the north viewing slot of TREAT, as the distance from the source increases, the stochastic uncertainty and spectra intensity also increase. However, as more features are added to these models, the spectra begin to portray the expected shape and the stochastic error decreases within reasonable confidence intervals.

7.2.1 Neutron Streaming Pipe

Upon showing the verification of tally characteristics for concentric spheres, a simplified model for the TREAT reactor was constructed to investigate the deformation of a traditional Watt fission spectrum as the distance from the center of the core increases. Described as the “Universe and Pipe” model, a small cell light enriched uranium (LEU) fuel was placed at the center of the model and surrounded by a separate model universe filled with either void or graphite. Nine identical tally boxes were

extending down the Y-axis in the positive direction to simulate the neutron path towards the north-viewing slot and the hodoscope. For each tally box, an *f4* tally of all neutron paths was recorded to show the spectral changes as the distance from the origin increased.

The first exercise utilized a void-filled universe surrounding the fuel cell to demonstrate the spectrum shift only as a function of distance from the source. Figure 26 shows the geometric construction of the "Deconstructed Universe and Pipe" model. For note, the 10 colored cells extending from the main body are filled with void, and they are colored only to more easily show the cell boundaries. This model uses a point source inside of the fuel cell with a Watt fission spectrum energy distribution and an isotropic angular distribution.

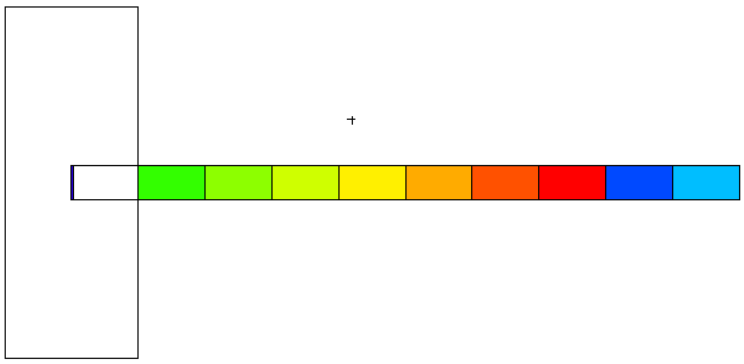

Figure 26. Neutron Streaming Pipe model with small fuel cell at the center and tally boxes extending down the Y-Axis.

From this model, simulations were run using SDEF mode at for $1x10^{10}$ particles over to generate the spectra show in Figure 27. As the distance from the fuel cell increases, the intensity of the observed flux decreases, and the accuracy of detection of

lower energy neutrons decreases. This is expected as the distance from the source increases. This model uses a point source inside of the fuel cell with a Watt fission spectrum energy distribution and an isotropic angular distribution.

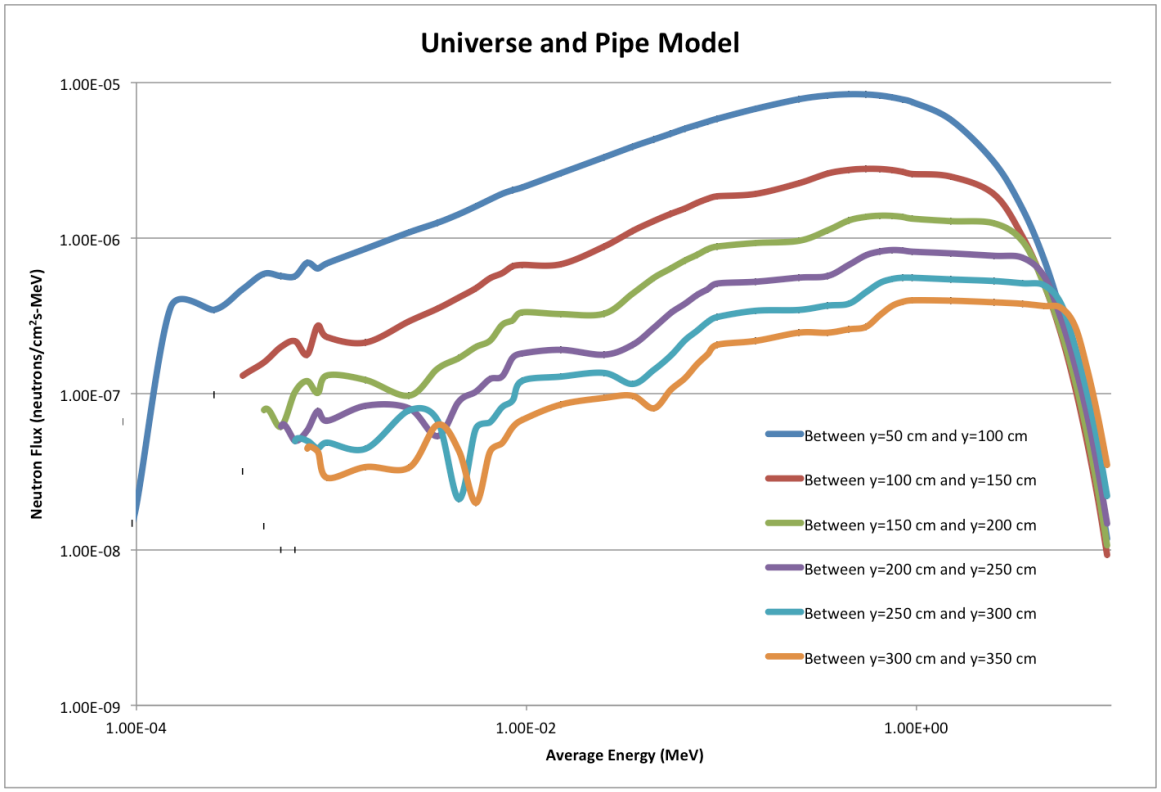

Figure 27. Plot showing Watt fission spectrum for Universe and Pipe model between y=50 cm and y=350 cm.

This plot should follow a "$1/r^2$" trend with the distance from the source. To show this, a ratio of the mid-point of the tally box was taken between two subsequent tally boxes and compared with the flux value tallied at 0.5 MeV. The results, shown in Table 6, prove this plot follows the $1/r^2$ trend expected.

Table 6. Comparison of square radii of analytical solution and MCNP tally for Neutron Streaming Pipe Model.

Ratio of Cells	Analytical Ratio	MCNP Tally Ratio
1:2	2.778	2.778
2:3	1.960	1.960
3:4	1.653	1.653
4:5	1.494	1.494
5:6	1.397	1.397

Next, to simulate the half-slotted configuration of TREAT, the main body universe was filled with the graphite material included in the M8CAL models. In doing this, the neutrons born in the fuel cell would be more channeled towards the tally cells. Figure 28 shows the addition of the graphite around the fuel cell. To more accurately demonstrate the TREAT system, air was added to the half slot prior to the tally cells. For the tally cells below, the colors from Fig. 26 have been removed to specifically show the boundaries. This model uses a point source inside of the fuel cell with a Watt fission spectrum energy distribution and an isotropic angular distribution.

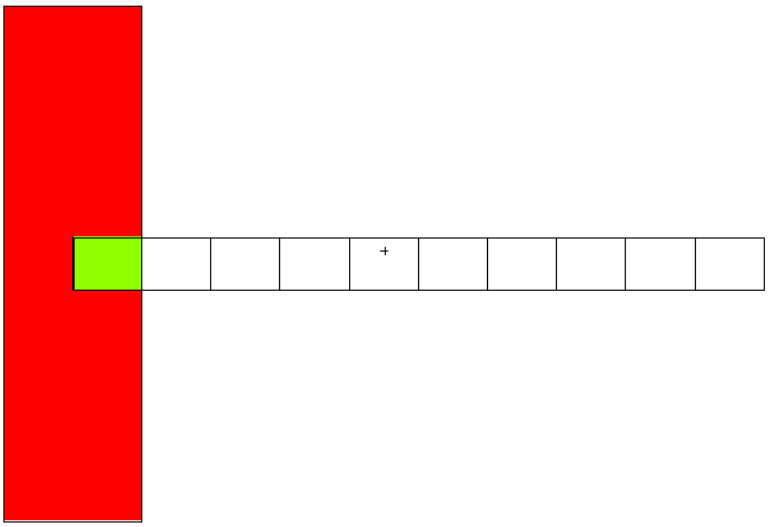

Figure 28. Deconstructed Universe and Pipe model with graphite placed around the fuel cell and air placed between the fuel and the tally boxes to more accurately simulate physics in TREAT core.

From this model, simulations were run using KCODE mode at for $1x10^6$ particles over 200 active cycles to generate the spectra show in Figure 29. The spectra demonstrate higher degrees of deformation than in Fig. 27, which is attributed mainly to the scattering from the graphite cell.

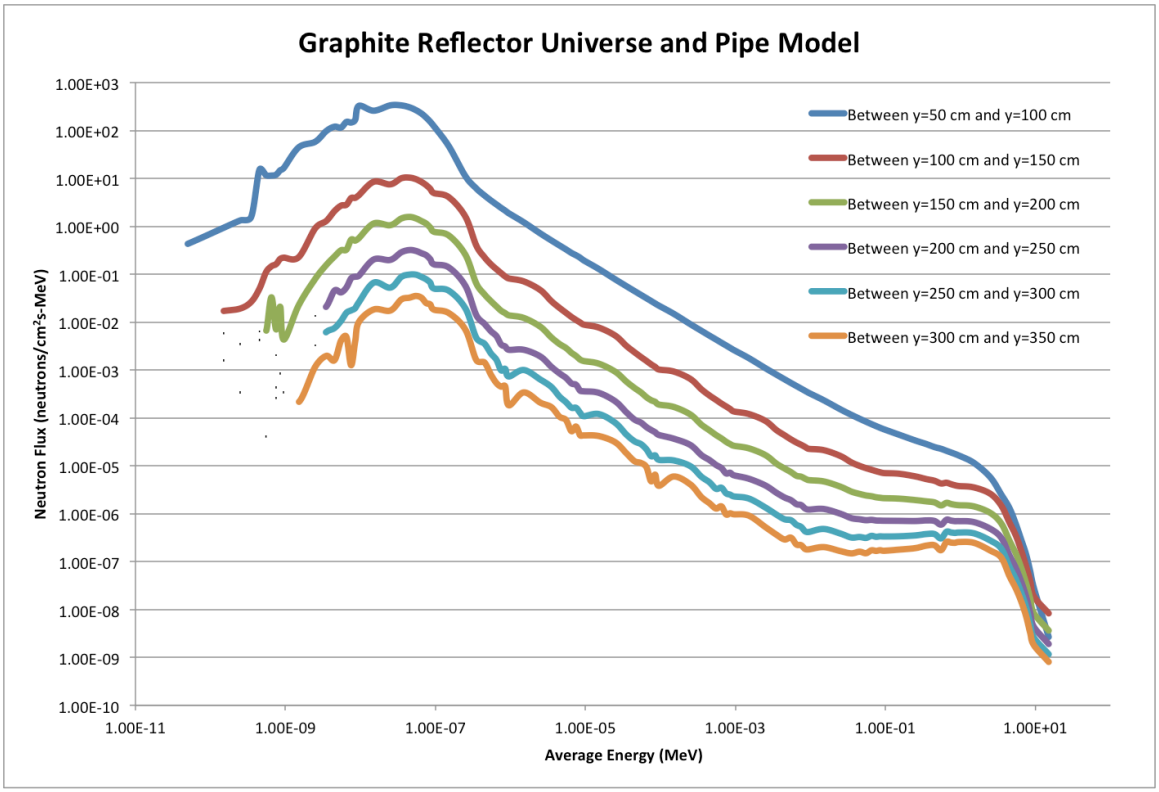

Figure 29. Plot showing Watt fission spectrum for Deconstructed Universe and Pipe model between y=50 cm and y=350 cm.

7.2.2 Graphite Wrapped Pipe Model

To more accurately simulate the neutron-channeling effects of the transient gap towards the hodoscope, a graphite wrap was added around the first three pipe tally bins. The idea is that in mimicking the channeling on neutrons, the neutron flux spectra will smooth out over the same distance as the Universe and Pipe Model. Figure 30 shows the MCNP model with the first three tally cells wrapped with graphite.

From this model, simulations were run using KCODE mode at for $1x10^6$ particles over 200 active cycles to generate the spectra show in Figure 31. The spectra demonstrate less spectral degradation than in Fig. 29. As the neutrons are channeled further down the pipe, it is expected that the stochastic uncertainty decreased and the

spectra appear smoother. In this model, all error bars are overtaken by the plot lines for all energies above $1x10^{-8}$ MeV. This model uses a point source inside of the fuel cell with a Watt fission spectrum energy distribution and an isotropic angular distribution.

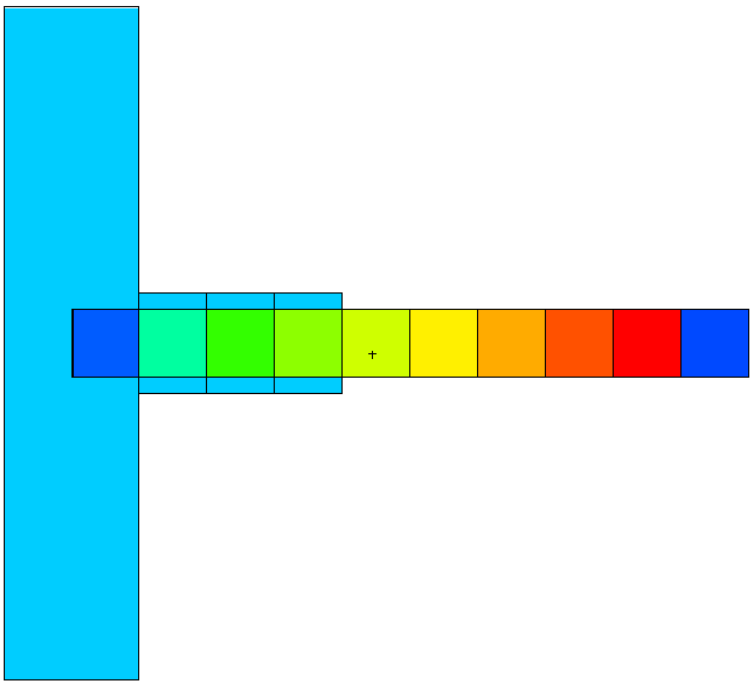

Figure 30. Elevation view of Universe and Pipe model shown with a graphite wrap along the first three tally bins to channel neutrons down the Y-Axis.

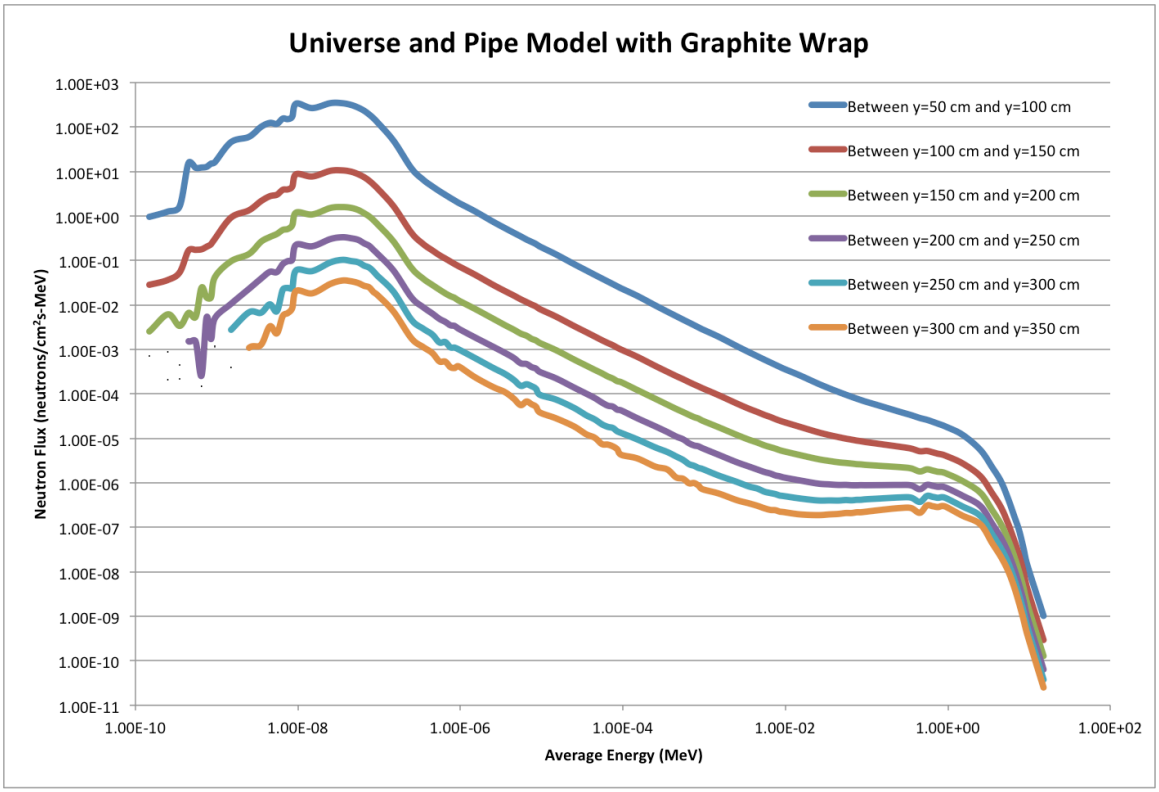

Figure 31. Plot showing Watt fission spectrum for Universe and Pipe model with Graphite Wrap between y=50 cm and y=350 cm.

7.2.3 Final Universe and Pipe Model

Finally, the TREAT Core model was inserted in the universe previously occupied by the graphite surrounding the fuel. Then, tally boxes covering the entirety of the half-slot opening were extended down the Y-axis toward the north-viewing slot. An elevation view of this model is shown in Figure 32. The tally cylinders are 50 cm in height with a radius on 40.64 cm.

The source was placed at the center of the core, and the same KCODE simulations using for $1x10^6$ particles over 200 active cycles to generate the spectra shown in Figure 33. A general degradation of the spectra is observed; however, the statistics on the model are low enough to attribute it solely to the distance from the

source in the center of the TREAT core. The plotted lines overlap this simulation's representative markers for the stochastic error, which fall well below 1%. This model uses a point source inside of the fuel cell with a Watt fission spectrum energy distribution and an isotropic angular distribution.

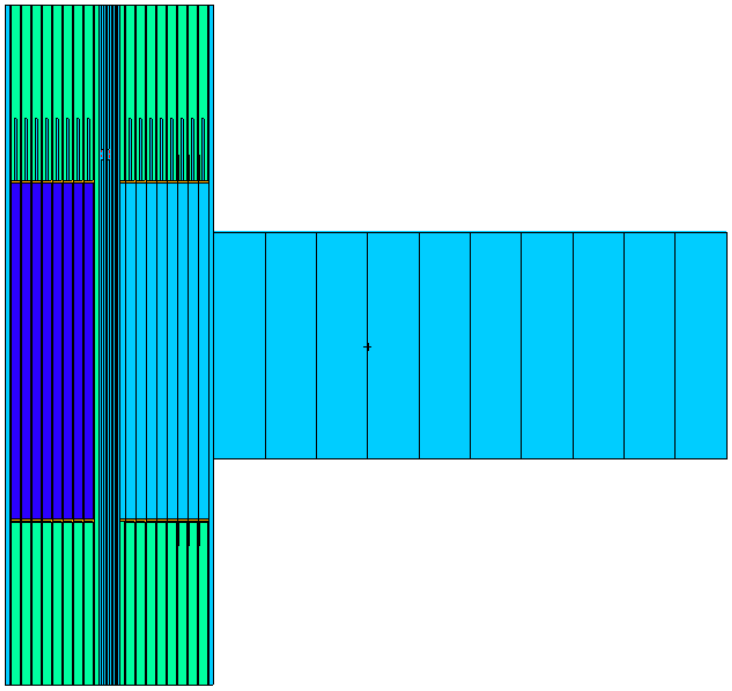

Figure 32. Elevation view of the TREAT core model inserted to where the block graphite universe was previously. Tally boxes extend down the Y-Axis.

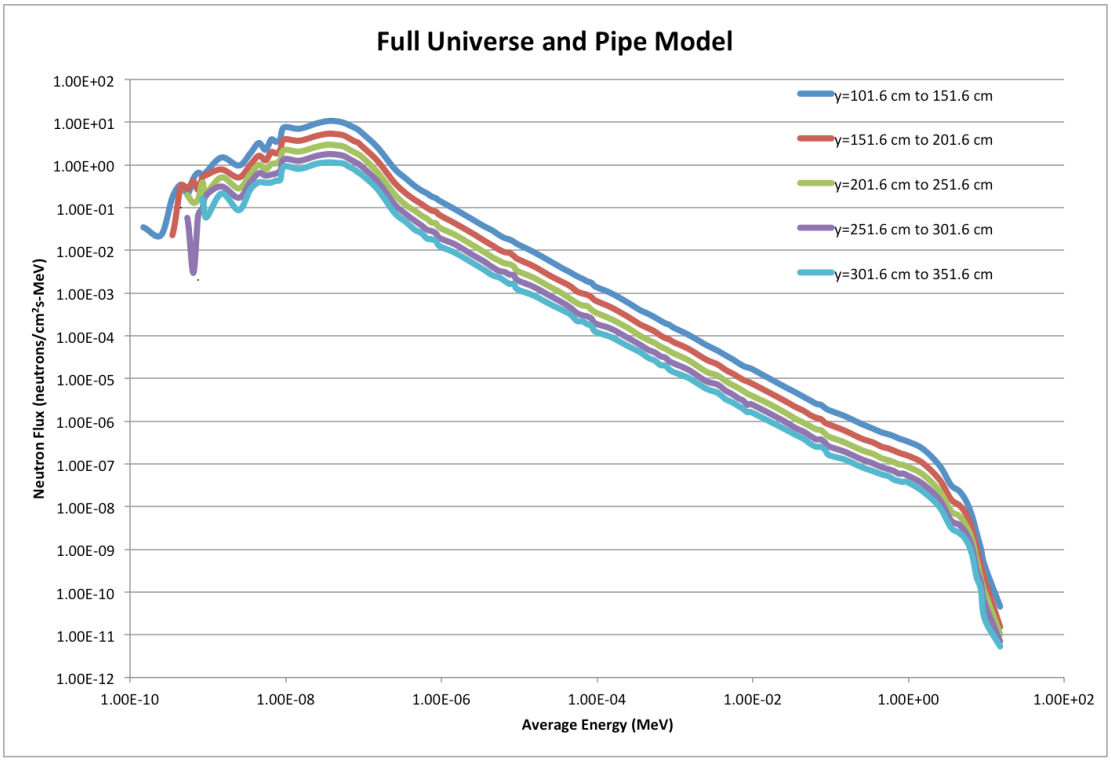

Figure 33. Plot showing Watt fission spectrum for Final Universe and Pipe model. While tallies extended to 501.6 cm from the center of the TREAT core, only the first five tally boxes are shown between y=101.6 cm and y=351.6 cm.

7.2.4 Flux Shape Investigations for Transient Gap Model

The primary test on the Transient Gap model was showing the flux recorded near the core was also seen at the transient gap-hodoscope interface. Knowing the TREAT core model using KCODE source mode will output a Watt fission spectrum, two volume tallies were set within the Transient Gap model within the transient gap cell and the front collimator phantom cell. An elevation view of this model is shown in Figure 34. The simulated spectra from this model are shown in Figure 35, generated from KCODE simulations using for $1x10^6$ particles over 200 active cycles. This model uses a point

source inside of the fuel cell with a Watt fission spectrum energy distribution and an isotropic angular distribution.

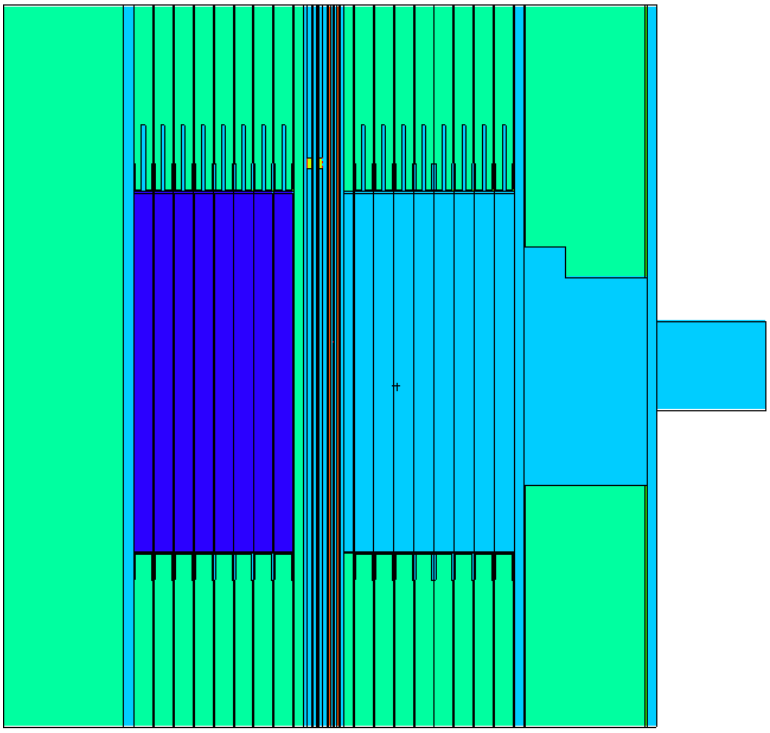

Figure 34. TREAT Transient Gap model used to tally neutron flux in the transient gap and the front collimator phantom cell.

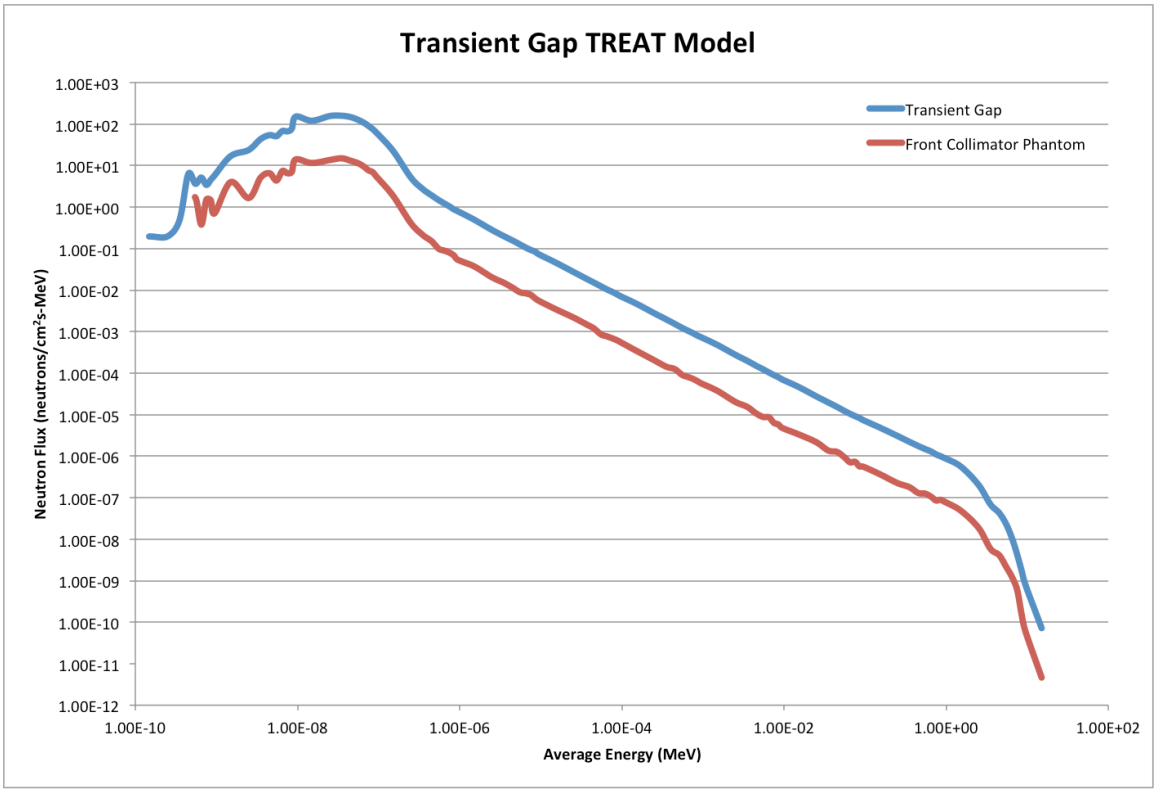

Figure 35. Neutron flux observed within the transient gap and the front collimator phantom.

Looking at the spectra from these tallies, we see that, again, the spectra resemble the Watt spectrum that degrades as the distance from the source increases. This, in combination with the temperature verification from the PWR fuel pin, allowed for an exercising of the model's response to temperature change in the experimental test tray.

7.3 Full-Core Model Analysis

With previous model iterations demonstrating the flux characteristic entering the front collimator, the Full-Core model was ready to test how changing the temperature in mSERTTA affected the flux observed at the front of the front-collimator. Models were developed to include source definitions with a typical Watt fission spectrum at the lower

and upper temperature bounds for fuel samples of 593 K and 2500 K, respectively. The models were then simulated for $1x10^8$ particles with an isotropic angular distribution.

However, these simulations never reached conclusion. Even utilizing the High-Performance Computing Center (HPC) at INL, the each particle history was taking a long time because of the moderating graphite in TREAT. As a particle would leave the mSERTTA boundaries, it would enter the TREAT reactor and scatter endlessly through the moderating graphite surrounding the fuel rods. Using an isotropic source, there appeared no clear way to simulate the model in a reasonable amount of time with meaningful statistics.

To correct this, the source was biased to channel neutrons down the north-viewing slot. This allowed for the neutrons to be born in the experimental fuel, travel through the mSERTTA unit, and stream towards the front of the front collimator. To minimize the contact with the moderating graphite, each source particle was biased with a given probabilistic angle about a specified vector. The elevation view of this model with its source bias vector is shown in Figure 36.

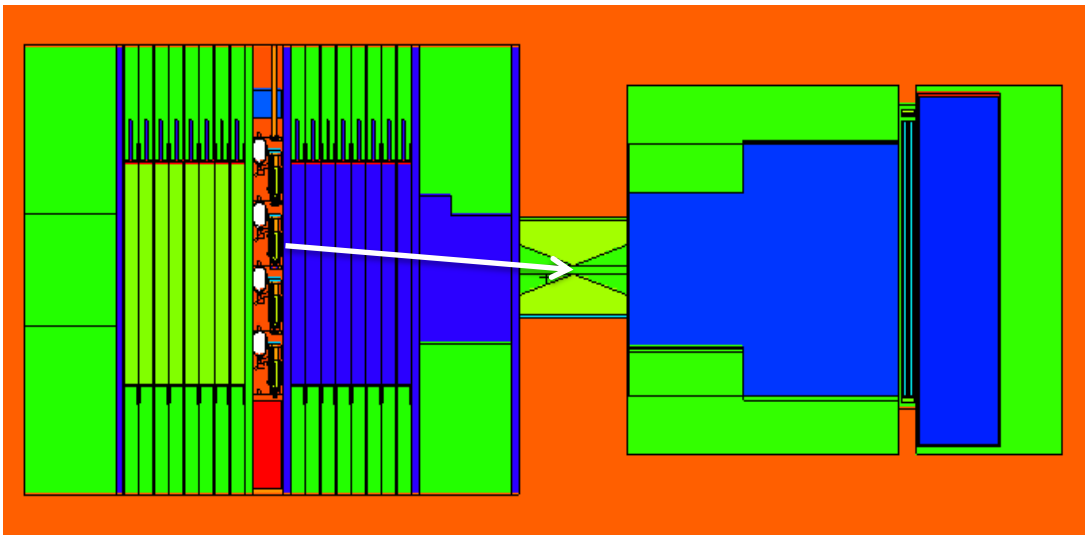

Figure 36. Elevation view of the Full-Core model with a characteristic bias vector.

Simulations were run with $1x10^{10}$ particles. At the opening of the front collimator, an f-mesh tally was placed to show the geometric distribution of the total flux entering the front collimator. Between the temperatures of 593 K and 2500 K, the observed neutron flux increases by roughly 10%. The flux shapes at 593 K, 2500 K, and the difference between the two fluxes are shown in Figure 37, Figure 38, and Figure 39, respectively.

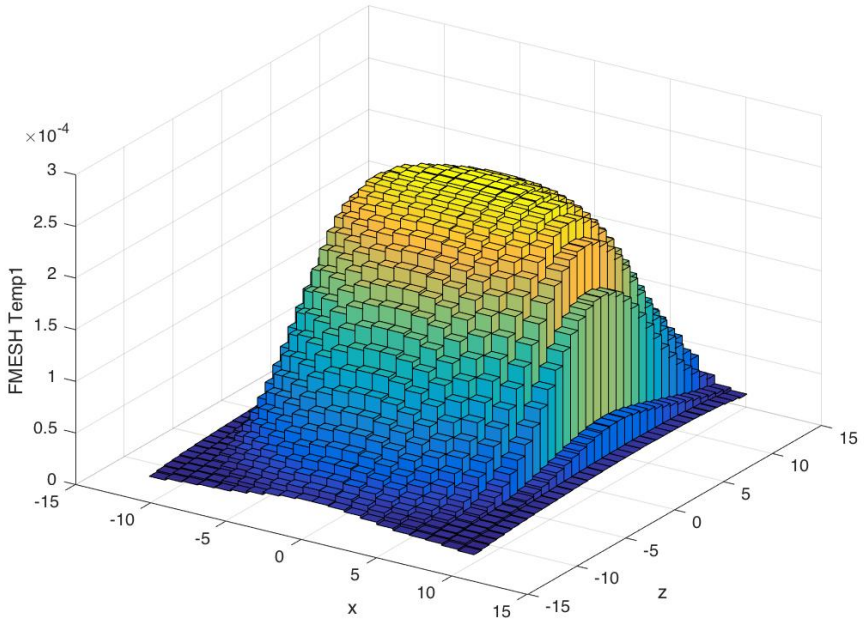

Figure 37. Total neutron flux profile at the front of the front collimator at 593 K.

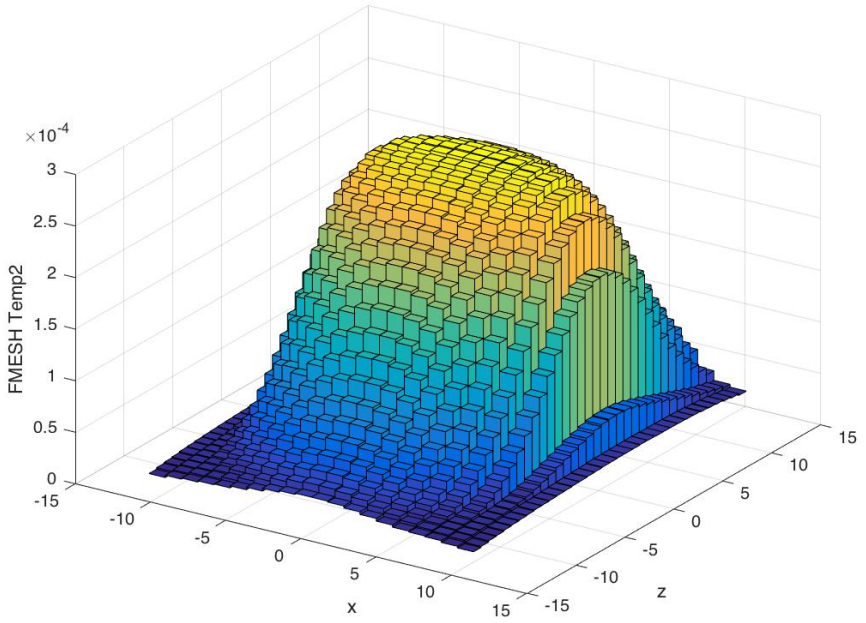

Figure 38. Total neutron flux profile at the front of the front collimator at 2500 K.

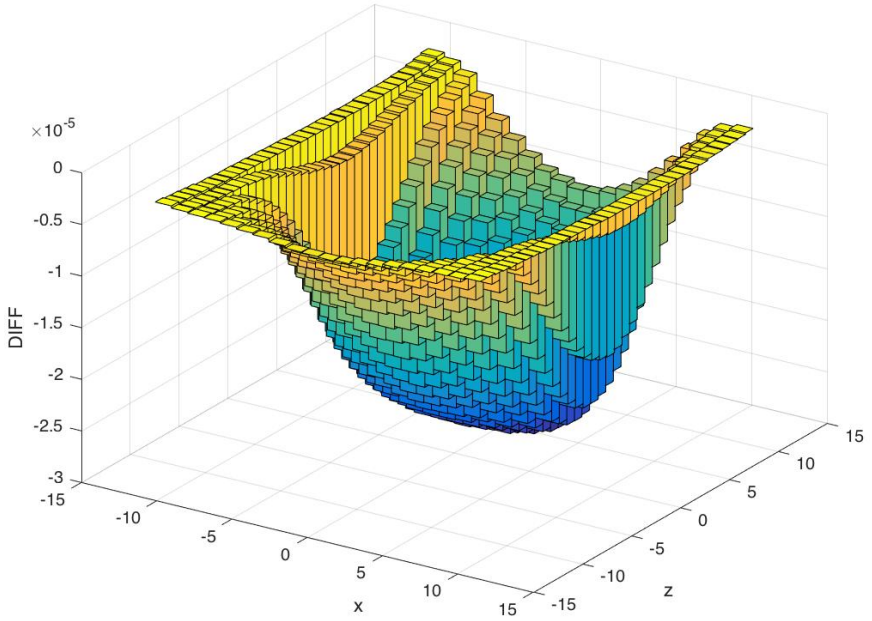

Figure 39. Difference between total neutron flux at the front of the front collimator at 593 K and 2500 K.

The only difference between the two simulations was the temperature change of the fuel and immediate surrounding instrumentation from 593 K to 2500 K. With this isolation of temperature change corresponding to a change in flux, it was originally believed that the change in temperature caused the change in neutron flux observed at the front collimator.

As a verification check, the TREAT fuel material, cladding, and water were input into the PWR fuel pin described previously. Simulations were then initiated by perturbing each material's temperature between the 293 K and 2500 K for material cross-sections and 293 K and 1200 K for S(α/β) cross-sections. Each model was simulated with a Watt fission spectrum energy definition and an isotropic angular distribution. A small volume tally was then set the same distance from the center of the

fuel rod as the mSERTTA to the front of the front collimator. It was believed that this would demonstrate the same flux increase that was observed in the Full-Core model, and it would also provide insight as to the degree to which each material contributed to the flux shift with temperature change.

However, no change in flux was observed outside statistical noise, regardless of temperature declaration for a given material. The results that seemed certain in the Full-Core model were now questionable. For several iterations of tally structure and temperature changes, no meaningful change in the neutron flux was ever observed.

In an effort to demonstrate the flux change in a simplified model, a series of compounding, simplified models were constructed to test the effects of various materials on the neutronic response at the front of the front collimator. Each model integrated more components from mSERTTA unit into the model in an attempt to isolate the material that caused the 10% shift at different temperatures.

Looking at all the results in culmination, it is hypothesized that the main effects from thermal neutrons are induced by the thermalization of fast neutrons by the water moderator. These thermalized neutrons then scatter back into the experimental fuel, causing secondary fissions. Because the current energy discretization only measures all neutrons between 0 and 0.1 MeV, the fraction of thermal neutrons observable is not discernable from the neutrons right at 0.1 MeV.

Each model was simulated using a Watt fission source definition for the energy distribution at temperatures of 593 K and 2500 K to be consistent with the Full-Core model. A series of tallies were implemented to investigate hypothetical neutronic

behavior. A surface tally was set up to show the surface flux of all neutrons at the fuel-cell boundary. Consistent with the full TREAT model with mSERTTA inserted, a mesh tally with the dimensions of the front-collimator opening was placed at the distance equivalent to the front-collimator opening in the full model (y=168.974).

7.3.1 Simple Model A: Simple Fuel Pin

To investigate the effects of the neutronic response at the front of the front collimator, a simplified model of the mSERTTA Unit #2 was constructed in MCNP. The model is a simplified version of a single experimental apparatus within mSERTTA. Ten 4.95% atom-enriched fuel pellets with a radius of 0.41 cm were placed at the origin of the model and combined into a single rodlet with a height of 10.16 cm. The rodlet was then wrapped with a small helium gap and zirconium-IV alloy cladding, and the supporting pins, comprised mainly of metallic alloys, were inserted at the base of the rodlet. This composition can be seen in Figure 40.

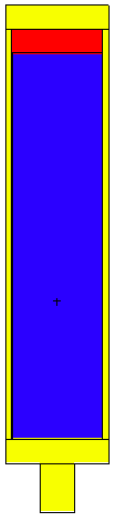

Figure 40. Model A: Simplified mSERTTA experimental pin and supporting apparati.

The source of the simulation was a Watt fission energy distribution of $1x10^{10}$ isotropic neutron particles, evenly distributed uniformly volume source within the fuel rodlet sample. An energy cut card was used at 0.099 MeV for one model and deleted for another for comparison of thermalizing neutrons. Concurrent with the Full-Core models, an identical mesh tally was set up to tally the neutron flux entering the front collimator. A summary of the tallies comparing the neutron flux tallied in a cell just below and west of the center of the mesh tally for each the four simulations are shown in Table 7.

Table 7. Summary table comparing the tallies recorded in the f-mesh cell to the left and below the center of the f-mesh grid.

Model	F-Mesh Tally at 593 K (Error, %)	F-Mesh Tally at 2500 K (Error, %)	Difference (%)
Isotropic Source; No Energy Cut	1.84411E-06 (0.80)	1.84480E-06 (0.80)	-0.00
Isotropic Source; Energy Cut at 0.099 MeV	1.80106E-06 (0.81)	1.80113E-06 (0.81)	-0.00

For the simple pin model simulated at two different temperatures, the neutron flux observed in it is clear that there is no significant difference in neutron flux because of temperature change. Thus, these tests were deemed inconclusive within stochastic error. For the center tally shown in Table 7, the results are indicative of the slot-by-slot comparison as a whole.

7.3.2 Simple Model B: Moderator Containment Vessel

Results for temperature dependence of neutronic behavior at the fmesh tallies was inconclusive for both the simple fuel model. In comparing the simplified model with the full core model, the main difference was the source definition within the MCNP physics cards. The simplified models utilized an isotropic source to show the neutron flux that leaves the fuel rodlet and is tallied on the surface of a large sphere. However, within the full core model, the source is defined such that it focuses on the geometric focal point of the front collimator to reduce computational time and allow more particles to be used without large effects from the scattering of moderator graphite. Moving forward, all models were simulated with both an isotropic angular distribution and a directionally biased angular distribution.

This vessel is a cylinder with an extended, rounded bottom. The moderator used was extracted directly from the mSERTTA model as compressed PWR Water at a pressure of 16 MPa and a temperature of 320°C. Usually, the moderator is contained in an aluminum-II alloy; however, for this simplified model, the water is suspended in form

around the mSERTTA experiment. This model configuration can be seen in Figure 41 with the water highlighted in red.

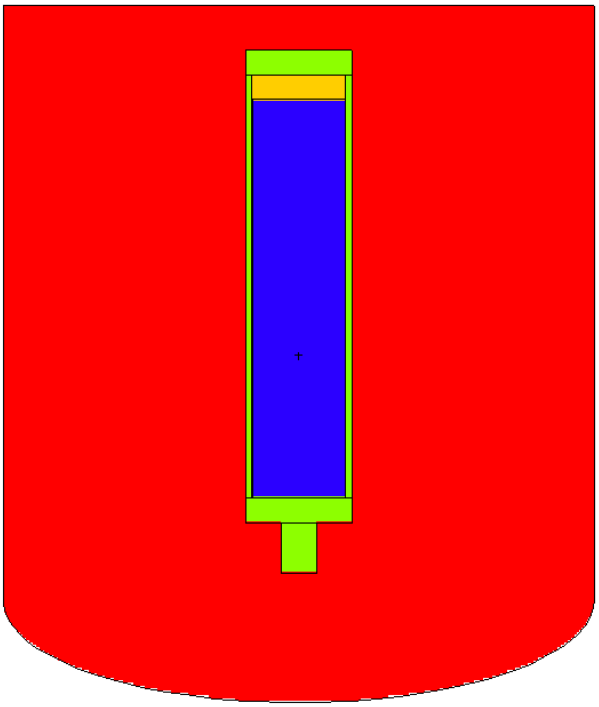

Figure 41. Model B: Simplified mSERTTA experimental pin with moderator containment and supporting apparati.

The source from the full core model was extracted, modified for the changes to origin relative position, and inserted into the simplified model. Figure 42 shows the general idea of the source, which declares a particle vector from the center of each pellet comprising the mSERTTA experimental rodlet. In the simplified model, the 10 pellets have been combined, so the source just samples from ten vectors all targeted on the y-axis at a distance of 205 cm.

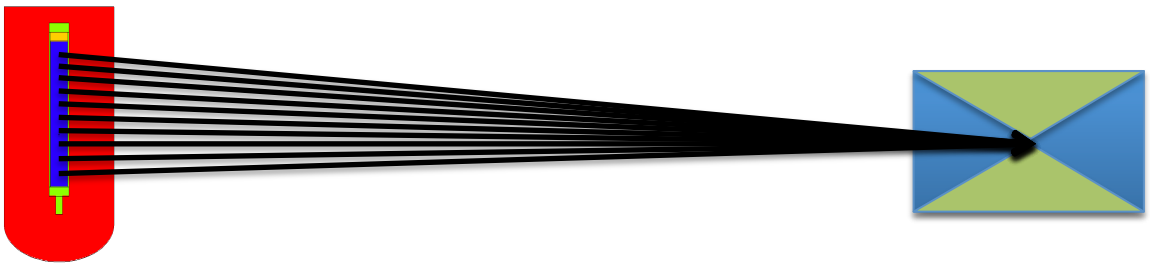

Figure 42. Example of more targeted source definition extracted from full core model, not drawn to scale. Arrows represent the vector definition for neutrons within the experimental fuel rodlet targeted at the geometric focal point.

The source of the simulation was a Watt fission energy distribution of $1x10^{10}$ isotropic neutron particles, evenly distributed uniformly volume source within the fuel rodlet sample. An energy cut card was used at 0.099 MeV for one model and deleted for another for comparison of thermalizing neutrons. A mesh tally was set up to tally the neutron flux entering the front collimator. A summary of the tallies comparing the neutron flux tallied in a cell near the origin for each the eight simulations are shown in Table 8.

Table 8. Summary table comparing the tallies recorded in the f-mesh cell to the left and below the center of the f-mesh grid for the simplified water model.

Model	F-Mesh Tally at 593 K (Error, %)	F-Mesh Tally at 2500 K (Error, %)	Difference (%)
Isotropic Source; No Energy Cut	2.34749E-06 (0.71)	2.34787E-06 (0.71)	-0.01
Isotropic Source; Energy Cut at 0.099 MeV	1.82055E-06 (0.81)	1.82073E-06 (0.81)	-0.01
Biased Source; No Energy Cut	5.14429E-04 (0.04)	5.14480E-04 (0.04)	-0.01
Biased Source; Energy Cut at 0.099 MeV	5.09925E-04 (0.04)	5.09924E-04 (0.04)	+0.00

For the moderator containment model simulated at two different temperatures with an energy cut at 0.099 MeV, the neutron flux showed minimal changes in the measured response from the f-mesh tally. However, all the changes in neutron flux for all models was smaller than the stochastic error, so these tests were also deemed inconclusive.

7.3.3 Simple Model C: Experimental Fuel Crucible

In addition to the moderator containment vessel, the ceramic crucible designed to catch any failed fuel was added to the simplified model. The crucible is an annular basket placed within the moderator containment with a high absorption cross section. While the actual material construction of the crucible is still under discussions, preliminary materials are composed of zirconium oxide ceramics absorption enriched with hafnium and magnesium in a 96 wt%-2 wt%-2 wt% ratio. A cross-section visualization of this model is shown in Figure 43, highlighting the crucible in orange.

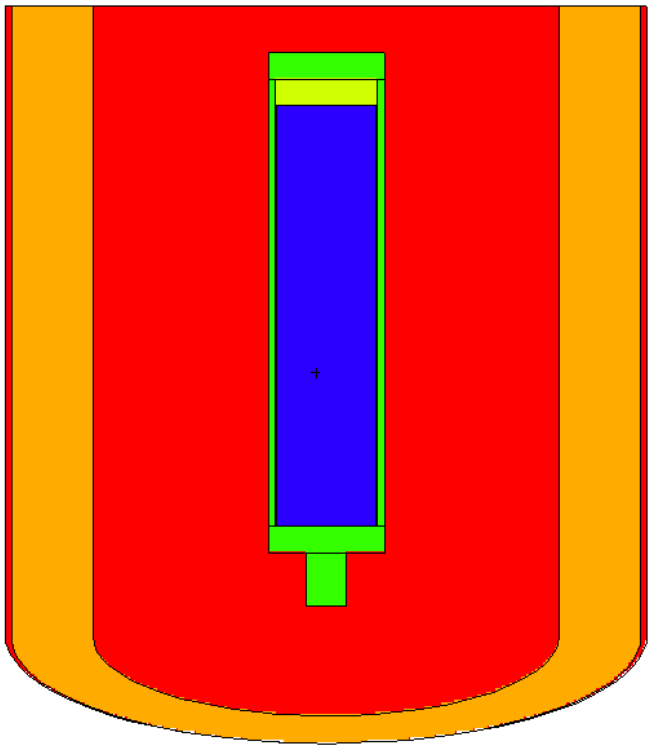

Figure 43. Model C: Simplified mSERTTA experimental pin with moderator containment, ceramic crucible, and supporting apparati.

The source of the simulation was a Watt fission energy distribution of $1x10^{10}$ isotropic neutron particles, evenly distributed uniformly volume source within the fuel rodlet sample. An energy cut card was used at 0.099 MeV for one model and deleted for another for comparison of thermalizing neutrons. A mesh tally was set up to tally the neutron flux entering the front collimator. A summary of the tallies comparing the neutron flux tallied in a cell near the origin for each the eight simulations are shown in Table 9.

Table 9. Summary table comparing the tallies recorded in the f-mesh cell to the left and below the center of the f-mesh grid for the simplified crucible model.

Model	F-Mesh Tally at 593 K (Error, %)	F-Mesh Tally at 2500 K (Error, %)	Difference (%)
Isotropic Source; No Energy Cut	2.32091E-06 (0.71)	2.32024E-06 (0.71)	+0.03
Isotropic Source; Energy Cut at 0.099 MeV	2.32087E-06 (0.71)	2.32024E-06 (0.71)	+0.03
Biased Source; No Energy Cut	4.83527E-04 (0.04)	4.83526E-04 (0.04)	+0.00
Biased Source; Energy Cut at 0.099 MeV	4.78456E-04 (0.04)	4.78456E-04 (0.04)	+0.00

Again, no change was significant outside the stochastic error of the simulation.

7.3.4 Simple Model D: Graphite Reflector Model

With still no clear correlation between the temperature of the experimental fuel and the recorded neutron flux at the front of the front collimator, a graphite block was placed around the simplified mSERTTA unit. The simple crucible model was placed in the center of a graphite cube with 400 cm sides. A slot was cut down the positive y-axis with a width of 10.67 cm and a height of 122.71 cm. This now acts as a simplified TREAT core model. A cross-section visualization of this model is shown in Figure 44, highlighting the graphite in red.

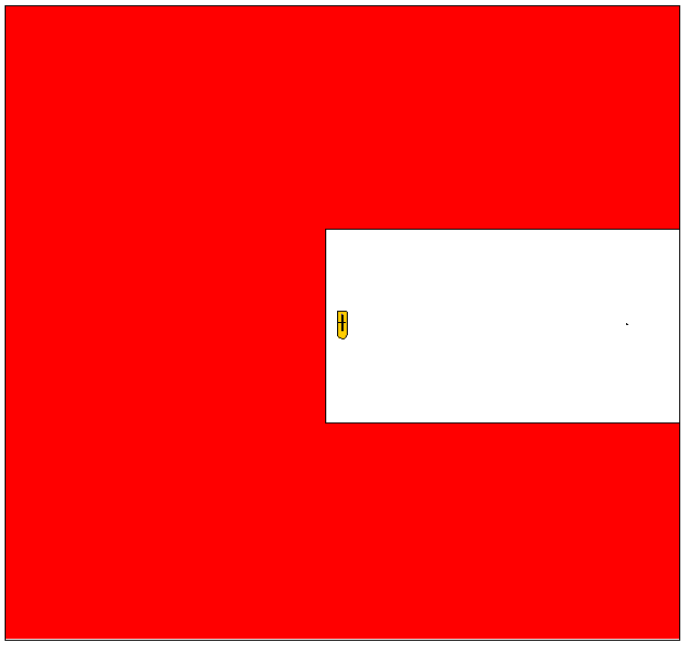

Figure 44. Model D: Simplified crucible model set inside of graphite block.

The source of the simulation was a Watt fission energy distribution of $1x10^{10}$ isotropic neutron particles, evenly distributed uniformly volume source within the fuel rodlet sample. An energy cut card was used at 0.099 MeV for one model and deleted for another for statistic comparison of thermalizing neutrons. A mesh tally was set up to tally the neutron flux entering the front collimator. A summary of the tallies comparing the neutron flux tallied in a cell near the origin for each the eight simulations are shown in Table 10.

Table 10. Summary table comparing the tallies recorded in the f-mesh cell to the left and below the center of the f-mesh grid for the simplified graphite block model.

Model	F-Mesh Tally at 593 K (Error, %)	F-Mesh Tally at 2500 K (Error, %)	Difference (%)
Isotropic Source; No Energy Cut	8.28047E-05 (0.95)	8.27747E-05 (0.95)	+0.03
Isotropic Source; Energy Cut at 0.099 MeV	4.09944E-06 (5.22)	4.09944E-06 (5.22)	+0.00
Biased Source; No Energy Cut	6.92435E-04 (0.60)	6.92416E-04 (0.60)	+0.00
Biased Source; Energy Cut at 0.099 MeV	5.65534E-04 (0.34)	5.65534E-04 (0.34)	+0.00

Different model produced the same results. Again, no simulation showed a change in observed neutron flux that was significant.

7.3.5 Investigation of Angular Source Biasing

Still, no simplified models could replicate any significant change in neutron flux paired with the change in experimental fuel temperature. While it was hypothesized that neutrons traveling from the fuel into the moderator water could result in thermalization of neutrons that return to the fuel and interact differently, there was no change in neutron flux for any containment vessel model between temperature when comparing simulations with and without an energy cut card. Also, for each of the simple models, directionally biased simulations also showed no significant change in neutron flux corresponding to changes in fuel temperature.

With no insight as to what produced the original 10% change in observed neutron flux when changing the experimental fuel temperature within the Full-Core model, the

investigation moved to look at the only remaining source definition option not yet analyzed: angular source particle biasing. As previously discussed, the source particles in the Full-Core model need to be directionally biased towards the north-viewing slot to allow simulations to run to completion in a realistic time frame. However, when setting the directional vector for source particles, the user can also set the cosine of angular rotation about that vector to create an angular distribution.

Two variations of the Full-Core model were constructed only changing the angular distribution of the directional bias. The first model used an angular distribution of 3.1°, which was the largest angle that provided a direct streaming line from the experimental fuel in mSERTTA unit #2 to the opening of the front collimator. The second model used a much wider angular distribution of 39.5°. The comparison of these two angular distributions is shown in Figure 45. The first model's distribution is shown in purple, and the second model's distribution is shown in white.

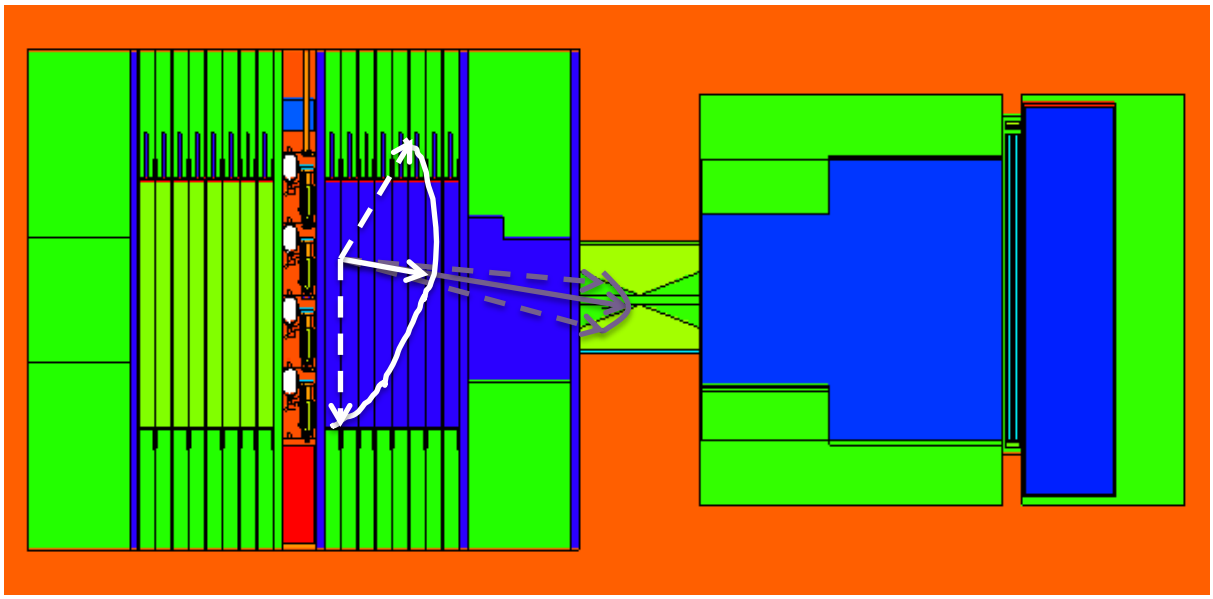

Figure 45. Elevation view of the Full-Core model with an angular distribution of the characteristic bias vector. Dotted lines represent the largest deviation from the directional vector.

The two models were simulated with the same source as previous Full-Core models for with $1x10^{11}$ particles. The resulting total neutron flux profiles at 593 K for the narrow-angle and the wide-angle models are shown in Figure 46 and Figure 47, respectively.

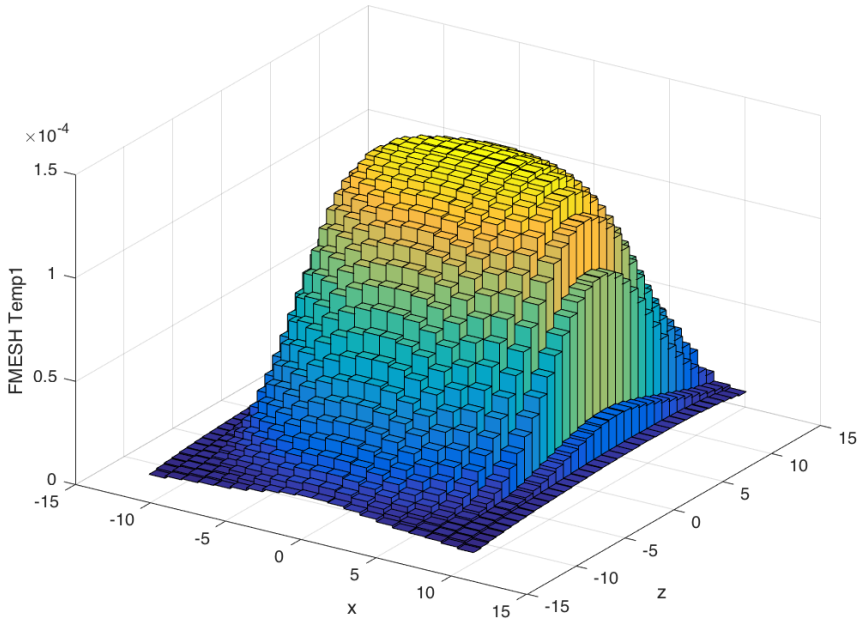

Figure 46. Total neutron flux profile observed for narrow angular distribution of 3.1°.

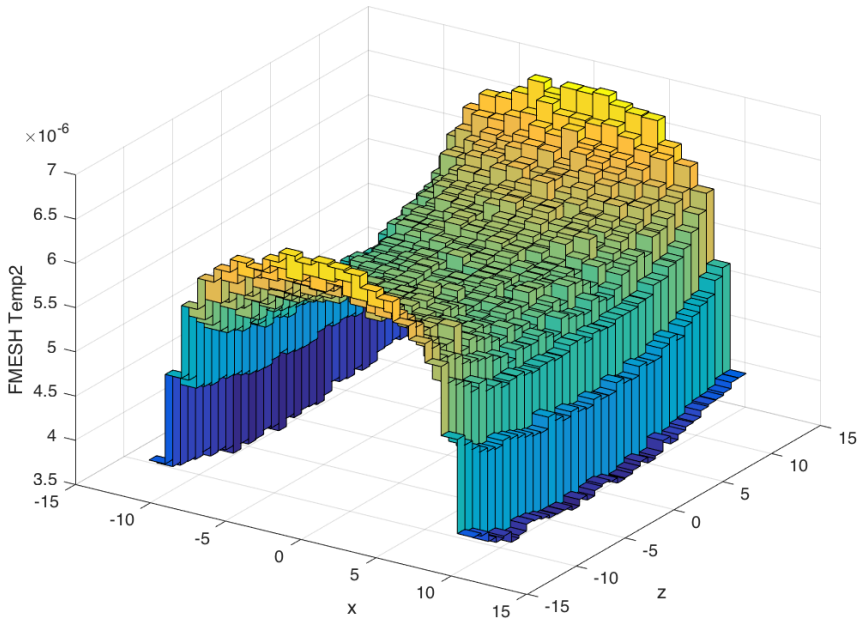

Figure 47. Total neutron flux profile observed for wide angular distribution of 39.5°.

These two spatial profiles are drastically different, which is expected because of the change in angular distribution about the same directional biasing vector. However, when the difference between the observed total neutron fluxes at different temperatures is plotted for each model, drastic results are shown. The narrow angle model shows a 35% decrease in observed neutron flux between temperatures of 593 K and 2500 K. By comparison, the wide angel model shows only a 0.3% decrease and more accurately aligns with results from the simplified models. These differences in total neutron flux profiles at 593 K for the narrow-angle and the wide-angle models are shown in Figure 48 and Figure 49, respectively.

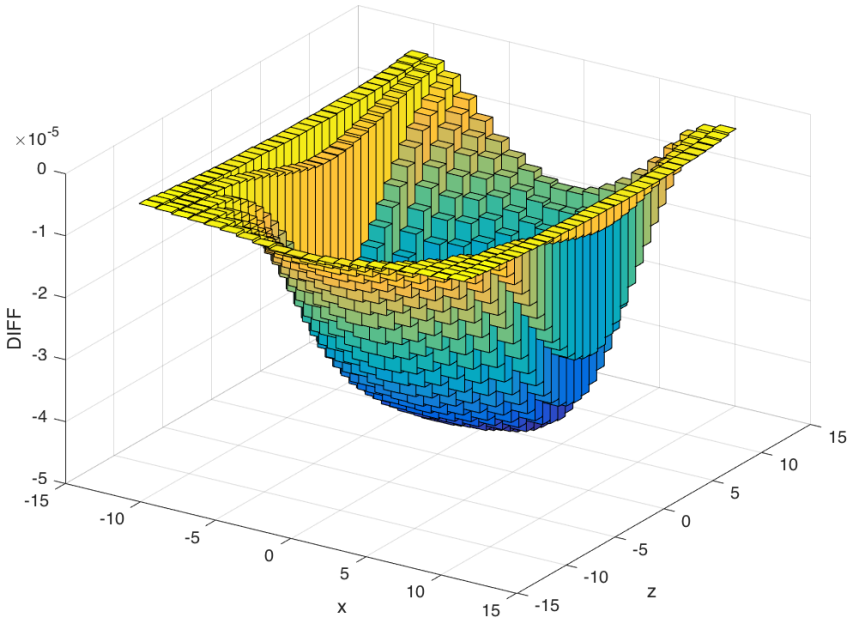

Figure 48. Difference in total neutron flux between simulations at 593 K and 2500 K for narrow angular distribution of 3.1°. Peak change is roughly 35% with a peak error of 0.04%.

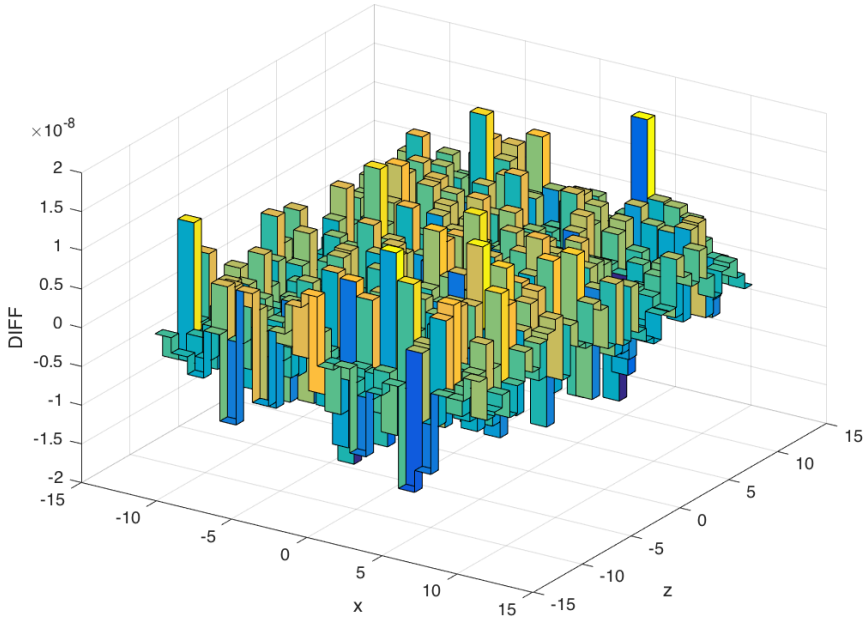

Figure 49. Difference in total neutron flux between simulations at 593 K and 2500 K for wide angular distribution of 39.5°. Peak change is roughly -0.2% with a peak error of 0.84%.

To show this change in angular distribution causes the change in mesh tally values at two different temperatures, a third model with an angle of 27.8°. The model was simulated with the same source as previous models for with $1x10^{11}$ particles. The resulting total neutron flux profiles at 593 K and the difference between the flux profiles at 593 K and 2500 K are shown in Figure 50 and Figure 51, respectively.

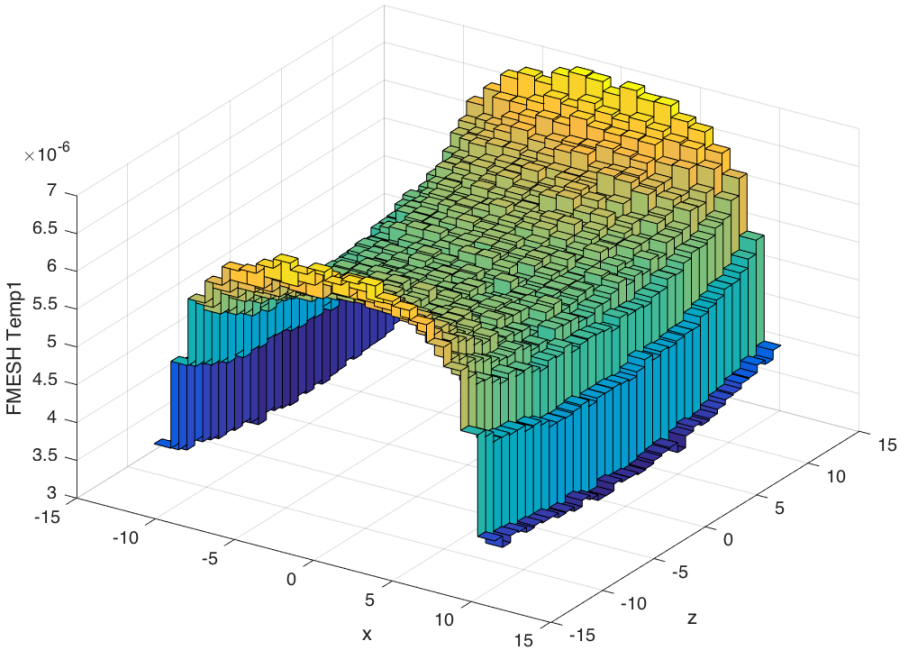

Figure 50. Total neutron flux profile observed for narrow angular distribution of 27.8° at 593 K.

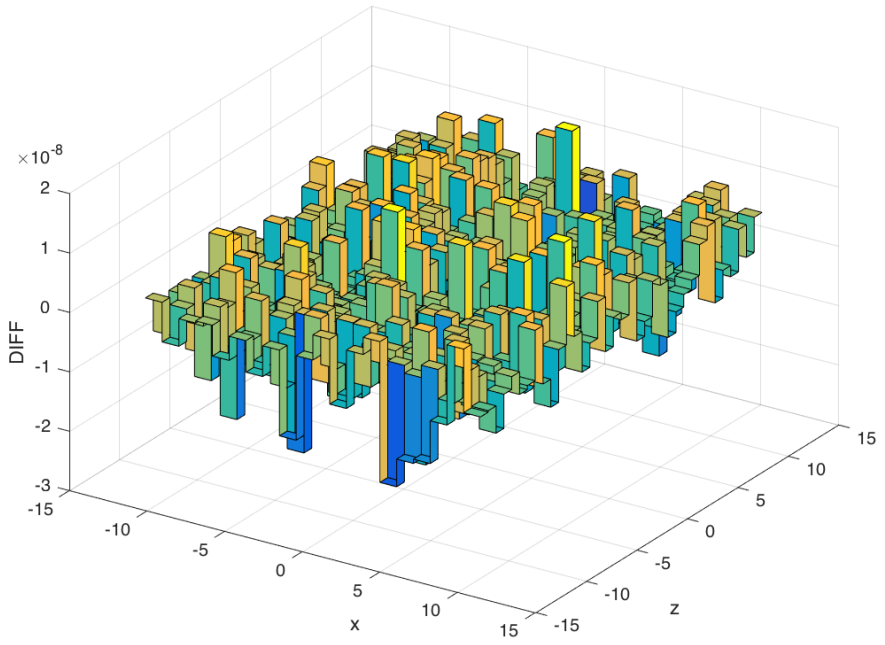

Figure 51. Difference in total neutron flux between simulations at 593 K and 2500 K for wide angular distribution of 27.8°. Peak change is roughly -2.6% with a peak error of 0.81%.

This showed a peak change of roughly -2.6% between temperatures of 593 K and 2500 K with an error of 0.81%. For the same number of particles with the same source definition, these three simulations show that the change in the angular distribution bias of a source definition results in different neutron fluxes at different temperatures.

7.3.6 Investigation of Lost Particles

While the angular distribution showed a change in the neutron flux observed at the front of the front collimator at two different temperatures, something still did not agree with the simplified models. In all the simplified models, an angular source and a biased source model was simulated with the same energy definition and number of particles. While the flux tally changed between the isotropic and angular biased simulations, the difference between temperatures for each model did not change. Initially, this was attributed to the complexity of the Full-Core model; however, something was overlooked.

As MCNP models become increasingly complex, a particle history will just become "lost" within the model. Generally, this occurs at poorly defined boundaries within the model geometry; however, complex models may just lose particle histories as prescribed in random chance. MCNP has a default setting for this number, and the run will terminate with statistical output if that number is reached by non-geometry lost particles.

In the first Full-Core model, the simulation was initiated for $1x10^{10}$ particles. As the simulation approached this number of particles, it lost its 10^{th} particle, the threshold within MCNP. The run concluded after $9.99x10^{9}$ particles, falling roughly 40,000 particles short of the full simulation. Similarly, the next simulation with $1x10^{11}$ particles was concluded after roughly $2.99x10^{10}$ particles. This resulted in the neutron flux difference between temperatures inconsistent as 3.1% and 35%, respectively.

To account for this, a feature was incorporated into the models to correct this. Declaring a lost neutron count allows the threshold to be set higher than the MCNP default of 10 particles. These two simulations, with an angular distribution of 3.1°, were rerun with a threshold of 200 lost particles. Each of the simulations was able to run to completion of $1x10^{10}$ and $1x10^{11}$ particles, respectively.

The neutron flux tallies were almost identical, regardless of particle number or temperature. Figure 52 through Figure 54 shows the difference between the simulations with $1x10^{10}$ particles, $1x10^{11}$ particles, and the comparison between the two simulations at 593 K. The difference is around $1x10^{-8}$, and the relative error is roughly $1x10^{-4}$.

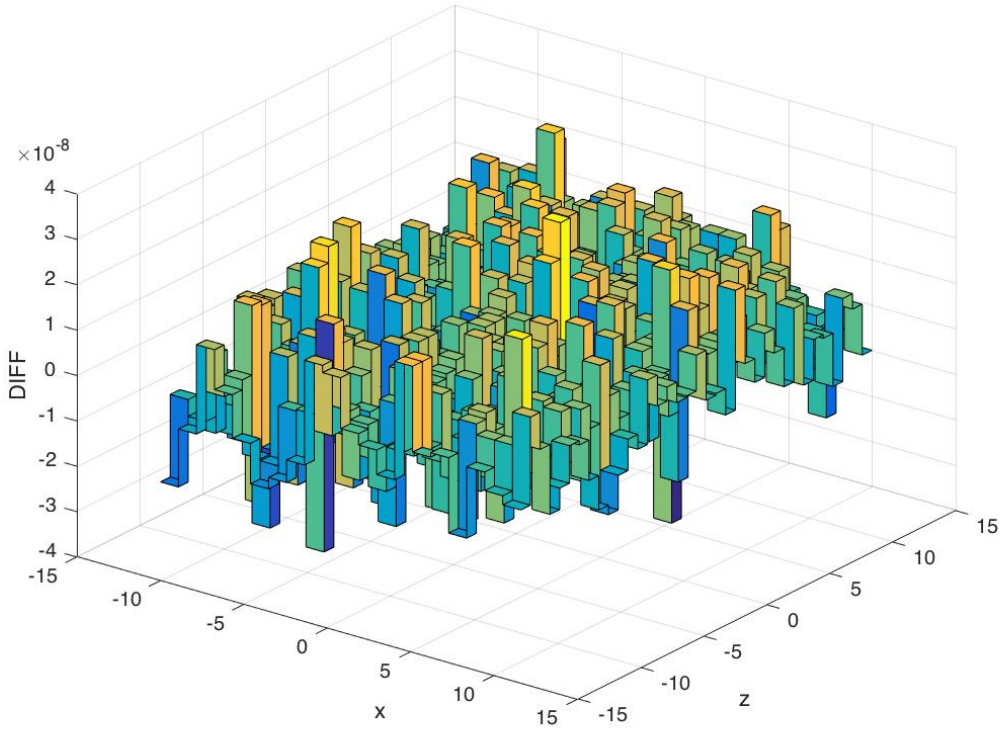

Figure 52. Difference between neutron flux tallies at the front collimator between 593 K and 2500 K for $1x10^{10}$ particles.

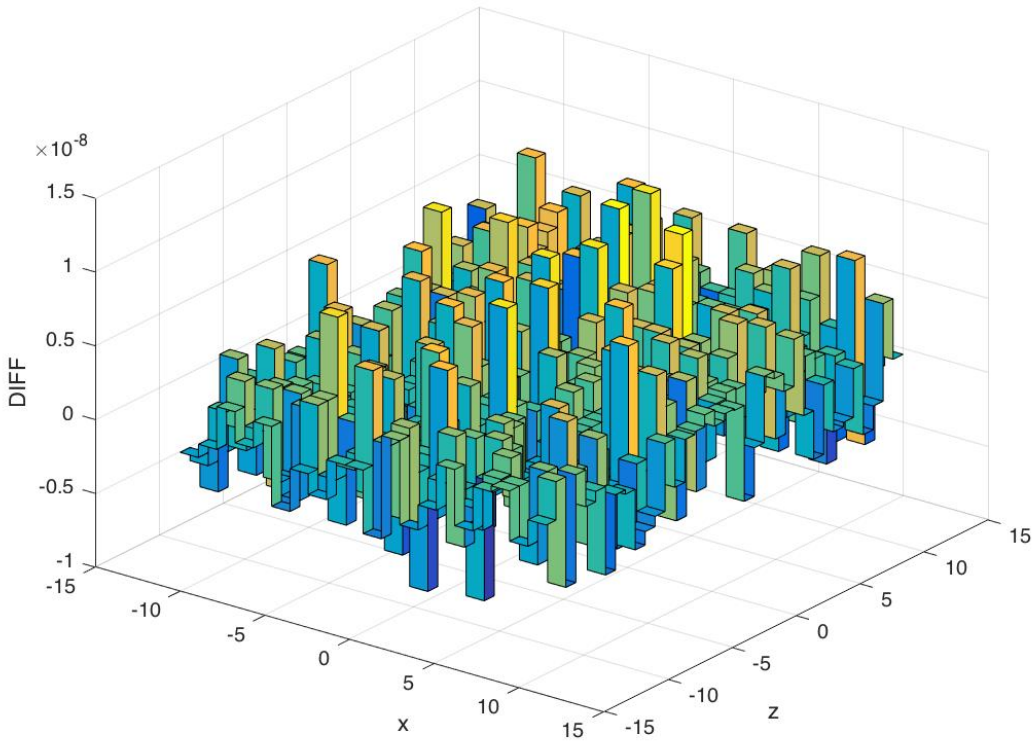

Figure 53. Difference between neutron flux tallies at the front collimator between 593 K and 2500 K for $1x10^{11}$ particles.

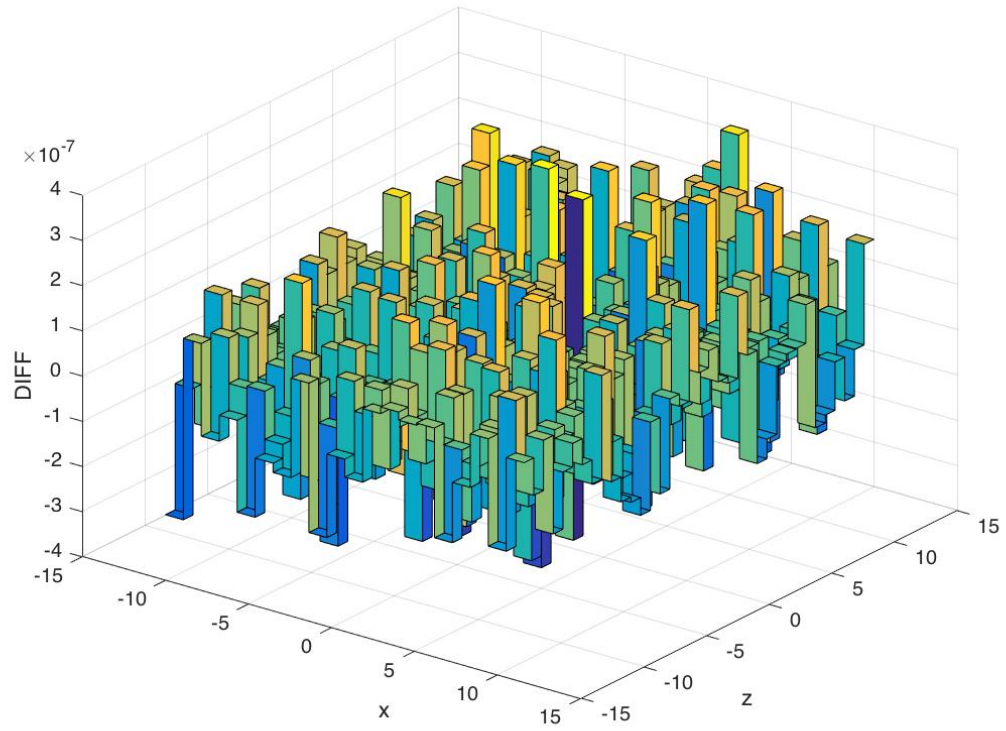

Figure 54. Difference between neutron flux tallies at the front collimator between simulations at $1x10^{10}$ particles and $1x10^{11}$ particles.

The differences show that the number of lost particles inappropriately normalized the number of particles. This error could have been propagated into the angular distribution to provide another false positive explanation for the change in neutron flux. These results more accurately demonstrate the trends from the simplified models, showing that the change in temperature within the experimental test tray does not affect the observed neutron flux.

8. CONCLUSIONS AND RECOMMENDATIONS

While the initial exercise of the Full-Core model showed a change in the temperature of the mSERTTA fuel causes a change in the neutron flux observed at the front collimator, these results could not be replicated using simplified mSERTTA models. Exercising the Full-Core model with different angular distributions of source particles showed a change in neutron flux when the temperature of the mSERTTA fuel was increased. However, as the angular distribution was widened to approach a truly isotropic distribution that would occur during actual testing conditions, the change in neutron flux observed with change with a change of temperature in the experimental fuel is less than the stochastic uncertainty of the simulation.

It is believed that the first exercises demonstrating a change in neutron flux with a change in the mSERTTA fuel temperature was a false positive result, attributable to the angular distribution biasing of the source particles. Based on the simulation results from the simplified models in conjunction with the Full-Core model simulations with varied angular distributions, it is concluded that a change temperature in the mSERTTA experimental fuel will not cause a significant change in the neutron flux characteristics at the front of the front collimator. For all isotropic simulations, there was no difference between neutron fluxes observed at different temperatures that were greater than the stochastic error of the simulations.

This study did have limitations. While various simulations approached an isotropic angular distribution, a Full-Core model could not be simulated with a fully

isotropic source definition because of the computational time this simulation would require. However, because simplified models did not show a change in neutron flux with for any isotropic simulations, it is believed that this would not have an effect in the Full-Core model. When the Full-Core model was simulated to completion, this observation was verified.

This study was also only concerned with the neutron flux response to the change in mSERTTA fuel temperature. It does not account for flux shaping or temperature response within the entire TREAT reactor core. Investigations to flux shaping and temperature coefficients for full core simulations should be done with the Full-Core model to ensure that the core does not drastically modify the mSERTTA fuel more than the temperature spike during transience.

Finally, it is still not fully understood why the change in angular distribution of source particles drastically affected neutron flux change when only the temperature of the mSERTTA fuel was modified. Simple model investigations demonstrated that it was not an effect of streaming fast neutrons overwhelming the observed total neutron flux, as there is still a minimal change in neutron flux when temperature of the mSERTTA fuel is modified using an energy cut card and without an energy cut card. Further investigations should be initiated to define the effect of angular distribution on source particle definition, both within a simulation framework and an MCNP code-debugging framework. This will allow for the verification that the change in neutron flux was caused by the definition of the source particles and not because of temperature change within the mSERTTA experimental fuel.

REFERENCES

[1] W. R. Robinson, and T. H. Bauer. *The M8 Power Calibration Experiment (M8CAL)*. ANL-IFR-232, Idaho National Laboratory, Idaho Falls, ID (1994). Print.

[3] J. D. Bess, and M. D. DeHart. "Baseline Assessment of TREAT for Modeling and Analysis Needs". INL/EXT-15-35372, Idaho National Laboratory, Idaho Falls, ID (2015). Print.

[4] M. D. DeHart. "TREAT Modeling and Simulation using MAMMOTH". Nuclear Engineering Seminar, Texas A&M Univeristy, 20 October 2015, Animal Industries Engineering Building, College Station, TX. Keynote Address.

[5] G. A. Freund, P. Elias, D. R. MacFarlane, J. D. Geier, J. F. Boland. "Design Summary Report on the Teansient Reactor Test Facility TREAT". ANL-6034, Argonne National Laboratory (1960). Print.

[6] A. De Volpi, R. R. Stewart, J. P. Regis, G. S. Stanford, E. A. Rhodes. "Fast-Neutron Hodoscope at TREAT: Data Processing, Analysis, and Results". *Nuclear Technology,* **30**, 398-421 (1976). Print.

[7] C. M. Hill, J. D. Bess, N. E. Woolstenhulme, J. R. Parry, S. E. Bays. "MCNP Water Physics Scoping Study to Support LWR Accident Tolerant Fuel Testing in TREAT". *PHYSOR 2016*, Sun Valley, ID, May 2016. Print.

[8] A. Beasley, C. Hill, G. Housley, C. Jensen, R. O'Brien, N. Woolstenhulme. *Treat Water Loop Status Report*. INL/LTD-15-36768, Idaho National Laboratory, Idaho Falls, ID (2015). Print.

[9] K. E. Holbert. "Thermal Neutrons". EEE460 Course Notes, Arizona State University (2013). Print.

[10] "Doppler Broadening of Resonances". *Reactor Physics*, Doppler Broadening-Doppler Effect. 10 February 2017. Web. http://www.nuclear-power.net/glossary/doppler-broadening/

[11] W. Stacey. *Nuclear Reactor Physics*. Wiley-VCH, Weinheim, Germany (2007). Print.

[12] F. B. Brown, W. R. Martin, G. Yesilyurt, S. A. Wilderman. "Progress with On-The-Fly Neutron Doppler Broadening in MCNP". LA-UR-12-22277, *2012 American Nuclear Society Summer Meeting*, Chicago, IL, June 24-28 (2012). Print.

[13] D. B. Pelowitz. *MCNP User's Manual*. LA-CP-13-00634, Vol. 1, pp. 119-122, Los Alamos National Laboratory, Los Alamos, NM (2013). Print.

[14] K. Shultis, R. E. Faw. *An MCNP Primer*. Mechanical and Nuclear Engineering Department, Kansas State University, Manhattan, KS (2011). Print.

[15] R. E. Macfarlane, A. C. Kahler. "Methods for Processing ENDF/B-VII with NJOY". LA-UR-10-04652, *Nuclear Data Sheets*, Vol. 111, (2010) 2739-2890. Print.

[16] F. B. Brown, W. R. Martin, G. Yesilyurt, S. A. Wilderman. “On-The-Fly Neutron Doppler Broadening for MCNP”. LA-UR-12-20338, Los Alamos National Laboratory, Los Alamos, NM (2012).

[17] W. R. Martin, G. Yesilyurt, F. B. Brown, S. A. Wilderman. *Implementation of On-the-Fly Doppler Broadening in MCNP for Multiphysics Simulation of Nuclear Reactors,* pp. 6-11, United States Department of Energy, Washington, DC (2012).

[18] W. R. Robinson, R. J. Page, A E. Wright. “TREAT NPR Calibration Experiment AN-CAL”. ANL/NPR-92/11, Argonne National Laboratory, Chicago, IL (1992).

APPENDIX A. SIMPLIFIED MODELS

A.1 mSERTTA Fuel Rodlet

```
mSERTTA Simplified Model
c by L. Scott
c The purpose of this model is to test the simplified neutronic response
c attributable directly to the temperature change. This will test various
c neutron cross sections, the OTFDB function, and the "tmp" declaration on the
c cell cards. The following are the ZAID numbers for materials tested.
c
c   -------------------- Doppler Broadening Temperatures --------------------
c   |                                                                        |
c   |  [ZAID].80c  --->  293.6 K   (original file)                           |
c   |  [ZAID].81c  --->  600.0 K                                             |
c   |  [ZAID].84c  --->  2500.0 K                                            |
c   |  [ZAID].70c  --->  On-the-Fly Doppler Broadening                       |
c   |                                                                        |
c   --------------------------------------------------------------------------
c
c ---------- Cell Cards ----------
c
c --------- Unit 1 (Top) ---------
c ------------ LEUO2 Fuel Pellets ------------
61001 6001 6.9759E-02  -60001  imp:n=1 tmp=5.11138E-08 $ Fuel Pellet 1 (Bottom)
(Top)
c
c ------------ Fuel Pin ------------
61041 6610 5.8248E-04  60001  -60041  imp:n=1 tmp=5.11138E-08 $ Helium Gap
61042 6700 8.6596E-02  -60044  imp:n=1 tmp=5.11138E-08 $ SS316 Spring
61043 6620 4.3360E-02  60041 60044 -60045  imp:n=1 tmp=5.11138E-08 $ Zr-4 Pin
Clad
61044 6620 4.3360E-02  -60042  imp:n=1 tmp=5.11138E-08 $ Zr-4 Fuel Pin End Tip
61045 6620 4.3360E-02  -60043  imp:n=1 tmp=5.11138E-08 $ Zr-4 Lower End Cap
61046 6620 4.3360E-02  -60046  imp:n=1 tmp=5.11138E-08 $ Zr-4 Upper End Cap
c
c ---------- Outside Universes ----------
999   0                -999    imp:n=1 tmp=5.11138E-08 $ f-mesh pipe
c
9998  0                -9999 #61001 #61041 #61042 #61043 #61044 #61045 #61046
                            #999  imp:n=1 tmp=5.11138E-08   $ Inside Universe
9999  0                +9999       imp:n=0 tmp=5.11138E-08   $ Outside Universe
c

c ---------- Surface Cards ----------
c --- Experimental Facilities ------------------------------------------------
-
c ------ Fuel Pin ------
c --------- Fuel Pellets ---------
60001 rcc 0 0 -5.080   0 0 10.16   0.41   $ Fuel Pellet #1 (Bottom)
c
60041 rcc 0 0 -5.080   0 0 10.16   0.415  $ Fuel/Clad Gap
60042 rcc 0 0 -7.0104  0 0 1.2954  0.159  $ Fuel Pin End Tip
60043 rcc 0 0 -5.715   0 0 0.635   0.475  $ Lower End Cap
60044 rcc 0 0 +5.080   0 0 0.635   0.415  $ Spring
```

```
60045 rcc 0 0 -5.08    0 0 10.795  0.475  $ Outer Clad Surface
60046 rcc 0 0 +5.715   0 0 0.635   0.475  $ Upper End Cap
c
999   RPP -1.07823 0 168.474 169.474 -0.775266667 0             $ f4 box
c
9999  SO   205                                                  $ Outside
Border

c
c ---------- Data Cards ----------
c --- Physics Cards ---
mode n
sdef pos=0 0 0 axs=0 0 1 ext=d3 rad=d2 erg=d6
SI2 0 0.41
SP2 -21 1
SI3 -5.08 5.08
SP3 -21 0
SI6 H
SP6 -3  0.965 2.29
nps 1e10
c --- Experimental ------------------------------------------------------------
-
c ------ UO2 Fuel Pellets (4.95% U-235) ------
m6001  8016.81c 4.6489E-02   8017.81c 1.7672E-05  92234.81c 7.0909E-06
      92235.81c 1.1650E-03  92236.81c 1.4061E-05  92238.81c 2.2067E-02
c         Total 6.9759E-02
mt6001 o2-u.20t u-o2.20t
c
c ------ Fuel-Clad Gap (Helium 350 psi 300 K) ------
m6610  2003.81c 7.8052E-10  2004.81c 5.8247E-04
c         Total 5.8248E-04
c
c ------ Zircaloy-4 Clad ------
m6620 50112.81c 4.6806E-06  50114.81c 3.1848E-06  50115.81c 1.6406E-06
      50116.81c 7.0161E-05  50117.81c 3.7059E-05  50118.81c 1.1687E-04
      50119.81c 4.1450E-05  50120.81c 1.5721E-04  50122.81c 2.2342E-05
      50124.81c 2.7939E-05  26054.81c 8.6830E-06  26056.81c 1.3631E-04
      26057.81c 3.1479E-06  26058.81c 4.1892E-07  24050.81c 3.3012E-06
      24052.81c 6.3660E-05  24053.81c 7.2186E-06  24054.81c 1.7969E-06
      28058.81c 1.6037E-06  28060.81c 6.1775E-07  28061.81c 2.6853E-08
      28062.81c 8.5620E-08  28064.81c 2.1805E-08  13027.81c 5.4906E-06
       5010.81c 1.8179E-08   5011.81c 7.3174E-08  48106.81c 1.0982E-10
      48108.81c 7.8194E-11  48110.81c 1.0974E-09  48111.81c 1.1246E-09
      48112.81c 2.1200E-09  48113.81c 1.0736E-09  48114.81c 2.5242E-09
      48116.81c 6.5806E-10  20040.81c 1.4333E-06  20042.81c 9.5662E-09
      20043.81c 1.9960E-09  20044.81c 3.0843E-08  20046.81c 5.9142E-11
      20048.81c 2.7649E-09   6000.81c 4.4404E-05  27059.81c 6.7033E-07
      29063.81c 1.0747E-06  29065.81c 4.7947E-07  72174.81c 1.7706E-09
      72176.81c 5.8209E-08  72177.81c 2.0584E-07  72178.81c 3.0189E-07
      72179.81c 1.5072E-07  72180.81c 3.8821E-07   1001.81c 4.8987E-05
       1002.81c 5.6341E-09  12024.81c 1.2839E-06  12025.81c 1.6254E-07
      12026.81c 1.7895E-07  25055.81c 1.7977E-06  42092.81c 1.5205E-07
      42094.81c 9.5015E-08  42095.81c 1.6368E-07  42096.81c 1.7171E-07
      42097.81c 9.8412E-08  42098.81c 2.4902E-07  42100.81c 9.9545E-08
      41093.81c 2.1261E-06   7014.81c 1.1241E-05   7015.81c 4.1066E-08
      14028.81c 7.7832E-06  14029.81c 3.9539E-07  14030.81c 2.6095E-07
      74180.81c 1.2893E-09  74182.81c 2.8473E-07  74183.81c 1.5375E-07
      74184.81c 3.2921E-07  74186.81c 3.0546E-07  22046.81c 1.6674E-07
      22047.81c 1.5037E-07  22048.81c 1.4899E-06  22049.81c 1.0934E-07
      22050.81c 1.0469E-07  92234.81c 1.5684E-12  92235.81c 2.0923E-10
```

```
      92238.81c 2.8833E-08  40090.81c 2.1875E-02  40091.81c 4.7704E-03
      40092.81c 7.2917E-03  40094.81c 7.3895E-03  40096.81c 1.1905E-03
c         Total 4.3360E-02
mt6620 al27.22t fe56.22t
c
c ------ Stainless Steel 316 ------
m6700  6000.81c 2.0056E-04  25055.81c 8.7693E-04  15031.81c 5.9323E-04
      16032.81c 3.0137E-05  16033.81c 1.9890E-05  16034.81c 3.4997E-05
      16036.81c 2.1408E-05  14028.81c 1.6903E-07  14029.81c 9.5783E-07
      14030.81c 2.2537E-09  24050.81c 6.8439E-04  24052.81c 1.3198E-02
      24053.81c 1.4965E-03  24054.81c 3.7252E-04  42092.81c 1.8542E-04
      42094.81c 1.1587E-04  42095.81c 1.9961E-04  42096.81c 2.0940E-04
      42097.81c 1.2002E-04  42098.81c 3.0368E-04  42100.81c 1.2140E-04
      28058.81c 6.7055E-03  28060.81c 2.5829E-03  28061.81c 1.1228E-04
      28062.81c 3.5799E-04  28064.81c 9.1170E-05   7014.81c 1.7135E-04
       7015.81c 6.2600E-07  26054.81c 3.3778E-03  26056.81c 5.3024E-02
      26057.81c 1.2246E-03  26058.81c 1.6297E-04
c         Total 8.6596E-02
mt6700 fe56.22t
c
c ---------- OTF Doppler Definition ----------
c OTFDB     8016.70c 8017.70c 92234.70c 92235.70c 92236.70c 92238.70c
c           1001.70c 3006.70c 1002.70c 5010.70c 3007.70c 5011.70c
c           50112.70c 50116.70c 50119.70c 50124.70c 26057.70c
c           24052.70c 28058.70c 28062.70c 48108.70c 48112.70c
c           48116.70c 20043.70c 20048.70c 29063.70c 72176.70c
c           72179.70c 12026.70c 42094.70c 42097.70c 41093.70c 14028.70c
c           74184.70c 22047.70c 22050.70c 40092.70c 50114.70c
c           50117.70c 50120.70c 26054.70c 26058.70c 24053.70c 28060.70c
c           28064.70c 48110.70c 48113.70c 20040.70c 20044.70c 6000.70c
c           29065.70c 72177.70c 72180.70c 12024.70c 25055.70c 42095.70c
c           42098.70c 7014.70c 14029.70c 74182.70c 74186.70c 22048.70c
c           40090.70c 40094.70c 50115.70c 50118.70c 50122.70c 26056.70c
c           24050.70c 24054.70c 28061.70c 13027.70c 48106.70c 48111.70c
c           48114.70c 20042.70c 20046.70c 27059.70c 72174.70c 72178.70c
c           12025.70c 42092.70c 42096.70c 42100.70c 7015.70c 14030.70c
c           74183.70c 22046.70c 22049.70c 40091.70c 40096.70c
c            2003.70c 2004.70c 16032.70c 16036.70c 16033.70c 15031.70c
c           16034.70c 73181.70c 18038.70c 18040.70c
c
c ---------- Tallies ----------
c ---------- Mesh Tally ----------
fmesh204:n GEOM=xyz origin= -10.7823 168.474 -13.9548
          IMESH= +10.7823 IINTS= 20
          JMESH= +169.474 JINTS= 1
          KMESH= +13.9548 KINTS= 36
          EMESH  0.1, 0.5, 1.00, 1.50, 1.75, 2.00
c
f04:n 999
e0      0.10 0.15 0.20 0.25 0.30 0.35 0.40 0.45 0.50 0.55 0.60 0.65 0.70 0.75
        0.80 0.85 0.90 0.95 1.00 1.05 1.10 1.15 1.20 1.25 1.30 1.35 1.40 1.45
        1.50 1.55 1.60 1.65 1.70 1.75 1.80 1.85 1.90 1.95 2.00 2.05 2.10 2.15
        2.20 2.25 2.30 2.35 2.40 2.45 2.50 2.55 2.60 2.65 2.70 2.75 2.80 2.85
        2.90 2.95 3.00 3.05 3.10
c
c
c e0    3.00E-09 5.00E-09 6.90E-09 1.00E-08 1.50E-08 2.00E-08 2.50E-08 3.00E-08
c      3.50E-08 4.20E-08 5.00E-08 5.80E-08 6.70E-08 7.70E-08 8.00E-08 9.50E-08
c      1.00E-07 1.15E-07 1.34E-07 1.40E-07 1.60E-07 1.80E-07 1.89E-07 2.20E-07
c      2.48E-07 2.80E-07 3.00E-07 3.15E-07 3.20E-07 3.50E-07 3.91E-07 4.00E-07
```

```
c      4.33E-07 4.85E-07 5.00E-07 5.40E-07 6.25E-07 7.05E-07 7.80E-07 7.90E-07
c      8.50E-07 8.60E-07 9.10E-07 9.30E-07 9.50E-07 9.72E-07 9.86E-07 9.96E-07
c      1.02E-06 1.04E-06 1.05E-06 1.07E-06 1.10E-06 1.11E-06 1.12E-06 1.15E-06
c      1.17E-06 1.24E-06 1.30E-06 1.34E-06 1.37E-06 1.44E-06 1.48E-06 1.50E-06
c      1.59E-06 1.67E-06 1.76E-06 1.84E-06 1.93E-06 2.02E-06 2.10E-06 2.13E-06
c      2.36E-06 2.55E-06 2.60E-06 2.72E-06 2.77E-06 3.30E-06 3.38E-06 4.00E-06
c      4.13E-06 5.04E-06 5.35E-06 6.16E-06 7.52E-06 8.32E-06 9.19E-06 9.91E-06
c      1.12E-05 1.37E-05 1.59E-05 1.95E-05 2.26E-05 2.50E-05 2.76E-05 3.05E-05
c      3.37E-05 3.73E-05 4.02E-05 4.55E-05 4.83E-05 5.16E-05 5.56E-05 6.79E-05
c      7.57E-05 9.17E-05 1.37E-04 1.49E-04 2.04E-04 3.04E-04 3.72E-04 4.54E-04
c      6.77E-04 7.49E-04 9.14E-04 1.01E-03 1.23E-03 1.43E-03 1.51E-03 2.03E-03
c      2.25E-03 3.35E-03 3.53E-03 5.00E-03 5.53E-03 7.47E-03 9.12E-03 1.11E-02
c      1.50E-02 1.66E-02 2.48E-02 2.74E-02 2.93E-02 3.70E-02 4.09E-02 5.52E-02
c      6.74E-02 8.23E-02 1.11E-01 1.23E-01 1.83E-01 2.47E-01 2.73E-01 3.02E-01
c      4.08E-01 4.50E-01 4.98E-01 5.50E-01 6.08E-01 8.21E-01 9.07E-01 1.00E+00
c      1.11E+00 1.22E+00 1.35E+00 1.65E+00 2.02E+00 2.23E+00 2.47E+00 3.01E+00
c      3.68E+00 4.49E+00 5.49E+00 6.07E+00 6.70E+00 8.19E+00 1.00E+01 1.16E+01
c      1.38E+01 1.49E+01 1.73E+01 1.96E+01   $ Energy bins for Tallies
```

A.2 Moderator Containment Vessel

```
mSERTTA Simplified Model
c by L. Scott
c The purpose of this model is to test the simplified neutronic response
c attributable directly to the temperature change. This will test various
c neutron cross sections, the OTFDB function, and the "tmp" declaration on the
c cell cards. The following are the ZAID numbers for materials tested.
c
c   -------------------- Doppler Broadening Temperatures --------------------
c   |                                                                        |
c   |  [ZAID].80c  --->  293.6 K   (original file)                           |
c   |  [ZAID].81c  --->  600.0 K                                             |
c   |  [ZAID].84c  --->  2500.0 K                                            |
c   |  [ZAID].70c  --->  On-the-Fly Doppler Broadening                       |
c   |                                                                        |
c   --------------------------------------------------------------------------
c
c ---------- Cell Cards ----------
c
c --------- Unit 1 (Top) ---------
c ------------ LEUO2 Fuel Pellets ------------
61001 6001 6.9759E-02  -60001  imp:n=1 tmp=5.11138E-08 $ Fuel Pellet 1 (Bottom)
(Top)
c
c ------------ Fuel Pin ------------
61041 6610 5.8248E-04  60001  -60041  imp:n=1 tmp=5.11138E-08 $ Helium Gap
61042 6700 8.6596E-02  -60044  imp:n=1 tmp=5.11138E-08 $ SS316 Spring
61043 6620 4.3360E-02  60041 60044 -60045  imp:n=1 tmp=5.11138E-08 $ Zr-4 Pin
Clad
61044 6620 4.3360E-02  -60042  imp:n=1 tmp=5.11138E-08 $ Zr-4 Fuel Pin End Tip
61045 6620 4.3360E-02  -60043  imp:n=1 tmp=5.11138E-08 $ Zr-4 Lower End Cap
61046 6620 4.3360E-02  -60046  imp:n=1 tmp=5.11138E-08 $ Zr-4 Upper End Cap
c
c ------------ Medium in Primary Vessel ------------
61198 7 6.8309E-02  -60199 (-60601:-60603) #61001 #61041
                    #61042 #61043 #61044 #61045
                    #61046 imp:n=1 tmp=5.11138E-08 $ Water
c
c ---------- Outside Universes ----------
998   0                -998        imp:n=1 tmp=5.11138E-08 $ f4 tally box
c 999   0                -999  #998  imp:n=1 tmp=5.11138E-08 $ f-mesh pipe
c
9997  0                +9997 -9999          imp:n=1 tmp=5.11138E-08   $ Shell
9998  0                -9999  #61001 #61041 #61042 #61043 #61044 #61045
                              #61046 #61198 #998 #9997
                                           imp:n=1 tmp=5.11138E-08   $ Inside
Universe
9999  0                +9999                imp:n=0 tmp=5.11138E-08   $ Outside
Universe
c

c ---------- Surface Cards ----------
c --- Experimental Facilities ----------------------------------------------
-
c ------ Fuel Pin ------
c --------- Fuel Pellets ---------
60001 rcc 0 0 -5.080   0 0 10.16   0.41   $ Fuel Pellet #1 (Bottom)
c
```

```
60041 rcc 0 0 -5.080   0 0 10.16   0.415  $ Fuel/Clad Gap
60042 rcc 0 0 -7.0104  0 0 1.2954  0.159  $ Fuel Pin End Tip
60043 rcc 0 0 -5.715   0 0 0.635   0.475  $ Lower End Cap
60044 rcc 0 0 +5.080   0 0 0.635   0.415  $ Spring
60045 rcc 0 0 -5.08    0 0 10.795  0.475  $ Outer Clad Surface
60046 rcc 0 0 +5.715   0 0 0.635   0.475  $ Upper End Cap
c
c ------ Primary Vessel Internals ------
60199 pz 7.496
c
60601 rcc 0 0.000 -7.695    0 0 22.015   2.625  $ Main Vessel ID
60602 rcc 0 0.000 -7.695    0 0 22.015   3.015  $ Main Vessel OD
60603 sph 0 0.000 -7.695                 2.625  $ Vessel Cup ID
c
998   RPP -1.07823 0 168.474 169.474 -0.775266667 0             $ f4 box
c 999   RPP -10.7823 +10.7823 +1.000 +169.974 -13.9548 +13.9548   $ f-mesh pipe
c
9997  SO   204                                                   $ Shell
9999  SO   205                                                   $ Outside
Border

c
c ---------- Data Cards ----------
c --- Physics Cards ---
mode n
sdef pos=0 0 0 axs=0 0 1 ext=d3 rad=d2 erg=d6
SI2 0 0.41
SP2 -21 1
SI3 -5.08 5.08
SP3 -21 0
SI6 H
SP6 -3  0.965 2.29
nps 1e10
c cut:n j 0.099
c --- Experimental ------------------------------------------------------------
-
c ------ UO2 Fuel Pellets (4.95% U-235) ------
m6001  8016.81c 4.6489E-02   8017.81c 1.7672E-05  92234.81c 7.0909E-06
      92235.81c 1.1650E-03  92236.81c 1.4061E-05  92238.81c 2.2067E-02
c         Total 6.9759E-02
mt6001 o2-u.20t u-o2.20t
c
c ------ Fuel-Clad Gap (Helium 350 psi 300 K) ------
m6610  2003.81c 7.8052E-10  2004.81c 5.8247E-04
c         Total 5.8248E-04
c
c ------ Zircaloy-4 Clad ------
m6620 50112.81c 4.6806E-06  50114.81c 3.1848E-06  50115.81c 1.6406E-06
      50116.81c 7.0161E-05  50117.81c 3.7059E-05  50118.81c 1.1687E-04
      50119.81c 4.1450E-05  50120.81c 1.5721E-04  50122.81c 2.2342E-05
      50124.81c 2.7939E-05  26054.81c 8.6830E-06  26056.81c 1.3631E-04
      26057.81c 3.1479E-06  26058.81c 4.1892E-07  24050.81c 3.3012E-06
      24052.81c 6.3660E-05  24053.81c 7.2186E-06  24054.81c 1.7969E-06
      28058.81c 1.6037E-06  28060.81c 6.1775E-07  28061.81c 2.6853E-08
      28062.81c 8.5620E-08  28064.81c 2.1805E-08  13027.81c 5.4906E-06
       5010.81c 1.8179E-08   5011.81c 7.3174E-08  48106.81c 1.0982E-10
      48108.81c 7.8194E-11  48110.81c 1.0974E-09  48111.81c 1.1246E-09
      48112.81c 2.1200E-09  48113.81c 1.0736E-09  48114.81c 2.5242E-09
      48116.81c 6.5806E-10  20040.81c 1.4333E-06  20042.81c 9.5662E-09
      20043.81c 1.9960E-09  20044.81c 3.0843E-08  20046.81c 5.9142E-11
```

```
      20048.81c 2.7649E-09   6000.81c 4.4404E-05  27059.81c 6.7033E-07
      29063.81c 1.0747E-06  29065.81c 4.7947E-07  72174.81c 1.7706E-09
      72176.81c 5.8209E-08  72177.81c 2.0584E-07  72178.81c 3.0189E-07
      72179.81c 1.5072E-07  72180.81c 3.8821E-07   1001.81c 4.8987E-05
       1002.81c 5.6341E-09  12024.81c 1.2839E-06  12025.81c 1.6254E-07
      12026.81c 1.7895E-07  25055.81c 1.7977E-06  42092.81c 1.5205E-07
      42094.81c 9.5015E-08  42095.81c 1.6368E-07  42096.81c 1.7171E-07
      42097.81c 9.8412E-08  42098.81c 2.4902E-07  42100.81c 9.9545E-08
      41093.81c 2.1261E-06   7014.81c 1.1241E-05   7015.81c 4.1066E-08
      14028.81c 7.7832E-06  14029.81c 3.9539E-07  14030.81c 2.6095E-07
      74180.81c 1.2893E-09  74182.81c 2.8473E-07  74183.81c 1.5375E-07
      74184.81c 3.2921E-07  74186.81c 3.0546E-07  22046.81c 1.6674E-07
      22047.81c 1.5037E-07  22048.81c 1.4899E-06  22049.81c 1.0934E-07
      22050.81c 1.0469E-07  92234.81c 1.5684E-12  92235.81c 2.0923E-10
      92238.81c 2.8833E-08  40090.81c 2.1875E-02  40091.81c 4.7704E-03
      40092.81c 7.2917E-03  40094.81c 7.3895E-03  40096.81c 1.1905E-03
c         Total 4.3360E-02
mt6620 al27.22t fe56.22t
c
c ------ Stainless Steel 316 ------
m6700  6000.81c 2.0056E-04  25055.81c 8.7693E-04  15031.81c 5.9323E-04
      16032.81c 3.0137E-05  16033.81c 1.9890E-05  16034.81c 3.4997E-05
      16036.81c 2.1408E-05  14028.81c 1.6903E-07  14029.81c 9.5783E-07
      14030.81c 2.2537E-09  24050.81c 6.8439E-04  24052.81c 1.3198E-02
      24053.81c 1.4965E-03  24054.81c 3.7252E-04  42092.81c 1.8542E-04
      42094.81c 1.1587E-04  42095.81c 1.9961E-04  42096.81c 2.0940E-04
      42097.81c 1.2002E-04  42098.81c 3.0368E-04  42100.81c 1.2140E-04
      28058.81c 6.7055E-03  28060.81c 2.5829E-03  28061.81c 1.1228E-04
      28062.81c 3.5799E-04  28064.81c 9.1170E-05   7014.81c 1.7135E-04
       7015.81c 6.2600E-07  26054.81c 3.3778E-03  26056.81c 5.3024E-02
      26057.81c 1.2246E-03  26058.81c 1.6297E-04
c         Total 8.6596E-02
mt6700 fe56.22t
c
c ------ Compressed PWR Water (16 MPa 320 C) ------
m7     1001.81c 4.5496E-02   1002.81c 5.2326E-06   8016.81c 2.2742E-02
       8017.81c 8.6452E-06   5010.81c 1.1333E-05   5011.81c 4.5619E-05
       3006.81c 1.5710E-08   3007.81c 1.9127E-07
c         Total 6.8309E-02
mt7    lwtr.26t hwtr.26t
c
c ---------- OTF Doppler Definition ----------
c OTFDB     8016.70c 8017.70c 92234.70c 92235.70c 92236.70c 92238.70c
c           1001.70c 3006.70c 1002.70c 5010.70c 3007.70c 5011.70c
c           50112.70c 50116.70c 50119.70c 50124.70c 26057.70c
c           24052.70c 28058.70c 28062.70c 48108.70c 48112.70c
c           48116.70c 20043.70c 20048.70c 29063.70c 72176.70c
c           72179.70c 12026.70c 42094.70c 42097.70c 41093.70c 14028.70c
c           74184.70c 22047.70c 22050.70c 40092.70c 50114.70c
c           50117.70c 50120.70c 26054.70c 26058.70c 24053.70c 28060.70c
c           28064.70c 48110.70c 48113.70c 20040.70c 20044.70c 6000.70c
c           29065.70c 72177.70c 72180.70c 12024.70c 25055.70c 42095.70c
c           42098.70c 7014.70c 14029.70c 74182.70c 74186.70c 22048.70c
c           40090.70c 40094.70c 50115.70c 50118.70c 50122.70c 26056.70c
c           24050.70c 24054.70c 28061.70c 13027.70c 48106.70c 48111.70c
c           48114.70c 20042.70c 20046.70c 27059.70c 72174.70c 72178.70c
c           12025.70c 42092.70c 42096.70c 42100.70c 7015.70c 14030.70c
c           74183.70c 22046.70c 22049.70c 40091.70c 40096.70c
c            2003.70c 2004.70c 16032.70c 16036.70c 16033.70c 15031.70c
c           16034.70c 73181.70c 18038.70c 18040.70c
```

```
c
c ---------- Tallies ----------
c ---------- Mesh Tally ----------
fmesh204:n GEOM=xyz origin= -10.7823 168.474 -13.9548
          IMESH= +10.7823 IINTS= 20
          JMESH= +169.474 JINTS= 1
          KMESH= +13.9548 KINTS= 36
          EMESH  0.1, 0.5, 1.00, 1.50, 1.75, 2.00
c
f04:n 998
f14:n 9997
c
f12:n (60001.1 60001.2 60001.3)
SD12  27.23
f22:n 998.3
SD22  601.856569
f32:n 9999
SD32  5.28E5
e0      0.10 0.15 0.20 0.25 0.30 0.35 0.40 0.45 0.50 0.55 0.60 0.65 0.70 0.75
        0.80 0.85 0.90 0.95 1.00 1.05 1.10 1.15 1.20 1.25 1.30 1.35 1.40 1.45
        1.50 1.55 1.60 1.65 1.70 1.75 1.80 1.85 1.90 1.95 2.00 2.05 2.10 2.15
        2.20 2.25 2.30 2.35 2.40 2.45 2.50 2.55 2.60 2.65 2.70 2.75 2.80 2.85
        2.90 2.95 3.00 3.05 3.10
c
c
c e0    3.00E-09 5.00E-09 6.90E-09 1.00E-08 1.50E-08 2.00E-08 2.50E-08 3.00E-08
c      3.50E-08 4.20E-08 5.00E-08 5.80E-08 6.70E-08 7.70E-08 8.00E-08 9.50E-08
c      1.00E-07 1.15E-07 1.34E-07 1.40E-07 1.60E-07 1.80E-07 1.89E-07 2.20E-07
c      2.48E-07 2.80E-07 3.00E-07 3.15E-07 3.20E-07 3.50E-07 3.91E-07 4.00E-07
c      4.33E-07 4.85E-07 5.00E-07 5.40E-07 6.25E-07 7.05E-07 7.80E-07 7.90E-07
c      8.50E-07 8.60E-07 9.10E-07 9.30E-07 9.50E-07 9.72E-07 9.86E-07 9.96E-07
c      1.02E-06 1.04E-06 1.05E-06 1.07E-06 1.10E-06 1.11E-06 1.12E-06 1.15E-06
c      1.17E-06 1.24E-06 1.30E-06 1.34E-06 1.37E-06 1.44E-06 1.48E-06 1.50E-06
c      1.59E-06 1.67E-06 1.76E-06 1.84E-06 1.93E-06 2.02E-06 2.10E-06 2.13E-06
c      2.36E-06 2.55E-06 2.60E-06 2.72E-06 2.77E-06 3.30E-06 3.38E-06 4.00E-06
c      4.13E-06 5.04E-06 5.35E-06 6.16E-06 7.52E-06 8.32E-06 9.19E-06 9.91E-06
c      1.12E-05 1.37E-05 1.59E-05 1.95E-05 2.26E-05 2.50E-05 2.76E-05 3.05E-05
c      3.37E-05 3.73E-05 4.02E-05 4.55E-05 4.83E-05 5.16E-05 5.56E-05 6.79E-05
c      7.57E-05 9.17E-05 1.37E-04 1.49E-04 2.04E-04 3.04E-04 3.72E-04 4.54E-04
c      6.77E-04 7.49E-04 9.14E-04 1.01E-03 1.23E-03 1.43E-03 1.51E-03 2.03E-03
c      2.25E-03 3.35E-03 3.53E-03 5.00E-03 5.53E-03 7.47E-03 9.12E-03 1.11E-02
c      1.50E-02 1.66E-02 2.48E-02 2.74E-02 2.93E-02 3.70E-02 4.09E-02 5.52E-02
c      6.74E-02 8.23E-02 1.11E-01 1.23E-01 1.83E-01 2.47E-01 2.73E-01 3.02E-01
c      4.08E-01 4.50E-01 4.98E-01 5.50E-01 6.08E-01 8.21E-01 9.07E-01 1.00E+00
c      1.11E+00 1.22E+00 1.35E+00 1.65E+00 2.02E+00 2.23E+00 2.47E+00 3.01E+00
c      3.68E+00 4.49E+00 5.49E+00 6.07E+00 6.70E+00 8.19E+00 1.00E+01 1.16E+01
c      1.38E+01 1.49E+01 1.73E+01 1.96E+01   $ Energy bins for Tallies
```

A.3 Experimental Fuel Crucible

```
mSERTTA Simplified Model
c by L. Scott
c The purpose of this model is to test the simplified neutronic response
c attributable directly to the temperature change. This will test various
c neutron cross sections, the OTFDB function, and the "tmp" declaration on the
c cell cards. The following are the ZAID numbers for materials tested.
c
c   -------------------- Doppler Broadening Temperatures --------------------
c   |                                                                        |
c   |  [ZAID].80c  --->  293.6 K   (original file)                           |
c   |  [ZAID].81c  --->  600.0 K                                             |
c   |  [ZAID].84c  --->  2500.0 K                                            |
c   |  [ZAID].70c  --->  On-the-Fly Doppler Broadening                       |
c   |                                                                        |
c   --------------------------------------------------------------------------
c
c ---------- Cell Cards ----------
c
c --------- Unit 1 (Top) ---------
c ------------ LEUO2 Fuel Pellets ------------
61001 6001 6.9759E-02  -60001  imp:n=1 tmp=5.11138E-08 $ Fuel Pellet 1 (Bottom)
(Top)
c
c ------------ Fuel Pin ------------
61041 6610 5.8248E-04  60001  -60041  imp:n=1 tmp=5.11138E-08 $ Helium Gap
61042 6700 8.6596E-02  -60044  imp:n=1 tmp=5.11138E-08 $ SS316 Spring
61043 6620 4.3360E-02  60041 60044 -60045  imp:n=1 tmp=5.11138E-08 $ Zr-4 Pin
Clad
61044 6620 4.3360E-02  -60042  imp:n=1 tmp=5.11138E-08 $ Zr-4 Fuel Pin End Tip
61045 6620 4.3360E-02  -60043  imp:n=1 tmp=5.11138E-08 $ Zr-4 Lower End Cap
61046 6620 4.3360E-02  -60046  imp:n=1 tmp=5.11138E-08 $ Zr-4 Upper End Cap
c
c ------------ Medium in Primary Vessel ------------
61198 7 6.8309E-02  -60199 (-60601:-60603) #61001 #61041
                    #61042 #61043 #61044 #61045 #61501
                    #61046 imp:n=1 tmp=5.11138E-08 $ Water
c
61501 6820 8.7321E-02 (60501 -60502):(60503 -60504 -60505)
                      imp:n=1 tmp=5.11138E-08 $ Zirconia Crucible
c ---------- Outside Universes ----------
998   0                -998        imp:n=1 tmp=5.11138E-08 $ f4 tally box
c 999   0                -999  #998  imp:n=1 tmp=5.11138E-08 $ f-mesh pipe
c
9997  0                +9997 -9999          imp:n=1 tmp=5.11138E-08   $ Shell
9998  0                -9999  #61001 #61041 #61042 #61043 #61044 #61045
                              #61046 #61198 #998 #9997 #61501
                                           imp:n=1 tmp=5.11138E-08   $ Inside
Universe
9999  0                +9999                imp:n=0 tmp=5.11138E-08   $ Outside
Universe
c

c ---------- Surface Cards ----------
c --- Experimental Facilities ------------------------------------------------
-
c ------ Fuel Pin ------
c --------- Fuel Pellets ---------
```

```
60001 rcc 0 0 -5.080   0 0 10.16   0.41   $ Fuel Pellet #1 (Bottom)
c
60041 rcc 0 0 -5.080   0 0 10.16   0.415  $ Fuel/Clad Gap
60042 rcc 0 0 -7.0104  0 0 1.2954  0.159  $ Fuel Pin End Tip
60043 rcc 0 0 -5.715   0 0 0.635   0.475  $ Lower End Cap
60044 rcc 0 0 +5.080   0 0 0.635   0.415  $ Spring
60045 rcc 0 0 -5.08    0 0 10.795  0.475  $ Outer Clad Surface
60046 rcc 0 0 +5.715   0 0 0.635   0.475  $ Upper End Cap
c
c ------ Primary Vessel Internals ------
60199 pz 7.496
c
c --------- Crucible ---------
60501 rcc 0 0.00 -7.745   0 0 15.241  1.905  $ Crucible ID
60502 rcc 0 0.00 -7.745   0 0 15.241  2.575  $ Crucible OD
60503 sph 0 0.00 -7.745               1.905  $ Crucible Cup ID
60504 sph 0 0.00 -7.745               2.575  $ Crucible Cup OD
60505 pz  -7.745
c
60601 rcc 0 0.000 -7.695    0 0 22.015   2.625  $ Main Vessel ID
60602 rcc 0 0.000 -7.695    0 0 22.015   3.015  $ Main Vessel OD
60603 sph 0 0.000 -7.695                 2.625  $ Vessel Cup ID
c
998   RPP -1.07823 0 168.474 169.474 -0.775266667 0             $ f4 box
c 999   RPP -10.7823 +10.7823 +1.000 +169.974 -13.9548 +13.9548   $ f-mesh pipe
c
9997  SO   204                                                   $ Shell
9999  SO   205                                                   $ Outside
Border

c
c ---------- Data Cards ----------
c --- Physics Cards ---
mode n
sdef pos=0 0 0 axs=0 0 1 ext=d3 rad=d2 erg=d6
SI2 0 0.41
SP2 -21 1
SI3 -5.08 5.08
SP3 -21 0
SI6 H
SP6 -3  0.965 2.29
nps 1e10
c cut:n j 0.099
c --- Experimental ------------------------------------------------------------
-
c ------ UO2 Fuel Pellets (4.95% U-235) ------
m6001  8016.81c 4.6489E-02   8017.81c 1.7672E-05  92234.81c 7.0909E-06
      92235.81c 1.1650E-03  92236.81c 1.4061E-05  92238.81c 2.2067E-02
c         Total 6.9759E-02
mt6001 o2-u.20t u-o2.20t
c
c ------ Fuel-Clad Gap (Helium 350 psi 300 K) ------
m6610  2003.81c 7.8052E-10  2004.81c 5.8247E-04
c         Total 5.8248E-04
c
c ------ Zircaloy-4 Clad ------
m6620 50112.81c 4.6806E-06  50114.81c 3.1848E-06  50115.81c 1.6406E-06
      50116.81c 7.0161E-05  50117.81c 3.7059E-05  50118.81c 1.1687E-04
      50119.81c 4.1450E-05  50120.81c 1.5721E-04  50122.81c 2.2342E-05
      50124.81c 2.7939E-05  26054.81c 8.6830E-06  26056.81c 1.3631E-04
```

```
      26057.81c 3.1479E-06  26058.81c 4.1892E-07  24050.81c 3.3012E-06
      24052.81c 6.3660E-05  24053.81c 7.2186E-06  24054.81c 1.7969E-06
      28058.81c 1.6037E-06  28060.81c 6.1775E-07  28061.81c 2.6853E-08
      28062.81c 8.5620E-08  28064.81c 2.1805E-08  13027.81c 5.4906E-06
       5010.81c 1.8179E-08   5011.81c 7.3174E-08  48106.81c 1.0982E-10
      48108.81c 7.8194E-11  48110.81c 1.0974E-09  48111.81c 1.1246E-09
      48112.81c 2.1200E-09  48113.81c 1.0736E-09  48114.81c 2.5242E-09
      48116.81c 6.5806E-10  20040.81c 1.4333E-06  20042.81c 9.5662E-09
      20043.81c 1.9960E-09  20044.81c 3.0843E-08  20046.81c 5.9142E-11
      20048.81c 2.7649E-09   6000.81c 4.4404E-05  27059.81c 6.7033E-07
      29063.81c 1.0747E-06  29065.81c 4.7947E-07  72174.81c 1.7706E-09
      72176.81c 5.8209E-08  72177.81c 2.0584E-07  72178.81c 3.0189E-07
      72179.81c 1.5072E-07  72180.81c 3.8821E-07   1001.81c 4.8987E-05
       1002.81c 5.6341E-09  12024.81c 1.2839E-06  12025.81c 1.6254E-07
      12026.81c 1.7895E-07  25055.81c 1.7977E-06  42092.81c 1.5205E-07
      42094.81c 9.5015E-08  42095.81c 1.6368E-07  42096.81c 1.7171E-07
      42097.81c 9.8412E-08  42098.81c 2.4902E-07  42100.81c 9.9545E-08
      41093.81c 2.1261E-06   7014.81c 1.1241E-05   7015.81c 4.1066E-08
      14028.81c 7.7832E-06  14029.81c 3.9539E-07  14030.81c 2.6095E-07
      74180.81c 1.2893E-09  74182.81c 2.8473E-07  74183.81c 1.5375E-07
      74184.81c 3.2921E-07  74186.81c 3.0546E-07  22046.81c 1.6674E-07
      22047.81c 1.5037E-07  22048.81c 1.4899E-06  22049.81c 1.0934E-07
      22050.81c 1.0469E-07  92234.81c 1.5684E-12  92235.81c 2.0923E-10
      92238.81c 2.8833E-08  40090.81c 2.1875E-02  40091.81c 4.7704E-03
      40092.81c 7.2917E-03  40094.81c 7.3895E-03  40096.81c 1.1905E-03
c         Total 4.3360E-02
mt6620 al27.22t fe56.22t
c
c ------ Stainless Steel 316 ------
m6700  6000.81c 2.0056E-04  25055.81c 8.7693E-04  15031.81c 5.9323E-04
      16032.81c 3.0137E-05  16033.81c 1.9890E-05  16034.81c 3.4997E-05
      16036.81c 2.1408E-05  14028.81c 1.6903E-07  14029.81c 9.5783E-07
      14030.81c 2.2537E-09  24050.81c 6.8439E-04  24052.81c 1.3198E-02
      24053.81c 1.4965E-03  24054.81c 3.7252E-04  42092.81c 1.8542E-04
      42094.81c 1.1587E-04  42095.81c 1.9961E-04  42096.81c 2.0940E-04
      42097.81c 1.2002E-04  42098.81c 3.0368E-04  42100.81c 1.2140E-04
      28058.81c 6.7055E-03  28060.81c 2.5829E-03  28061.81c 1.1228E-04
      28062.81c 3.5799E-04  28064.81c 9.1170E-05   7014.81c 1.7135E-04
       7015.81c 6.2600E-07  26054.81c 3.3778E-03  26056.81c 5.3024E-02
      26057.81c 1.2246E-03  26058.81c 1.6297E-04
c         Total 8.6596E-02
mt6700 fe56.22t
c
c ------ Crucible [ZrOx 86 (96wt% zirconia, 2wt% magnesia, 2wt% hafnia)] ------
m6820 40090.81c 1.4473E-02  40091.81c 3.1562E-03  40092.81c 4.8243E-03
      40094.81c 4.8890E-03  40096.81c 7.8765E-04   8016.81c 5.7997E-02
       8017.81c 2.2047E-05  12024.81c 4.6292E-04  12025.81c 5.8605E-05
      12026.81c 6.4524E-05  72174.81c 9.3767E-07  72176.81c 3.0826E-05
      72177.81c 1.0900E-04  72178.81c 1.5987E-04  72179.81c 7.9819E-05
      72180.81c 2.0558E-04
c         Total 8.7321E-02
c
c ------ Compressed PWR Water (16 MPa 320 C) ------
m7     1001.81c 4.5496E-02   1002.81c 5.2326E-06   8016.81c 2.2742E-02
       8017.81c 8.6452E-06   5010.81c 1.1333E-05   5011.81c 4.5619E-05
       3006.81c 1.5710E-08   3007.81c 1.9127E-07
c         Total 6.8309E-02
mt7    lwtr.26t hwtr.26t
c
c ---------- OTF Doppler Definition ----------
```

```
c OTFDB     8016.70c 8017.70c 92234.70c 92235.70c 92236.70c 92238.70c
c           1001.70c 3006.70c 1002.70c 5010.70c 3007.70c 5011.70c
c           50112.70c 50116.70c 50119.70c 50124.70c 26057.70c
c           24052.70c 28058.70c 28062.70c 48108.70c 48112.70c
c           48116.70c 20043.70c 20048.70c 29063.70c 72176.70c
c           72179.70c 12026.70c 42094.70c 42097.70c 41093.70c 14028.70c
c           74184.70c 22047.70c 22050.70c 40092.70c 50114.70c
c           50117.70c 50120.70c 26054.70c 26058.70c 24053.70c 28060.70c
c           28064.70c 48110.70c 48113.70c 20040.70c 20044.70c 6000.70c
c           29065.70c 72177.70c 72180.70c 12024.70c 25055.70c 42095.70c
c           42098.70c 7014.70c 14029.70c 74182.70c 74186.70c 22048.70c
c           40090.70c 40094.70c 50115.70c 50118.70c 50122.70c 26056.70c
c           24050.70c 24054.70c 28061.70c 13027.70c 48106.70c 48111.70c
c           48114.70c 20042.70c 20046.70c 27059.70c 72174.70c 72178.70c
c           12025.70c 42092.70c 42096.70c 42100.70c 7015.70c 14030.70c
c           74183.70c 22046.70c 22049.70c 40091.70c 40096.70c
c            2003.70c 2004.70c 16032.70c 16036.70c 16033.70c 15031.70c
c           16034.70c 73181.70c 18038.70c 18040.70c
c
c ---------- Tallies ----------
c ---------- Mesh Tally ----------
fmesh204:n GEOM=xyz origin= -10.7823 168.474 -13.9548
          IMESH= +10.7823 IINTS= 20
          JMESH= +169.474 JINTS= 1
          KMESH= +13.9548 KINTS= 36
          EMESH  0.1, 0.5, 1.00, 1.50, 1.75, 2.00
c
f04:n 998
f14:n 9997
c
f12:n (60001.1 60001.2 60001.3)
SD12  27.23
f22:n 998.3
SD22  601.856569
f32:n 9999
SD32  5.28E5
e0      0.10 0.15 0.20 0.25 0.30 0.35 0.40 0.45 0.50 0.55 0.60 0.65 0.70 0.75
        0.80 0.85 0.90 0.95 1.00 1.05 1.10 1.15 1.20 1.25 1.30 1.35 1.40 1.45
        1.50 1.55 1.60 1.65 1.70 1.75 1.80 1.85 1.90 1.95 2.00 2.05 2.10 2.15
        2.20 2.25 2.30 2.35 2.40 2.45 2.50 2.55 2.60 2.65 2.70 2.75 2.80 2.85
        2.90 2.95 3.00 3.05 3.10
c
c
c e0    3.00E-09 5.00E-09 6.90E-09 1.00E-08 1.50E-08 2.00E-08 2.50E-08 3.00E-08
c      3.50E-08 4.20E-08 5.00E-08 5.80E-08 6.70E-08 7.70E-08 8.00E-08 9.50E-08
c      1.00E-07 1.15E-07 1.34E-07 1.40E-07 1.60E-07 1.80E-07 1.89E-07 2.20E-07
c      2.48E-07 2.80E-07 3.00E-07 3.15E-07 3.20E-07 3.50E-07 3.91E-07 4.00E-07
c      4.33E-07 4.85E-07 5.00E-07 5.40E-07 6.25E-07 7.05E-07 7.80E-07 7.90E-07
c      8.50E-07 8.60E-07 9.10E-07 9.30E-07 9.50E-07 9.72E-07 9.86E-07 9.96E-07
c      1.02E-06 1.04E-06 1.05E-06 1.07E-06 1.10E-06 1.11E-06 1.12E-06 1.15E-06
c      1.17E-06 1.24E-06 1.30E-06 1.34E-06 1.37E-06 1.44E-06 1.48E-06 1.50E-06
c      1.59E-06 1.67E-06 1.76E-06 1.84E-06 1.93E-06 2.02E-06 2.10E-06 2.13E-06
c      2.36E-06 2.55E-06 2.60E-06 2.72E-06 2.77E-06 3.30E-06 3.38E-06 4.00E-06
c      4.13E-06 5.04E-06 5.35E-06 6.16E-06 7.52E-06 8.32E-06 9.19E-06 9.91E-06
c      1.12E-05 1.37E-05 1.59E-05 1.95E-05 2.26E-05 2.50E-05 2.76E-05 3.05E-05
c      3.37E-05 3.73E-05 4.02E-05 4.55E-05 4.83E-05 5.16E-05 5.56E-05 6.79E-05
c      7.57E-05 9.17E-05 1.37E-04 1.49E-04 2.04E-04 3.04E-04 3.72E-04 4.54E-04
c      6.77E-04 7.49E-04 9.14E-04 1.01E-03 1.23E-03 1.43E-03 1.51E-03 2.03E-03
c      2.25E-03 3.35E-03 3.53E-03 5.00E-03 5.53E-03 7.47E-03 9.12E-03 1.11E-02
c      1.50E-02 1.66E-02 2.48E-02 2.74E-02 2.93E-02 3.70E-02 4.09E-02 5.52E-02
```

```
c      6.74E-02 8.23E-02 1.11E-01 1.23E-01 1.83E-01 2.47E-01 2.73E-01 3.02E-01
c      4.08E-01 4.50E-01 4.98E-01 5.50E-01 6.08E-01 8.21E-01 9.07E-01 1.00E+00
c      1.11E+00 1.22E+00 1.35E+00 1.65E+00 2.02E+00 2.23E+00 2.47E+00 3.01E+00
c      3.68E+00 4.49E+00 5.49E+00 6.07E+00 6.70E+00 8.19E+00 1.00E+01 1.16E+01
c      1.38E+01 1.49E+01 1.73E+01 1.96E+01   $ Energy bins for Tallies
```

A.4 Graphite Reflector Model

```
mSERTTA Simplified Model
c by L. Scott
c The purpose of this model is to test the simplified neutronic response
c attributable directly to the temperature change. This will test various
c neutron cross sections, the OTFDB function, and the "tmp" declaration on the
c cell cards. The following are the ZAID numbers for materials tested.
c
c   -------------------- Doppler Broadening Temperatures --------------------
c   |                                                                        |
c   |  [ZAID].80c  --->  293.6 K   (original file)                           |
c   |  [ZAID].81c  --->  600.0 K                                             |
c   |  [ZAID].84c  --->  2500.0 K                                            |
c   |  [ZAID].70c  --->  On-the-Fly Doppler Broadening                       |
c   |                                                                        |
c   --------------------------------------------------------------------------
c
c ---------- Cell Cards ----------
c
c --------- Unit 1 (Top) ---------
c ------------ LEUO2 Fuel Pellets ------------
61001 6001 6.9738672E-02  -60001  imp:n=1 tmp=5.11138E-08 $ Fuel Pellet 1
(Bottom) (Top)
c
c ------------ Fuel Pin ------------
61041 6610 5.8248E-04  60001  -60041  imp:n=1 tmp=5.11138E-08 $ Helium Gap
61043 6620 4.80140975E-02  60041 60044 -60045  imp:n=1 tmp=5.11138E-08 $ Zr-4
Pin Clad
c
c ------------ Medium in Primary Vessel ------------
61198 7 6.8238E-02  -60199 (-60601:-60603) #61001 #61041
                    #61043   imp:n=1 tmp=5.11138E-08 $ Water
c
c ---------- Outside Universes ----------
998   0               -998        imp:n=1 tmp=5.11138E-08 $ f4 tally box
c
9000  0               -9000  #61001 #61041 #61043
                             #61198 #998        imp:n=1 tmp=5.11138E-08
9001  500 8.3721E-02  -9001  #9000  #61001 #61041 #61043
                             #61198 #998        imp:n=1 tmp=5.11138E-08
9998  0                -9999  #9000 #9001 #61001 #61041 #61043
                             #61198 #998            imp:n=1 tmp=5.11138E-08   $
Inside Universe
9999  0                +9999                    imp:n=0 tmp=5.11138E-08   $
Outside Universe
c

c ---------- Surface Cards ----------
c --- Experimental Facilities ------------------------------------------------
-
c ------ Fuel Pin ------
c --------- Fuel Pellets ---------
60001 rcc 0 0 -5.080   0 0 10.16   0.41   $ Fuel Pellet #1 (Bottom)
c
60041 rcc 0 0 -5.080   0 0 10.16   0.415  $ Fuel/Clad Gap
60042 rcc 0 0 -7.0104  0 0 1.2954  0.159  $ Fuel Pin End Tip
60043 rcc 0 0 -5.715   0 0 0.635   0.475  $ Lower End Cap
60044 rcc 0 0 +5.080   0 0 0.635   0.415  $ Spring
```

```
60045 rcc 0 0 -5.08    0 0 10.795  0.475  $ Outer Clad Surface
60046 rcc 0 0 +5.715   0 0 0.635   0.475  $ Upper End Cap
c
c ------ Primary Vessel Internals ------
60199 pz 7.496
c
60601 rcc 0 0.000 -7.695    0 0 22.015   2.625  $ Main Vessel ID
60602 rcc 0 0.000 -7.695    0 0 22.015   3.015  $ Main Vessel OD
60603 sph 0 0.000 -7.695                 2.625  $ Vessel Cup ID
c
998   RPP -1.07823 0 168.474 169.474 -0.775266667 0            $ f4 box
c
9000  RPP -5.3340 +5.3340 -10.2743 +200 -63.4206 +59.2931      $ Air Box (Void
in Model)
9001  RPP -200     +200 -200    +200    -200     +200          $ Graphite
c 9997  SO   204                                                 $ Shell
9999  SO   350                                                 $ Outside
Border

c
c ---------- Data Cards ----------
c --- Physics Cards ---
mode n
sdef pos=0 0 0 axs=0 0 1 ext=d3 rad=d2 erg=d4
SI2 0 0.41
SP2 -21 1
SI3 -5.08 5.08
SP3 -21 0
SI4 H
SP4 -3  0.965 2.29
nps 1e8
c --- Experimental ------------------------------------------------------------
-
c ------ UO2 Fuel Pellets (4.95% U-235) ------
m6001  8016.84c 4.6489E-02   8017.84c 1.7672E-05
      92235.84c 1.1650E-03   92238.84c 2.2067E-02
c         Total 6.9738672E-02
mt6001 o2-u.20t u-o2.20t
c
c ------ Fuel-Clad Gap (Helium 350 psi 300 K) ------
m6610    2004.81c 1.00
c
c ------ Zircaloy-4 Clad ------
m6620   40090.81c 2.1875E-02  40091.81c 4.7704E-03
        40092.81c 7.2917E-03  40094.81c 7.3895E-03  40096.81c 1.1905E-03
c         Total 6.2378372E-02
mt6620 al27.22t fe56.22t
c
c ------ Compressed PWR Water (16 MPa 320 C) ------
m7     1001.81c 4.5496E-02   8016.81c 2.2742E-02
c         Total 6.8238E-02
mt7    lwtr.26t hwtr.26t
c ------ CP-2 Graphite ------
m500   3006.81c  7.3682E-09   3007.81c  8.9709E-08   4009.81c  2.7898E-09
       5010.81c  6.4792E-09   5011.81c  2.6079E-08   9019.81c  2.6468E-09
      11023.81c  1.0936E-09  12024.81c  1.9611E-09  12025.81c  2.4827E-10
      12026.81c  2.7334E-10  13027.81c  8.2001E-08  14028.81c  2.3116E-06
      14029.81c  1.1743E-07  14030.81c  7.7503E-08  15031.81c  2.1105E-08
      16032.81c  1.3407E-06  16033.81c  1.0585E-08  16034.81c  5.9984E-08
      16036.81c  1.4114E-10  17035.81c  9.6708E-09  17037.81c  3.0943E-09
```

19039.81c	1.1994E-09	19040.81c	1.5047E-13	19041.81c	8.6557E-11
20040.81c	3.8921E-06	20042.81c	2.5977E-08	20043.81c	5.4202E-09
20044.81c	8.3752E-08	20046.81c	1.6060E-10	20048.81c	7.5079E-09
21045.81c	1.1185E-10	22046.81c	2.0800E-08	22047.81c	1.8758E-08
22048.81c	1.8586E-07	22049.81c	1.3640E-08	22050.81c	1.3060E-08
23050.81c	5.9226E-09	23051.81c	2.3631E-06	24050.81c	2.1010E-10
24052.81c	4.0515E-09	24053.81c	4.5941E-10	24054.81c	1.1436E-10
25055.81c	3.6612E-10	26054.81c	6.5261E-09	26056.81c	1.0245E-07
26057.81c	2.3659E-09	26058.81c	3.1486E-10	27059.81c	8.5325E-11
28058.81c	1.6331E-08	28060.81c	6.2905E-09	28061.81c	2.7344E-10
28062.81c	8.7186E-10	28064.81c	2.2204E-10	29063.81c	1.6416E-09
29065.81c	7.3236E-10	30064.81c	1.8554E-10	30066.81c	1.0753E-10
30067.81c	1.5767E-11	30068.81c	7.3125E-11	30070.81c	2.4255E-12
31069.81c	4.3350E-11	31071.81c	2.8770E-11	32070.81c	7.0540E-11
32072.81c	9.4526E-11	32073.81c	2.6859E-11	32074.81c	1.2710E-10
32076.81c	2.7101E-11	33075.81c	3.3558E-10	34074.81c	2.8339E-12
34076.81c	2.9836E-11	34077.81c	2.4295E-11	34078.81c	7.5688E-11
34080.81c	1.5797E-10	34082.81c	2.7798E-11	35079.81c	3.1900E-10
35081.81c	3.1031E-10	37085.81c	2.1230E-10	37087.81c	8.1868E-11
38084.81c	7.7131E-11	38086.81c	1.3581E-09	38087.81c	9.6414E-10
38088.81c	1.1374E-08	39089.81c	5.6559E-10	40090.81c	1.9285E-09
40091.81c	4.2056E-10	40092.81c	6.4283E-10	40094.81c	6.5145E-10
40096.81c	1.0495E-10	41093.81c	2.7062E-10	42092.81c	3.8707E-11
42094.81c	2.4188E-11	42095.81c	4.1668E-11	42096.81c	4.3712E-11
42097.81c	2.5053E-11	42098.81c	6.3393E-11	42100.81c	2.5341E-11
44096.81c	1.3781E-11	44098.81c	4.6518E-12	44099.81c	3.1742E-11
44100.81c	3.1344E-11	44101.81c	4.2439E-11	44102.81c	7.8484E-11
44104.81c	4.6319E-11	45103.81c	4.8865E-11	46102.81c	2.4098E-12
46104.81c	2.6319E-11	46105.81c	5.2756E-11	46106.81c	6.4569E-11
46108.81c	6.2513E-11	46110.81c	2.7689E-11	47107.81c	1.2083E-10
47109.81c	1.1226E-10	48106.81c	2.7958E-12	48108.81c	1.9906E-12
48110.81c	2.7936E-11	48111.81c	2.8629E-11	48112.81c	5.3970E-11
48113.81c	2.7332E-11	48114.81c	6.4259E-11	48116.81c	1.6752E-11
49113.81c	9.3940E-12	49115.81c	2.0958E-10	50112.81c	2.0544E-12
50114.81c	1.3979E-12	50115.81c	7.2011E-13	50116.81c	3.0795E-11
50117.81c	1.6266E-11	50118.81c	5.1297E-11	50119.81c	1.8193E-11
50120.81c	6.9003E-11	50122.81c	9.8061E-12	50124.81c	1.2263E-11
51121.81c	1.1813E-10	51123.81c	8.8357E-11	52120.81c	1.7734E-13
52122.81c	5.0245E-12	52123.81c	1.7537E-12	52124.81c	9.3397E-12
52125.81c	1.3931E-11	52126.81c	3.7122E-11	52128.81c	6.2540E-11
52130.81c	6.7151E-11	53127.81c	3.9624E-11	55133.81c	1.8917E-10
56130.81c	1.9407E-13	56132.81c	1.8491E-13	56134.81c	4.4251E-12
56135.81c	1.2069E-11	56136.81c	1.4379E-11	56137.81c	2.0564E-11
56138.81c	1.3127E-10	57138.81c	1.6290E-13	57139.81c	1.8084E-10
58136.81c	3.3196E-13	58138.81c	4.5039E-13	58140.81c	1.5871E-10
58142.81c	1.9943E-11	59141.81c	1.7843E-10	60142.81c	4.7411E-11
60143.81c	2.1265E-11	60144.81c	4.1485E-11	60145.81c	1.4467E-11
60146.81c	2.9981E-11	60148.81c	9.9355E-12	60150.81c	9.7611E-12
62144.81c	1.0267E-12	62147.81c	5.0131E-12	62148.81c	3.7590E-12
62149.81c	4.6218E-12	62150.81c	2.4681E-12	62152.81c	8.9459E-12
62154.81c	7.6082E-12	63151.81c	1.5820E-11	63153.81c	1.7270E-11
64152.81c	6.3955E-14	64154.81c	6.9711E-13	64155.81c	4.7327E-12
64156.81c	6.5458E-12	64157.81c	5.0045E-12	64158.81c	7.9432E-12
64160.81c	6.9903E-12	65159.81c	3.1640E-11	66156.81c	1.7329E-14
66158.81c	2.9397E-14	66160.81c	7.2069E-13	66161.81c	5.8451E-12
66162.81c	7.8831E-12	66163.81c	7.7039E-12	66164.81c	8.7449E-12
67165.81c	3.0488E-11	68162.81c	4.1789E-14	68164.81c	4.8132E-13
68166.81c	1.0072E-11	68167.81c	6.8753E-12	68168.81c	8.1106E-12
68170.81c	4.4825E-12	69169.81c	2.9766E-11	71175.81c	2.7995E-11
71176.81c	7.4435E-13	72174.81c	4.5075E-14	72176.81c	1.4819E-12

```
      72177.81c  5.2400E-12  72178.81c  7.6854E-12  72179.81c  3.8371E-12
      72180.81c  9.8828E-12  73180.81c  3.3347E-11  73181.81c  2.7786E-07
      74180.81c  1.6411E-13  74182.81c  3.6242E-11  74183.81c  1.9571E-11
      74184.81c  4.1904E-11  74186.81c  3.8881E-11  75185.81c  1.0100E-11
      75187.81c  1.6905E-11  77191.81c  9.7578E-12  77193.81c  1.6403E-11
      79197.81c  2.5529E-10  80196.81c  3.7602E-13  80198.81c  2.4993E-11
      80199.81c  4.2290E-11  80200.81c  5.7908E-11  80201.81c  3.3040E-11
      80202.81c  7.4854E-11  80204.81c  1.7222E-11  81203.81c  3.6314E-11
      81205.81c  8.6701E-11  82204.81c  1.6988E-12  82206.81c  2.9244E-11
      82207.81c  2.6817E-11  82208.81c  6.3584E-11  83209.81c  1.2031E-10
      90232.81c  1.0835E-10  92234.81c  5.7039E-15  92235.81c  7.6094E-13
      92238.81c  1.0486E-10   1001.81c  2.2327E-05   1002.81c  2.5679E-09
       8016.81c  1.1161E-05   8017.81c  4.2426E-09   6000.81c  8.3677E-02
c        Total  8.3721E-02
mt500 grph.20t al27.22t fe56.22t
c
c ---------- Tallies ----------
c ---------- Mesh Tally ----------
fmesh204:n GEOM=xyz origin= -10.7823 168.474 -13.9548
          IMESH= +10.7823 IINTS= 20
          JMESH= +169.474 JINTS= 1
          KMESH= +13.9548 KINTS= 36
          EMESH  0.1, 0.5, 1.00, 1.50, 1.75, 2.00
c
f04:n 998
c
f22:n 998.3
SD22  601.856569
c
e0    3.00E-09 5.00E-09 6.90E-09 1.00E-08 1.50E-08 2.00E-08 2.50E-08 3.00E-08
      3.50E-08 4.20E-08 5.00E-08 5.80E-08 6.70E-08 7.70E-08 8.00E-08 9.50E-08
      1.00E-07 1.15E-07 1.34E-07 1.40E-07 1.60E-07 1.80E-07 1.89E-07 2.20E-07
      2.48E-07 2.80E-07 3.00E-07 3.15E-07 3.20E-07 3.50E-07 3.91E-07 4.00E-07
      4.33E-07 4.85E-07 5.00E-07 5.40E-07 6.25E-07 7.05E-07 7.80E-07 7.90E-07
      8.50E-07 8.60E-07 9.10E-07 9.30E-07 9.50E-07 9.72E-07 9.86E-07 9.96E-07
      1.02E-06 1.04E-06 1.05E-06 1.07E-06 1.10E-06 1.11E-06 1.12E-06 1.15E-06
      1.17E-06 1.24E-06 1.30E-06 1.34E-06 1.37E-06 1.44E-06 1.48E-06 1.50E-06
      1.59E-06 1.67E-06 1.76E-06 1.84E-06 1.93E-06 2.02E-06 2.10E-06 2.13E-06
      2.36E-06 2.55E-06 2.60E-06 2.72E-06 2.77E-06 3.30E-06 3.38E-06 4.00E-06
      4.13E-06 5.04E-06 5.35E-06 6.16E-06 7.52E-06 8.32E-06 9.19E-06 9.91E-06
      1.12E-05 1.37E-05 1.59E-05 1.95E-05 2.26E-05 2.50E-05 2.76E-05 3.05E-05
      3.37E-05 3.73E-05 4.02E-05 4.55E-05 4.83E-05 5.16E-05 5.56E-05 6.79E-05
      7.57E-05 9.17E-05 1.37E-04 1.49E-04 2.04E-04 3.04E-04 3.72E-04 4.54E-04
      6.77E-04 7.49E-04 9.14E-04 1.01E-03 1.23E-03 1.43E-03 1.51E-03 2.03E-03
      2.25E-03 3.35E-03 3.53E-03 5.00E-03 5.53E-03 7.47E-03 9.12E-03 1.11E-02
      1.50E-02 1.66E-02 2.48E-02 2.74E-02 2.93E-02 3.70E-02 4.09E-02 5.52E-02
      6.74E-02 8.23E-02 1.11E-01 1.23E-01 1.83E-01 2.47E-01 2.73E-01 3.02E-01
      4.08E-01 4.50E-01 4.98E-01 5.50E-01 6.08E-01 8.21E-01 9.07E-01 1.00E+00
      1.11E+00 1.22E+00 1.35E+00 1.65E+00 2.02E+00 2.23E+00 2.47E+00 3.01E+00
      3.68E+00 4.49E+00 5.49E+00 6.07E+00 6.70E+00 8.19E+00 1.00E+01 1.16E+01
      1.38E+01 1.49E+01 1.73E+01 1.96E+01   $ Energy bins for Tallies
```